Surface Interaction Mechanisms between Deformable Bubbles and Hydrophobic Surfaces in Aqueous
Solutions

by

Xin Cui

A thesis submitted in partial fulfillment of the requirements for the degree of

Doctor of Philosophy

in

Materials Engineering

Department of Chemical and Materials Engineering
University of Alberta

Abstract

Deformable bubbles in complex fluidic systems are crucial components in a variety of traditional and emerging industrial processes, where their surface interactions with hydrophobic surfaces play an important role in realizing the targeted functionalities. In this project, a bubble probe atomic force microscopy (AFM) technique was applied to directly measure the interactions between air bubbles and various hydrophobic surfaces under different aqueous conditions, and the measured interaction forces were theoretically analyzed based on a Stokes-Reynolds-Young-Laplace model which incorporated the effect of disjoining pressure. By virtue of this methodology, the project systematically investigated the critical roles of the surface interactions including van der Waals (VDW), electrical double-layer (EDL) and hydrophobic (HB) interactions in the bubble-surface interaction processes. The VDW and EDL interactions could be well explained by the classical Derjaguin-Landau-Verwey-Overbeek (DLVO) theory, which tended to stabilize the thin water film and prevent the bubble attachment onto the hydrophobic surface. The non-DLVO HB interaction originating from the water structuring effect at the hydrophobic interface was responsible for the bubble attachment, which could be quantified using an exponentially decaying model derived from the thermodynamic consideration.

Besides, the effects of a series of principal factors which could modulate the HB interactions between air bubbles and hydrophobic surfaces have been elucidated. Firstly, it was found that altering aqueous salinity and pH could hardly affect the HB interactions between air bubbles and hydrocarbon self-assembled monolayers (SAMs) composed of octadecyltrichlorosilane (OTS), with the decay length D_0 remaining ~ 1.0 nm across all the investigated cases. However, for the cases involving hydrophobic polystyrene (PS) surfaces, interfacial nanobubbles (INBs) could spontaneously form on the PS surfaces and significantly

affect the measurement of the bubble-PS interactions. As verified by the AFM imaging results, high salinity (e.g., 1000 mM NaCl) could sufficiently suppress the nanobubble formation and simplify the quantification of the intrinsic HB interaction between the air bubble and the pristine PS surface, and the decay length D_0 was theoretically fitted to be ~ 0.75 nm. Moreover, the bubble-polymer HB interactions were found to be subject to ion specificity. The selective binding of the cations with low charge density (e.g., K^+ and NH_4^+) to the aromatic benzene groups, the so-called "cation-π interaction" could shorten the range of the bubble-PS HB interaction with D_0 declining from ~ 0.75 nm to ~ 0.60 nm; while the preferential adsorption of heavy halide anion (e.g., I^-) onto the poly (methyl methacrylate) (PMMA) and polydimethylsiloxane (PDMS) surfaces could reduce the corresponding D_0 from ~ 0.63 nm and ~ 0.72 nm to ~ 0.50 nm and ~ 0.59 nm, respectively. Furthermore, the range of the HB interaction could also be evidently modulated by altering the surface properties. By coadsorbing two components of alkanethiols with different chain length or tail groups, surface mobility and nano-scaled chemistry heterogeneity could be introduced into the SAM surfaces, which could effectively relax the physical restriction that orderly rearranges the interfacial water molecules and shorten the range of the HB interaction.

This project provides a useful method to quantitatively study the interactions between deformable droplets (e.g., air bubbles) and hydrophobic surfaces in complex aqueous media, and contributes to an improved understanding of the surface interaction mechanisms. The results of quantifying the HB interactions under different experimental conditions comprehensively illustrate the effects of the influencing factors such as water chemistry and surface properties, and sheds novel light on the physical mechanism underlying the HB interaction, which is of both fundamental and practical significance.

Preface

Chapter 3 of this thesis has been published as X. Cui, C. Shi, S. Zhang, L. Xie, J Liu, D. Jiang, H. Zeng, "Probing the Effect of Salinity and pH on Surface Interactions between Air Bubbles and Hydrophobic Solids: Implications for Colloidal Assembly at Air/Water Interfaces.", *Chemistry-an Asian Journal*, vol. 12, 1568-1577. I was responsible for AFM force measurement, data analysis, and manuscript composition. C. Shi, L. Xie J. Liu assisted with the AFM force measurement. S Zhang was responsible for surface tension measurement. Dr. D. Jiang contributed to manuscript edition. Dr. Hongbo Zeng was the supervisory author and was involved in concept formation and manuscript composition.

Chapter 4 of this thesis has been published as X. Cui, C. Shi, L. Xie, J. Liu, H. Zeng, "Probing Interactions between Air Bubble and Hydrophobic Polymer Surface: Impact of Solution Salinity and Interfacial Nanobubbles.", *Langmuir*, vol. 32, issue 43, 11236-11244. I was responsible for AFM force measurement, AFM imaging, data analysis, and manuscript composition. C. Shi, and L. Xie assisted with the AFM force measurement. J. Liu contributed to the AFM imaging. Dr. Hongbo Zeng was the supervisory author and was involved in concept formation and manuscript composition.

Chapter 5 of this thesis will be submitted for publication as X. Cui, J. Liu, L. Xie, J. Huang, H. Zeng, "Probing Effects of Ion Specificity on Hydrophobic Interactions between Air Bubbles and Hydrophobic Polymer Surfaces Using Bubble Probe AFM.". I was responsible for experimental force measurement via bubble probe AFM, AFM imaging characterization, data analysis, and manuscript composition. J. Liu and L. Xie assisted with the AFM force measurement. J. Liu, L. Xie and J. Huang contributed to the manuscript edition. Dr. Hongbo

Zeng was the supervisory author and was involved in concept formation and manuscript composition.

Chapter 6 of this thesis will be submitted for publication as X. Cui, C. Shi, L. Xie, L. Zhang, J. Liu, H. Zeng, "Modulation of Hydrophobic Interaction by Mediating Surface Mobility and Chemistry.". I was responsible for AFM force measurement, AFM imaging, data analysis, and manuscript composition. C. Shi, and L. Xie assisted with the AFM force measurement. J. Liu contributed to the AFM imaging. L. Zhang conducted the characterization of the sample thickness. Dr. Hongbo Zeng was the supervisory author and was involved in concept formation and manuscript composition.

Chapters 1, 2, and 7 are originally written by Xin Cui, and have never been published before.

Acknowledgement

I would like to express my sincere gratitude to Prof. Hongbo Zeng for his insightful guidance and considerate encouragement throughout the whole period of my PhD study. His ingenious mind and brilliant suggestions have enlightened me every time when I was confronted with research difficulties during these years. I am also impressed by his enthusiasm and aspire for scientific research which inspires me to fight for my career goal as a dedicated researcher. Besides, Prof. Zeng has also set an excellent example for me because of his cautiousness into every detail in academic work.

I wish to thank all my group members for their strong support and generous help during my study. Especially, I am grateful to Dr. Chen Shi and Dr. Lei Xie for their valuable advice for the completion of my research and revision of my manuscripts during my PhD study.

I want to acknowledge Dr. Shihong Xu in nanoFAB for his assistance with the XPS characterizations.

Last but not least, my deepest gratitude goes to my family. I am sincerely grateful to my parents and my wife Ms. Jing Liu for their endless love and support.

Table of Contents

List of Tables

List of Figures

List of Acronyms and Symbols

AFM   Atomic force microscopy

DLVO   Derjaguin-Landau-Verwey-Overbeek

EDL   Electrical double-layer

HB   Hydrophobic

INB   Interfacial nanobubbles

MD   Molecular dynamics

OTS   Octadecyltrichlorosilane

PF-QNM   PeakForce quantitative nano-mechanics

PDMS   Polydimethylsiloxane

PMMA   Poly (methyl methacrylate)

PS   Polystyrene

RICM   Reflection interference contrast microscopy

RMS   Root-mean-square

SAM   Self-assembled monolayer

SFA   Surface forces apparatus

SFG   Sum-frequency generation

TM	Tapping mode
VDW	Van der Waals
WCA	Water contact angle
XPS	X-ray photoelectron spectroscopy
A_H	Hamaker constant
C_0	Pre-exponential factor of hydrophobic interaction
D_0	Decay length of hydrophobic interaction
F	Measured interaction force
h	Separation between two surfaces
k_B	Boltzmann constant
R	Radius of bubble or particle
T	Temperature
ΔP	Laplace pressure
Ψ	Surface potential
γ	Interfacial tension
θ_c	Water contact angle
κ	Inverse of Debye length
μ	Solution viscosity

$\varepsilon_0\varepsilon$ dielectric permittivity

ρ Ion density in solution

z Ion valency

Chapter 1   Introduction

1.1. Interactions between Deformable Bubbles and Solid Surfaces.

Deformable bubbles are important components in a variety of technological and bioengineering processes, such as froth flotation, stabilization of emulsions and foams,[1] ultrasound contrast imaging,[2] controlled drug delivery and therapeutics,[3] water-driven micromotor[4] and soft templates for preparation of advanced materials.[5] In many of these applications, the surface interactions involving bubbles are essential in achieving the desired characteristics and functionalities. Different from a solid material, the behavior of a bubble in a fluid system is strongly determined by its interfacial tension with the surrounding liquid phase. Consequently, the bubble can easily change its shape, which is governed by the balance between the Laplace pressure inside the bubble and the external forces including hydrodynamic force and disjoining pressure arising from surface interactions. It is such complex that makes it challenging to quantitatively determine the exact force law of the surface interactions involving deformable bubbles.[6-7] Figure 1.1 illustrates the interaction process of a deformable bubble with a solid flat substrate. When the bubble approaches the substrate, the confined water film between the bubble and the substrate starts to drain out, and the resultant hydrodynamic repulsion tend to flatten the central part of the bubble. As the bubble moves closer to the substrate, the effect of disjoining pressure grows increasingly evident, especially at a relatively low interaction velocity which sufficiently weakens the hydrodynamic effect. If the disjoining pressure is repulsive, the thin water film will be stabilized at a critical separation where the Laplace pressure is fully balanced by the external pressure. Further driving the bubble to the substrate will not reduce the bubble-substrate separation but enlarge the flattened area. On the contrary, for the case of attractive disjoining pressure, the drainage process of the thin water film will be accelerated which

facilitates the approaching process of the bubble. When the Laplace pressure is not able to resist the attractive disjoining pressure, the confined thin water film will rupture, resulting in the bubble attachment onto the substrate. Whether the disjoining pressure is repulsive or attractive depends on the features and strength of all the surface interactions which are determined by the specific properties of the interacting objects and the media. For the interactions of deformable bubbles in aqueous media, three major surface interactions are generally taken into account, i.e., the van der Waals (VDW) interaction and electrical double-layer (EDL) interaction which can be well interpreted by the classical DLVO theory, and the hydrophobic (HB) interaction (the primary focus in this project) that deviates from the DLVO theory.[8]
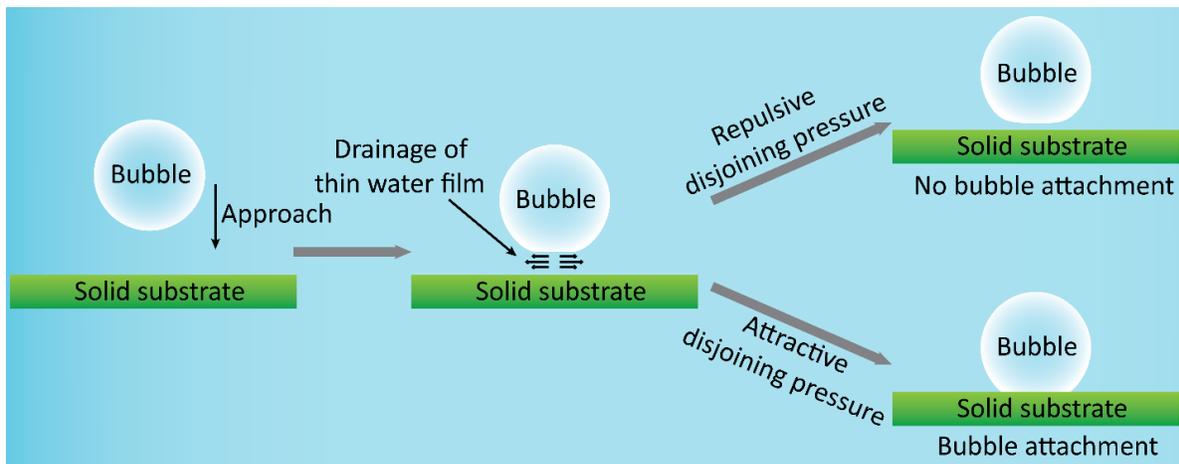
Figure 1.1. Schematic illustration of the interaction process of a deformable droplet with a solid substrate in aqueous environment.

1.1.1. Van der Waals interaction.

Van der Waals (VDW) interaction is generally defined as the totality of the attractions and repulsions between atoms and molecules originating from the electrostatic correlations in the fluctuating polarizations.[8] Three representative components, the orientation interaction between two permanent dipoles (Keesom interaction), induction interaction between a permanent dipole

and its induced dipole (Debye interaction), and dispersion interaction between an instantaneous dipole and its induced dipoles (London interaction), varying with the inverse six power of distance, collectively contribute to the overall VDW interaction.

The VDW interaction between two macroscopic bodies through a medium can be calculated based on Lifshitz theory which incorporates the influence of surrounding molecules on the interaction between each pair of molecules in the two interacting bodies.[8] Treating the macroscopic bodies as continuous media and ignoring the molecular structure, Liftshitz theory is derived in terms of the bulk parameters including dielectric constants and refractive indices. equation 1.1 illustrates the approximate expression for the nonretarded VDW interaction energy per unit area between two macroscopic non-conducting objects 1 and 2 through a medium 3,

$$W_{VDW}(h) = -\frac{A_H}{12\pi h^2}$$

$$A \approx \frac{3}{4}k_B T \left(\frac{\varepsilon_1 - \varepsilon_3}{\varepsilon_1 + \varepsilon_3}\right)\left(\frac{\varepsilon_2 - \varepsilon_3}{\varepsilon_2 + \varepsilon_3}\right) + \frac{3h\upsilon_e}{8\sqrt{2}} \frac{\left(n_1^2 - n_3^2\right)\left(n_2^2 - n_3^2\right)}{\sqrt{\left(n_1^2 + n_3^2\right)}\sqrt{\left(n_2^2 + n_3^2\right)}\left\{\sqrt{\left(n_1^2 + n_3^2\right)} + \sqrt{\left(n_2^2 + n_3^2\right)}\right\}} \tag{1.1}$$

where h in the top equation is the separation between two macroscopic surfaces, A_H is the non-retarded Hamaker constant, ε is the dielectric constant, n is the refractive index, k_B and h in the bottom equation are the Boltzmann's and Plank's constants, T is the temperature, υ_e is the main electronic absorption frequency. For a symmetric interaction between two identical condensed materials in a medium, the value of A_H is always positive, leading to an attractive VDW interaction. For an asymmetric interaction, the VDW interaction could be attractive or repulsive, depending on the specific values of ε and n. Taking the interaction between an air bubble and a solid substrate (e.g., mica, silica and gold) in water as an example, the values of ε and n of the media water are smaller than those of the air bubble but larger than those of the solid substrate. As a result, the corresponding A_H keeps negative at any separation and the VDW interaction of

the air/water/solid system is repulsive which tends to prevent the bubble from attaching onto the solid substrate.

1.1.2. Electrical double-layer interaction.

The surfaces of gas bubbles, liquid droplets and solid particles suspended in water usually carry charges, which can be possibly due to the ionization or dissociation of surface groups, the adsorption of ions from aqueous environment, and protons or electrons-hop. Regardless of the charging mechanism, the surface charge will be balanced by an equal number of oppositely charged counterions. Some counterions are transiently bound to the charged surface forming the Stern or Helmholtz layer, while others construct a diffuse region near the charged surface owing to the mutual repulsion among those counterions, and this is the so-called "electrical double-layer (EDL)" model. Nonetheless, the origin of the EDL interaction between two charged surfaces in water is entropic (osmotic) rather than electrostatic. When two similarly charged surfaces are brought close to each other, the overlapping of the two double-layers increases the counterion concentration and forces the counterions back onto the surfaces. Consequently, the osmotic pressure between these two surfaces is increased and the entropy of the system is decreased, which is against the preferred equilibrium state of the counterions and leads to the EDL repulsion.[8]

Equation 1.2 describes the EDL interaction energy per unit area between two identical surfaces in electrolyte solution. Derived based on Poisson-Boltzmann equation and Grahame equation, this equation demonstrates that EDL interaction decays exponentially with separation and the characteristic decay length, Debye length κ^{-1}, can roughly estimate the "thickness" of the diffuse double-layer.

$$W_{EDL}(h) = 64 k_B T \rho_\infty \tanh^2 \left(\frac{ze\psi}{4kT} \right) \kappa^{-1} \exp \left(-\frac{h}{\kappa^{-1}} \right)$$

$$\kappa^{-1} = \left(\sum_i \rho_{\infty i} e^2 z_i^2 / \varepsilon_0 \varepsilon k_B T \right)^{-\frac{1}{2}}$$

(1.2)

where z is the ionic valency, Ψ is the surface potential of interacting objects, ρ_∞ is the number density of ion in bulk reservoir, e is the elementary charge, and $\varepsilon_0\varepsilon$ is the dielectric permittivity of the aqueous medium. For the case of asymmetric EDL interaction between two surfaces of unequal but constant potentials, the "Hogg-Healy-Fuerstenau" equation can be applied to quantify the EDL interaction, as shown in Equation 1.3.[9-10]

$$W_{EDL}(h) = \frac{\varepsilon_0 \varepsilon \kappa \left[2\psi_1 \psi_2 - \left(\psi_1^2 + \psi_2^2 \right) \exp(-\kappa h) \right]}{[\exp(\kappa h) - \exp(-\kappa h)]}$$

(1.3)

It is noteworthy that some corresponding modifications need to be imposed on the expressions for the EDL interaction energy mentioned above, when it comes to the cases where the assumption of constant surface charge is applied, or the separation between two surfaces is reduced within a Debye length, or the complexity of divalent ions or high surface potential is involved.

The combination of the VDW and EDL interactions underlies the famous DLVO theory in the colloidal and interfacial science. According to the DLVO theory, the VDW interaction is insensitive to the change in the aqueous condition, but depends on the dielectric constants and refractive indices of the interacting objects and media. In contrast, the EDL interaction can be readily modulated by altering the ionic strength, electrolyte type, aqueous pH and the surface charge and potential. In addition, several non-DLVO surface interactions can also extensively participate in the interaction processes involving deformable droplets, such as solvation, structural, hydration and hydrophobic (HB) interaction.[8] Among them, HB interaction is ubiquitously present in the interaction of a deformable bubble with a hydrophobic surface, which

is the driving force behind a number of colloidal and interfacial phenomena and relevant engineering applications.

1.1.3. Hydrophobic interaction.

Hydrophobic (HB) interaction, also known as hydrophobic effect or hydrophobic force, generally describes the exceptional attraction between hydrophobic species in aqueous media which deviates from the classical DLVO theory. Manifested as the strong tendency of nonpolar substances to aggregate in aqueous media, HB interaction is responsible for many phenomena in aqueous environment including rapid coalescence of oil droplets, formation of lipids and micelles, protein folding, and self-assembling behaviors of macromolecules, proteins and colloidal particles at interfaces.[6, 8] As one of the most important nonspecific surface interactions, HB interaction also plays a crucial role in a wide range of water-based engineering and industrial processes, such as froth flotation,[11] oil/water separation,[12] stabilization of foams and emulsions,[13] gas transport,[14] and protein purification and separation.[15]

Even though its exact physical mechanism has not been fully elucidated, HB interaction has been well recognized as an entropy-driven process highly associated with the water structuring effect in proximity to hydrophobic surfaces.[16] To be specific, hydrophobic surfaces are incapable of forming hydrogen bonds or electrostatically interacting with the neighboring water molecules. Therefore, the introduction of hydrophobic surfaces can notably disrupt the dynamic hydrogen bonding network, and physically restricts the interfacial water molecules to reorient and rearrange into a more ordered structure as compared to those in the bulk. Such a water structuring effect can significantly decrease the configurational entropy which is thermodynamically unfavorable. Therefore, the hydrophobic substances tend to aggregate

together to minimize their area exposed to the aqueous environment and lower the surface free energy of the entire system. The intensity of the HB interaction is closely related to the surface hydrophobicity of the interacting materials which is manifested as the antipathy against water. The hydrophobicity of a solid surface is usually gauged by measuring its water contact angle (WCA) in air, and a solid surface with higher WCA is considered more hydrophobic.[6] For agas bubble or an oil droplet, its immiscibility and interfacial tension with water are often applied as the criterion to roughly assess its hydrophobicity, with larger values implying higher hydrophobicity.[17]

1.2. Direct measurement of the interactions between hydrophobic surfaces.

In 1982, Israelachvili and Pashley directly measured the interaction between two hydrophobic self-assembled monolayers (SAMs) deposited on mica substrates for the first time, reporting that HB interaction could follow an exponentially decaying force law.[18] This pioneering work has inspired a huge wave of research interest in quantifying the HB interactions involved in a variety of hydrophobic systems and probing the roles of potential influencing factors in modulating the HB interactions. Two major nanomechanical techniques have been commonly used to measure the interactions between two hydrophobic surfaces, i.e., surface forces apparatus (SFA) and atomic force microscope (AFM), as shown in Figures 1.2A and 1.2B, respectively. Many previous studies have been focused on the force measurement of the interactions between two solid hydrophobic surfaces, which are intrinsically hydrophobic (e.g., hydrophobic polymers and minerals), chemically modified by hydrophobic agents (e.g., alkylsilanes and alkanethiols), and physically treated by adsorbing amphiphilic surfactants through electrostatic interaction (e.g., hexadecyltrimethylammonium bromide, CTAB).[19-25]

Besides, quite a few studies have also been conducted to measure the interaction forces between deformable droplets/bubbles and hydrophobic solids via a modified SFA and a colloidal probe AFM (Figures 1.3A and 1.3B, respectively).[26-28] However, some issues convoluted with these two techniques impede their wide application in quantitatively probing the surface interactions, such as the relatively large droplet size, limited range of applicable hydrophobic solids, and the difficulty in interpreting droplet deformation and correlating the interaction forces with surface separation. Notably, a novel droplet/bubble probe AFM technique has been successfully developed and extensively adopted to directly measure the interactions between deformable droplets and solid substrates during the recent decade (Figure 1.3C).[29-33] The measured interaction forces can be theoretically analyzed through a model based on Reynolds lubrication theory and augmented Young-Laplace equation incorporating the effect of disjoining pressure. This Stokes-Reynolds-Young-Laplace model is capable of precisely calculating the droplet/bubble deformation and establishing the accurate force-separation profiles of the involved surface interactions.[34] Recently, the droplet/bubble probe AFM technique has been coupled with confocal microscopy and reflection interference contrast microscopy (RICM). Such innovative researches allow the synchronous measurement of the interaction forces and the visualization of the spatiotemporal evolution of the confined thin water film, and more importantly confirm the validity of the theoretical model.[30, 35]
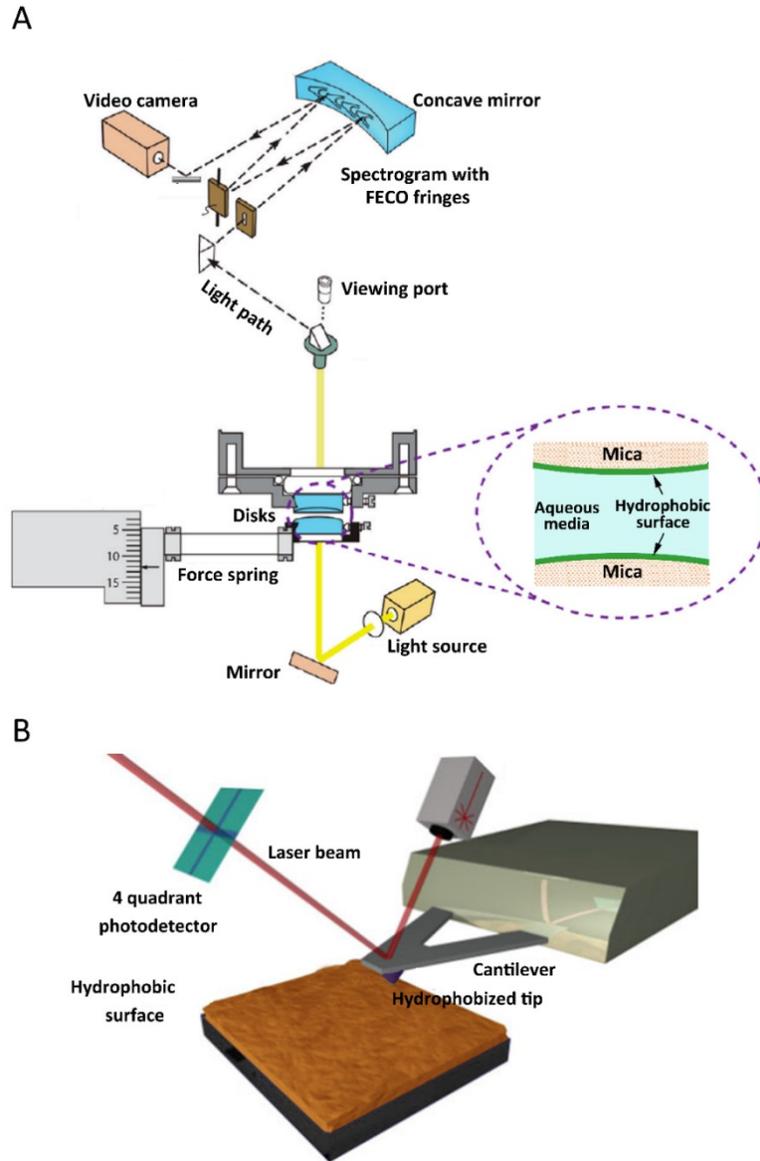
Figure 1.2. Schematic diagrams of force measurement of the interaction between two hydrophobic solid surfaces by (A) SFA and (B) AFM, respectively.[19, 36]
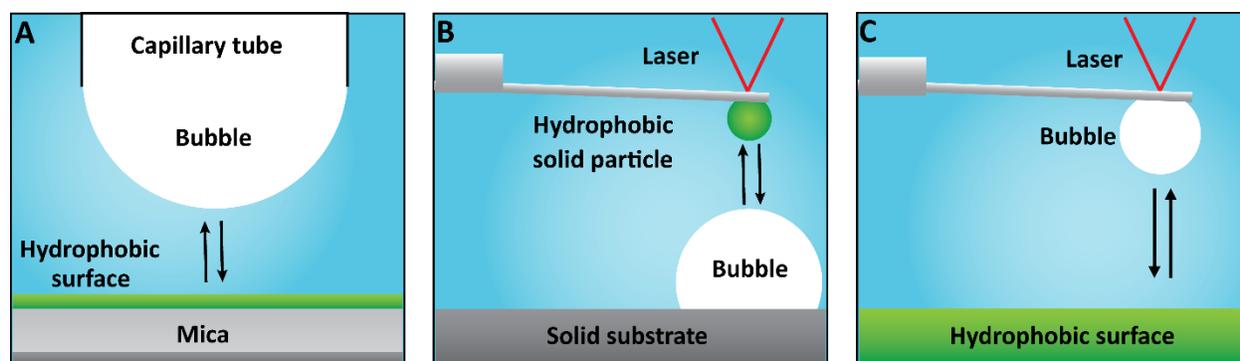
Figure 1.3. Schematic diagrams of force measurement involving deformable droplets (e.g., gas bubble) by using (A) a modified SFA incorporating a capillary tube, (B) colloidal probe AFM, and (C) bubble/droplet probe AFM, respectively.

1.2.1. Challenges in quantification of hydrophobic interaction.

Despite so many efforts dedicated to probing HB interaction over the last three decades, a profound understanding of HB interaction has not been achieved up to date. Due to the remarkable disagreement in the reported range and magnitude of HB interaction across the previous studies, no current theory can comprehensively interpret all the experimental results and elucidating the effects of the potential influencing parameters such as water chemistry and surface properties. One possible reason could be that several long-ranged (up to > 100 nm) attractions between two hydrophobic surfaces turn out to be some system-specific, indirectly hydrophobic, or even non-hydrophobic "artifacts", which can adversely affect the precise quantification of the short-ranged "intrinsic" HB interaction arsing from water structuring effect at the hydrophobic interfaces.

One major source of these long-ranged pseudo-hydrophobic interactions roots in the defective methodology to hydrophobize solid surfaces. For example, Langmuir-Blodgett (LB) deposition of cationic surfactant monolayers on mica has been frequently used to prepare

hydrophobic SAMs in early attempts to explore HB interaction via SFA. However, the observed long-ranged attractions in many of those cases have been proven to originate from electrostatics rather than hydrophobicity. By virtue of AFM imaging, it was found that the physisorbed monolayers, even though smooth and uniform in air, could be highly unstable and transform into a number of patchy bilayers distributed on the mica surface after being immersed in water, and this molecular rearrangement of the cationic surfactants can also result in the partial exposure of the mica substrate to the aqueous environment (Figure 1.4A.). Upon bring such two surfaces close, the electrostatic interaction between the positively charged bilayer domains and the negatively charged bare mica regions on the opposing surfaces gives rise to the observed long-ranged attraction.[23]

Besides, it has been reported that some long-ranged attractive artifacts can still exist despite the application of inherently hydrophobic or chemically hydrophobized solid surfaces. Most of these observed attractions are strongly associated with the presence of interfacial nanobubbles (INBs) on two opposing surfaces (Figure 1.4B), which complicates the quantification of the intrinsic HB interaction. INBs generally refer to the nanoscopic gaseous domains nucleated on some hydrophobic solid surfaces immersed in water, which can spontaneously form or be artificially generated through solvent exchanges processes. Interestingly, the existence of INBs were first speculated based on some stepwise-featured behaviors observed in the force curves between two hydrophobic solid surfaces, and then confirmed with the help of AFM imaging.[37-38] Thereafter, considerable research interest has been devoted to investigating the formation, morphology and stability of INBs, and the relevant influencing factors such as aqueous salinity and pH, ion specificity and degassing.[39] The critical role of INBs in the interaction between two

hydrophobic surfaces lies in that the coalescence of the INBs on the opposing surfaces results in a bridging capillary force driving the two surfaces suddenly jump into contact.[6, 40]
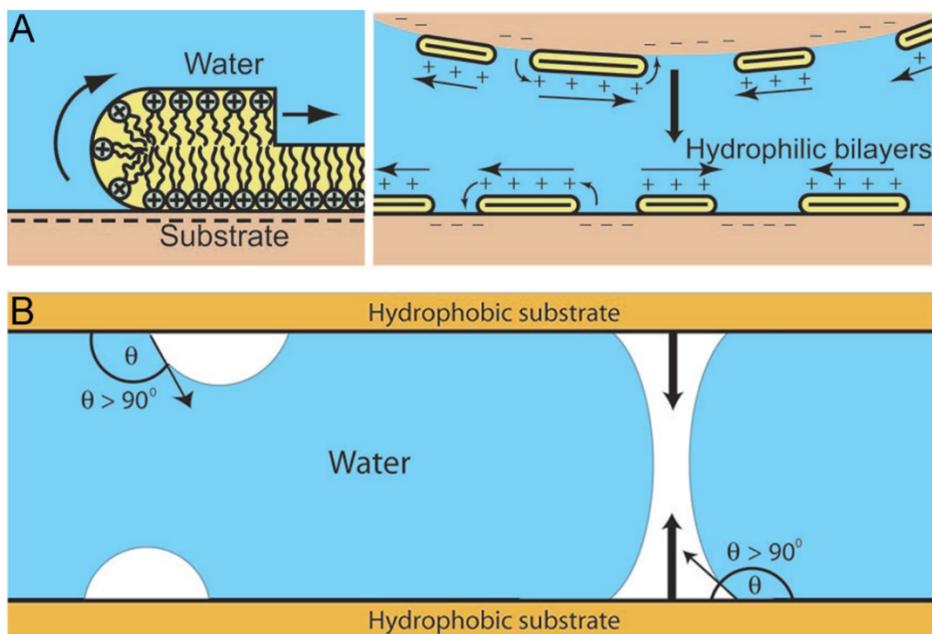
Figure 1.4. Schematic illustration of the mechanisms of long-ranged indirectly hydrophobic or non-hydrophobic artifacts. (A) Electrostatic interaction due to the molecular rearrangement of cationic surfactants. (B) Bridging capillary attraction due to the coalescence of interfacial nanobubbles on the apposing hydrophobic substrates.[40]

The negative influences from the long-ranged pseudo-HB interactions mentioned above could be effectively ruled out by improving the hydrophobization methods or optimizing the experimental conditions, such as decreasing surface roughness, lowering gas solubility, and altering water chemistry (e.g., salinity, ion type, and pH), which makes it possible to quantify the short-ranged intrinsic HB interaction. Nonetheless, there still exists a remarkable discrepancy in the range and magnitude of the intrinsic HB interactions across the relevant studies, which can be

attributed to the complexity caused by the interplay between the different water chemistry and the specific properties of the applied hydrophobic materials.

1.2.2. Theoretical models of hydrophobic interaction.

It has been commonly accepted that the intrinsic HB interaction energy decays exponentially with separation, as described in Equation 1.4,[18]

$$W_{HB}(h) = -C_0 \exp(-\frac{h}{D_0})$$
(1.4)

where C_0 is the pre-exponential factor related to the change in the interfacial free energy of the system, D_0 is the characteristic decay length and h denotes the separation between the two hydrophobic surfaces. However, the values of C_0 and D_0 are found to vary significantly in the previous reports, depending on the specificity of the applied hydrophobic systems. For instance, Donaldson *et al*. has proposed a "Hydra model" to quantify the HB interaction between two hydrophobic solid surfaces, as shown in Equation 1.5,[20]

$$W_{HB}(h) = -2\gamma H_y \exp(-\frac{h}{D_0})$$
(1.5)

where γ is the interfacial energy of the hydrophobic substrate with water, H_y is the defined non-dimensional Hydra parameter based on the surface hydrophobicity. Generally, H_y is > 0 for HB interactions between two partially hydrophobic surfaces, with ~ 1 corresponding to the maximum HB interactions between two fully hydrophobic surfaces. Applying $H_y \sim 1$, D_0 was determined to be ~ 1.7 nm for the HB interaction between two homogeneous and smooth hydrophobic substrates composed of chemically grafted polydimethylsiloxane (PDMS) with $\gamma \sim$ 44 mJ/m^2, while $\sim$ 1.0 nm between two stable surfactant SAMs of dioctadecyldimethylammonium bromide (DODAB) with $\gamma \sim 50$ mJ/m^2. Besides, Tabor *et al*.

innovatively measured the HB interaction between two oil droplets using droplet probe AFM technique. The VDW attraction was minimized by applying a specific mixture of perfluorooctane (PFO) and perfluorobezene (PFB) whose refractive index is equal to that of water, and the EDL repulsion was drastically suppressed by concentrating the salt solution and adjusting the aqueous pH to the isoelectric point of the oil droplets. The measured interaction force could be well interpreted by the model in Equation 1.6 describing the interaction energy of the oil/water/oil system,[41]

$$W_{HB}(h) = -2\gamma \exp(-\frac{h}{D_0}) \tag{1.6}$$

where γ is the oil/water interfacial energy, $\sim$ 50 mJ/m^2 in their work. According to the theoretically modeling result, D_0 was determined to be $\sim$ 0.3 nm, much smaller than that between two hydrophobic solid surfaces. Furthermore, the interactions between air bubbles and a variety of hydrophobic solid surfaces (e.g., hydrocarbon SAMs, minerals and polymers) have also been directly measured via bubble probe AFM technique, and the involved HB interactions can be precisely quantified using the model derived by Shi *et al*. from thermodynamic consideration by incorporating the Young-Duprè equation, as shown in Equation 1.7,[30, 42]

$$W_{HB}(h) = -\gamma_{AW}(1-\cos\theta_c)\exp(-\frac{h}{D_0}) \tag{1.7}$$

where γ_{AW} is the air/water interfacial energy ranging from 72 mJ/m^2 to 74 mJ/m^2, which depends on the applied aqueous salinity, and θ_c is the static WCA of the hydrophobic solid surface. For the asymmetric HB interactions between air bubbles and various hydrophobic solid surfaces, the values of D_0 were found to fall in a relatively wide range from 0.6 nm to 1.6 nm.

Despite the difference in the defining the pre-exponential factor C_0, these theoretical models mentioned above are not contradicted in fact. Instead, these three models are the modified

expressions of the exponentially decaying law of the HB interaction energy when it comes to the specific cases of symmetric solid-solid, droplet-droplet and asymmetric droplet-solid hydrophobic systems, respectively, and C_0 in each case is derived from the aspect of thermodynamics by calculating the change in the surface free energy during the corresponding interaction process. Figure 1.5 incorporates the curves of HB interaction energy of the solid-solid (PDMS-PDMS), droplet-droplet (perfluoro oil), and droplet-solid (bubble-hydrocarbon SAM) systems, showing that the range of HB interaction (denoted by the decay length D_0) varies significantly for different hydrophobic systems. This apparent discrepancy can be attributed to the difference in the inherent specificity of the applied hydrophobic materials.[6-7] As mentioned before, HB interaction is highly related to the reorientation and rearrangement of water molecules at hydrophobic interfaces. Such surface-induced water structuring effect can be subject to the variation in the intensity of the physical restriction imposed by the hydrophobic surfaces that orderly reorganize the interfacial water molecules. As a result, the extent of the water structuring effect could greatly differ at hydrophobic surfaces with distinctive properties, which is responsible for the notable difference in the range of the HB interactions. In general, a solid hydrophobic surface is thermodynamically immobilized, giving rise to a stronger physical restriction that rearranges the interfacial water molecules into a more ordered structure. As a result, the water structuring effect can extend over up to tens of water molecule layers, which is responsible for the relatively longer-ranged HB interaction. On the contrary, for the gas/water and oil/water interfaces which can reach thermodynamic equilibrium easily, the physical restriction is significantly relaxed. Therefore, the network of the interfacial water molecules appears to be more disordered, which reduces the extent of the water structuring effect down to even one or two layers of water molecules and significantly shortens the range of HB interaction.

However, despite so many previous studies on HB interaction, little information has been obtained on what kinds of experimental parameters or conditions can significantly impact the water structuring effects at different hydrophobic interfaces and modulate the range and magnitude of the intrinsic HB interaction, and further investigation needs to be done to probe the exact physical mechanism of the HB interaction.

$$W_{HB}(h) = -C_0 \exp(-\frac{h}{D_0})$$
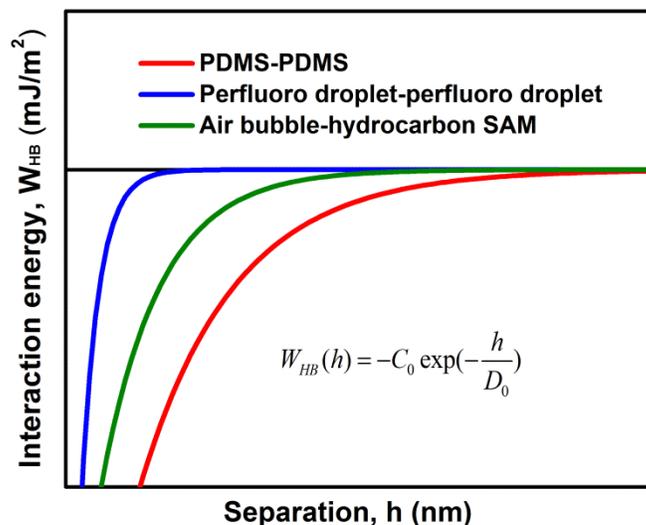
Figure 1.5. Hydrophobic interaction energy of the solid-solid (PDMS-PDMS), droplet-droplet (perfluoro oil), and bubble-solid (bubble-hydrocarbon SAM) systems.

1.3. Objectives.

A deep and comprehensive understanding of the surface interactions between deformable bubbles and hydrophobic solid surfaces in aqueous media is of great importance not only in explaining a variety of colloidal and interfacial phenomena, but also in providing theoretical guidance on the operation of relevant engineering processes and development of novel advanced materials. Despite many previous related studies, the knowledge in the mechanisms of such surface interactions, especially HB interaction, still remains incomplete, and intensive efforts are

required to be made. In this project, bubble probe AFM technique was applied to directly to measure the interactions between deformable bubbles and various hydrophobic solid surfaces under different aqueous conditions. The primary objectives of this thesis are to quantify involved the surface interactions, particularly HB interaction, through the theoretical model based on Reynolds lubrication theory and augmented Young-Laplace equation incorporating the effects of disjoining pressure, and to explicate the effects of various potential influencing factors, such as water chemistry (e.g., salinity, aqueous pH, and ion specificity) and inherent surface properties (e.g., hydrophobicity, chemical composition, and surface mobility). This work will shed novel light on the mechanisms of the surface interactions between deformable bubbles and hydrophobic solids. The specific objectives are as follows.

(1). Measure the interactions between air bubbles and mica substrates hydrophobized by octadecyltrichlorosilane (OTS) through silane chemistry in aqueous solutions with different salinity and pH, and quantify the involved surface interactions under the corresponding conditions, in order to investigate the effects of salinity and pH on the interactions between air bubbles and hydrophobic solid surfaces.

(2). Characterize the surface morphology of hydrophobic polymer surfaces such as polystyrene (PS) in aqueous solutions with different salinity and probe the effects of solution salinity on the morphology and distribution of INBs on the hydrophobic polymer surfaces. Measure the interactions between air bubbles and hydrophobic polymer surfaces in the corresponding conditions, aiming to clarify the effects of the presence of INBs on the bubble-polymer interactions under different aqueous conditions.

(3). Measure the interactions between air bubbles and various hydrophobic polymer surfaces in high salinity solutions with different electrolytes, and quantify the HB interaction in

each case, so as to probe the effect of ion specificity, particular to explore the impacts of the selective adsorption of specific ions onto the polymer surfaces due to cation-π or other interactions on the HB interactions.

(4). Measure the interactions of air bubbles with alkanethiol SAMs composed of hydrocarbon chains with different length and different tail moieties and slippery liquid-infused porous surfaces (SLIPSs) in high salinity solutions. By quantifying the involved HB interactions, the effects of surface mobility and chemistry on the range and magnitude of HB interactions are expected to be elucidated.

1.4. Structure of Thesis.

Chapter 1 introduces the interactions between deformable droplets and solid surfaces and the roles of surface interactions in the interaction processes, and particularly highlights the physical mechanism of hydrophobic interaction, methodology and challenges in measuring and quantifying hydrophobic interaction, and the current theoretical models for the force laws hydrophobic interactions in solid-solid, droplet-droplet and droplet-solid systems. Besides, the objectives of thesis are proposed as well.

Chapter 2 presents the experiment methods including the AFM force measurement via bubble probe AFM technique, theoretical model to analyze the measured interaction force, and preparation and characterization of hydrophobic solid surfaces.

Chapter 3 investigates the effects of solution salinity and aqueous pH on the surface interactions especially the HB interaction between air bubbles and mica substrates hydrophobized by OTS, and predicts the self-assembly behaviors of OTS-hydrophobized colloidal particles at the air/water interface from the aspect of surface interactions.

Chapter 4 demonstrates that the INBs could nucleate on hydrophobic PS surfaces and their morphology and distribution can be greatly affected by aqueous salinity, and illustrates that the presence of the INBs prevents the bubble from attaching onto the PS surfaces at a intermediate salinity ~ 100 mM where the EDL repulsion is highly suppressed and HB interaction should have triggered the bubble attachment, owing to a hydration force.

Chapter 5 probes the effects of ion specificity on the HB interactions between air bubbles and three different hydrophobic polymer surfaces, and demonstrates that the selective adsorption of specific ions onto particular polymers could obviously affect the water structuring effect at the hydrophobic interfaces and modulate the range of the HB interactions.

Chapter 6 studies the HB interactions of air bubbles with alkanethiol SAMs composed of different species and SLIPSs, and reveals that the range and magnitude of the HB interaction can be effectively modulated by altering the regularity, chemistry and state of the hydrophobic surfaces which determines the ordering degree of the water molecules in proximity to hydrophobic surfaces.

Chapter 7 presents the main conclusions and the original contributions of this thesis. The future work is also proposed.

1.5. References.

1.   Dickinson, E., Food Emulsions and Foams: Stabilization by Particles. *Curr. Opin. Colloid Interface Sci.* **2010**, *15*, 40-49.

2.   Park, J. I.; Jagadeesan, D.; Williams, R.; Oakden, W.; Chung, S.; Stanisz, G. J.; Kumacheva, E., Microbubbles Loaded with Nanoparticles: A Route to Multiple Imaging Modalities. *ACS Nano* **2010**, *4*, 6579-6586.

3.   Klibanov, A. L., Microbubble Contrast Agents: Targeted Ultrasound Imaging and Ultrasound-Assisted Drug-Delivery Applications. *Invest. Radiol.* **2006**, *41*, 354-362.

4.   Gao, W.; Pei, A.; Wang, J., Water-Driven Micromotors. *ACS Nano* **2012**, *6*, 8432-8438.

5.   Lou, X. W. D.; Archer, L. A.; Yang, Z., Hollow Micro-/Nanostructures: Synthesis and Applications. *Adv. Mater.* **2008**, *20*, 3987-4019.

6.   Zeng, H.; Shi, C.; Huang, J.; Li, L.; Liu, G.; Zhong, H., Recent Experimental Advances on Hydrophobic Interactions at Solid/Water and Fluid/Water Interfaces. *Biointerphases* **2016**, *11*, 018903.

7.   Xie, L.; Shi, C.; Cui, X.; Zeng, H., Surface Forces and Interaction Mechanisms of Emulsion Drops and Gas Bubbles in Complex Fluids. *Langmuir* **2017**, *33*, 3911-3925.

8.   Israelachvili, J. N., *Intermolecular and Surface Forces*; Academic press, 2011.

9.   Hogg, R.; Healy, T. W.; Fuerstenau, D., Mutual Coagulation of Colloidal Dispersions. *Trans. Faraday Soc.* **1966**, *62*, 1638-1651.

10.   Carnie, S. L.; Chan, D. Y.; Gunning, J. S., Electrical Double Layer Interaction between Dissimilar Spherical Colloidal Particles and between a Sphere and a Plate: The Linearized Poisson-Boltzmann Theory. *Langmuir* **1994**, *10*, 2993-3009.

11.   Ralston, J.; Fornasiero, D.; Hayes, R., Bubble–Particle Attachment and Detachment in Flotation. *Int. J. Miner. Process.* **1999**, *56*, 133-164.

12.   Gu, J.; Xiao, P.; Chen, J.; Zhang, J.; Huang, Y.; Chen, T., Janus Polymer/Carbon Nanotube Hybrid Membranes for Oil/Water Separation. *ACS Appl. Mater. Interfaces* **2014**, *6*, 16204-16209.

13.   Gonzenbach, U. T.; Studart, A. R.; Tervoort, E.; Gauckler, L. J., Ultrastable Particle-Stabilized Foams. *Angew. Chem. Int. Ed.* **2006**, *45*, 3526-3530.

14.   Yu, C.; Zhu, X.; Li, K.; Cao, M.; Jiang, L., Manipulating Bubbles in Aqueous Environment Via a Lubricant-Infused Slippery Surface. *Adv. Funct. Mater.* **2017**.

15.   Janson, J.-C., *Protein Purification: Principles, High Resolution Methods, and Applications*; John Wiley & Sons, 2012; Vol. 151.

16.   Chandler, D., Interfaces and the Driving Force of Hydrophobic Assembly. *Nature* **2005**, *437*, 640.

17.   Tabor, R. F.; Grieser, F.; Dagastine, R. R.; Chan, D. Y., The Hydrophobic Force: Measurements and Methods. *Phys. Chem. Chem. Phys.* **2014**, *16*, 18065-18075.

18.   Israelachvili, J.; Pashley, R., The Hydrophobic Interaction Is Long Range, Decaying Exponentially with Distance. *Nature* **1982**, *300*, 341-342.

19.   Faghihnejad, A.; Zeng, H., Hydrophobic Interactions between Polymer Surfaces: Using Polystyrene as a Model System. *Soft Matter* **2012**, *8*, 2746-2759.

20.   Donaldson Jr, S. H.; Røyne, A.; Kristiansen, K.; Rapp, M. V.; Das, S.; Gebbie, M. A.; Lee, D. W.; Stock, P.; Valtiner, M.; Israelachvili, J., Developing a General Interaction Potential for Hydrophobic and Hydrophilic Interactions. *Langmuir* **2014**, *31*, 2051-2064.

21.   Xie, L.; Wang, J.; Shi, C.; Cui, X.; Huang, J.; Zhang, H.; Liu, Q.; Liu, Q.; Zeng, H., Mapping the Nanoscale Heterogeneity of Surface Hydrophobicity on the Sphalerite Mineral. *J. Phys. Chem. C* **2017**, *121*, 5620-5628.

22.   Stock, P.; Utzig, T.; Valtiner, M., Direct and Quantitative Afm Measurements of the Concentration and Temperature Dependence of the Hydrophobic Force Law at Nanoscopic Contacts. *J. Colloid Interface Sci.* **2015**, *446*, 244-251.

23.   Meyer, E. E.; Lin, Q.; Hassenkam, T.; Oroudjev, E.; Israelachvili, J. N., Origin of the Long-Range Attraction between Surfactant-Coated Surfaces. *Proc. Natl. Acad. Sci. U.S.A.* **2005**, *102*, 6839-6842.

24.   Nguyen, A. V.; Nalaskowski, J.; Miller, J. D.; Butt, H.-J., Attraction between Hydrophobic Surfaces Studied by Atomic Force Microscopy. *Int. J. Miner. Process.* **2003**, *72*, 215-225.

25.   Ishida, N.; Sakamoto, M.; Miyahara, M.; Higashitani, K., Attraction between Hydrophobic Surfaces with and without Gas Phase. *Langmuir* **2000**, *16*, 5681-5687.

26.   Pushkarova, R. A.; Horn, R. G., Surface Forces Measured between an Air Bubble and a Solid Surface in Water. *Colloids Surf., A* **2005**, *261*, 147-152.

27.   Fielden, M. L.; Hayes, R. A.; Ralston, J., Surface and Capillary Forces Affecting Air Bubble− Particle Interactions in Aqueous Electrolyte. *Langmuir* **1996**, *12*, 3721-3727.

28.   Preuss, M.; Butt, H.-J., Direct Measurement of Particle− Bubble Interactions in Aqueous Electrolyte: Dependence on Surfactant. *Langmuir* **1998**, *14*, 3164-3174.

29.   Dagastine, R. R.; Manica, R.; Carnie, S. L.; Chan, D.; Stevens, G. W.; Grieser, F., Dynamic Forces between Two Deformable Oil Droplets in Water. *Science* **2006**, *313*, 210-213.

30.   Shi, C.; Cui, X.; Xie, L.; Liu, Q.; Chan, D. Y.; Israelachvili, J. N.; Zeng, H., Measuring Forces and Spatiotemporal Evolution of Thin Water Films between an Air Bubble and Solid Surfaces of Different Hydrophobicity. *ACS Nano* **2014**, *9*, 95-104.

31.   Tabor, R. F.; Manica, R.; Chan, D. Y.; Grieser, F.; Dagastine, R. R., Repulsive Van Der Waals Forces in Soft Matter: Why Bubbles Do Not Stick to Walls. *Phys. Rev. Lett.* **2011**, *106*, 064501.

32.   Cui, X.; Shi, C.; Xie, L.; Liu, J.; Zeng, H., Probing Interactions between Air Bubble and Hydrophobic Polymer Surface: Impact of Solution Salinity and Interfacial Nanobubbles. *Langmuir* **2016**, *32*, 11236-11244.

33.   Cui, X.; Shi, C.; Zhang, S.; Xie, L.; Liu, J.; Jiang, D.; Zeng, H., Probing the Effect of Salinity and Ph on Surface Interactions between Air Bubbles and Hydrophobic Solids: Implications for Colloidal Assembly at Air/Water Interfaces. *Chem. - Asian J.* **2017**, 12, 1568-1577.

34.   Chan, D. Y.; Klaseboer, E.; Manica, R., Film Drainage and Coalescence between Deformable Drops and Bubbles. *Soft Matter* **2011**, *7*, 2235-2264.

35.   Tabor, R. F.; Lockie, H.; Mair, D.; Manica, R.; Chan, D. Y.; Grieser, F.; Dagastine, R. R., Combined Afm− Confocal Microscopy of Oil Droplets: Absolute Separations and Forces in Nanofilms. *J. Phys. Chem. Lett.* **2011**, *2*, 961-965.

36.   Barrett. J.C. www.Barrett-Group.Mcgill.Ca. **2008**.

37.   Parker, J. L.; Claesson, P. M.; Attard, P., Bubbles, Cavities, and the Long-Ranged Attraction between Hydrophobic Surfaces. *J. Phys. Chem.* **1994**, *98*, 8468-8480.

38.   Yakubov, G. E.; Butt, H.-J.; Vinogradova, O. I., Interaction Forces between Hydrophobic Surfaces. Attractive Jump as an Indication of Formation of "Stable" Submicrocavities. *J. Phys. Chem. B* **2000**, *104*, 3407-3410.

39.   Lohse, D.; Zhang, X., Surface Nanobubbles and Nanodroplets. *Rev. Mod. Phys.* **2015**, *87*, 981.

40.   Meyer, E. E.; Rosenberg, K. J.; Israelachvili, J., Recent Progress in Understanding Hydrophobic Interactions. *Proc. Natl. Acad. Sci.* **2006**, *103*, 15739-15746.

41.   Tabor, R. F.; Wu, C.; Grieser, F.; Dagastine, R. R.; Chan, D. Y., Measurement of the Hydrophobic Force in a Soft Matter System. *J. Phys. Chem. Lett.* **2013**, *4*, 3872-3877.

42.   Shi, C.; Chan, D. Y.; Liu, Q.; Zeng, H., Probing the Hydrophobic Interaction between Air Bubbles and Partially Hydrophobic Surfaces Using Atomic Force Microscopy. *J. Phys. Chem. C* **2014**, *118*, 25000-25008.

Chapter 2   Experimental Methodology

2.1. Preparation and characterization of hydrophobic surfaces.

Three categories of hydrophobic surfaces were applied in this project: hydrocarbon SAMs prepared by hydrophobizing mica substrates using alkylsilane (e.g., OTS) and gold substrates using alkanethiols, hydrophobic polymer surfaces prepared by spin-coating and chemically grafting methods, and SLIPSs fabricated by wetting nano/microstructured materials using lubricants with low surface energy and viscosity. The detailed preparation procedures are listed below.

(1). The OTS-hydrophobized mica substrates were prepared through a vapor deposition process. To be specific, the freshly cleaved mica substrates were treated in UV/Ozone device or 15 min to generate a large number of surface hydroxyl groups which act as the reactive sites for the silane chemistry. Then, the mica substrates were placed in a vacuumed desiccator containing an open chamber filled with 50 μL for 48 h. Afterwards, the substrates were transferred into a vacuum oven and annealed at 80 ºC for 12 h. Finally, the substrates were washed with toluene to remove the unreacted OTS molecules, dried with nitrogen and kept under vacuum for further use. The alkanethiol SAMs on gold substrates were also applied as the sample surfaces for the AFM force measurements. Specifically, the gold substrates were prepared using a template-stripping method in which a layer of gold was deposited on a fresh mica using an electro-beam-equipped evaporation system and then the mica was peeled off with the gold facing the glue on another mica, leaving a molecularly smooth gold substrate. Then, the gold substrates were immersed in ethanol solutions containing 10 mM single-component or binary-component alkanethiol molecules with different tail groups or chain lengths. After being incubated for 24 h at room

temperature, the substrates were rinsed with ethanol, dried with nitrogen thoroughly and transferred into a vacuum environment and ready for further use.

(2). Three types of hydrophobic polymers with distinct pedant groups and inherent properties, i.e., polystyrene (PS), poly(methyl methacrylate) (PMMA), and polydimethylsiloxane (PDMS) were applied as the model materials to investigate their interactions with air bubbles under different aqueous conditions. The PS and PMMA surfaces were prepared by spin-coating 3-4 drops (~ 15 µL) of the toluene solutions containing the corresponding polymers on pre-cleaned silica wafers (1 cm × 1 cm) at a speed of 2000 rpm for 30 s. Then, the prepared PS and PMMA surfaces were placed in a vacuum oven at room temperature overnight to remove the residual solvent and ready for further use. The preparation of PDMS surface follows a click reaction procedure. At first, the silica wafer was treated by UV/Ozone plasma for 30 min and then modified by (3-aminopropyl) triethoxysilane (APTES) through a vapor deposition process under vacuum at room temperature for ~ 48 h, which was followed by annealing at 60 °C for ~ 12 h, rising with toluene and drying with nitrogen. Afterwards, the NH_2-silica substrates were immersed in a liquid of monoglycidyl ether-terminated PDMS and the reaction was conducted under vacuum at 80 °C for 12 h. Then, the PDMS-silica substrates were rinsed with toluene and dried with nitrogen thoroughly.

(3). The SLIPSs were prepared by infusing lubricating oils with low surface energy and viscosity (e.g., FC-70 and silicone oil) into polytetrafluoroethylene (PTFE) filter membrane (pore size ~ 0.2 µm). The PTFE membrane was immersed in the lubricant liquid and the lubricant can immediately spread throughout the whole porous texture. Then, the completely wetted membrane was taken out and treated by nitrogen flow and water flush to remove the excessive lubricants.

The thickness of the OTS monolayers on mica surfaces, alkanethiol SAMs on gold surfaces and hydrophobic polymer surfaces was characterized by ellipsometry, while the thickness of the lubricant over-layer of the SLIPSs was calculated based on the weight of the pristine and wetted membranes, the surface area and the thickness of the membrane and the density of the PTFE and the lubricants. The static WCA on the prepared hydrophobic surfaces were measured using a contact angle tensiometer. The topography of the hydrophobic solid surfaces was characterized by AFM tapping mode or PeakForce quantitative nano-mechanics (PF-QNM) imaging in specific aqueous environment. The surface composition of the alkanethiol SAMs was characterized using X-ray photoelectron spectroscopy (XPS). All the aqueous solutions were prepared by dissolving the corresponding electrolytes with Milli-Q water with a resistance of $\geq$ 18.2 MΩ cm.

2.2. Bubble probe AFM technique.

The AFM force measurements of the interactions between air bubbles and hydrophobic solid surfaces were conducted in a fluid cell filled with different aqueous solutions, based on an MFP-3D AFM incorporated with an inverted optical microscope. The experimental setup of the bubble probe AFM technique is illustrated in Figure 2.1. A customized tipless rectangular silicone cantilever (400 × 70 × 2 μm) with a circular gold patch (~ 65 μm in diameter, ~30 nm in thickness) at its front end was applied. The spring constant of the tipless cantilever was determined to be ~ 0.3-0.4 nN/nm using Hutter and Bechhoefer method.[1] Prior to the AFM force measurement, the bottom glass slide of the fluid cell (~ 70 mm in diameter) has been mildly hydrophobized through silane chemistry by immersing it in a toluene of OTS for ~10 seconds and the resultant static WCA reached ~ 30°-40°, which is favorable for capturing the air bubbles

generated through a custom-made ultrasharp glass pipet.[2-3] Besides, the gold patch of the tipless cantilever has been hydrophobized by placing the cantilever in an ethanol solution containing 10 mM dodecanethiol overnight, aiming to make it easier to pick up the bubble and facilitate the bubble immobilization.[4-6] At first, the tipless cantilever was slowly lowered down to make it contact with an applicable bubble (radius ~ 50-100 μm). Then the cantilever was lifted carefully to detach the bubble from the glass slide and then moved above the hydrophobic solid surface which has been previously placed in the fluid cell. Afterwards, the bubble probe was manipulated to approach and retract from the sample surface at a specific nominal velocity, and the deflection of the cantilever and the interaction force were recorded by the AFM software and ready for the theoretical analysis.[3, 7-11]
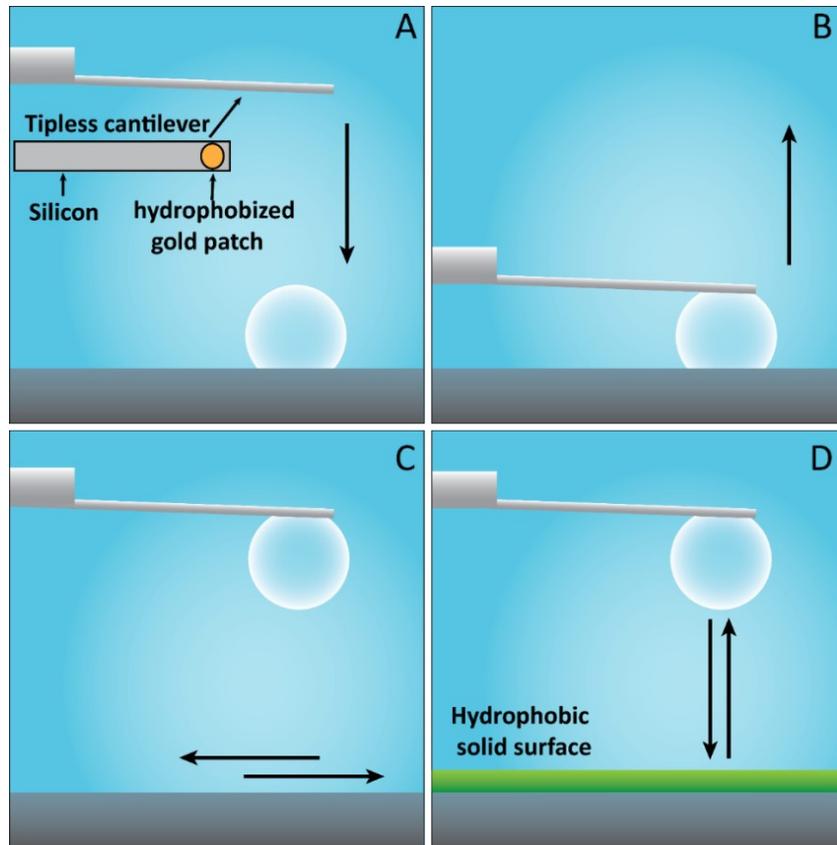
Figure 2.1. Schematic illustration of the experimental setup of the bubble probe AFM technique. (A). Lower the AFM tipless cantilever slowly to make it contact with an applicable air bubble (radius ~ 50-100 μm) on the glass slide of the fluid cell. (B). Lift the cantilever carefully to detach the bubble from the glass slide. (C). Move the cantilever horizontally above the hydrophobic solid surface previously placed in the fluid cell. (D). Drive the AFM bubble probe to approach and retract from the hydrophobic solid surface at a nominal velocity.

2.3. Theoretical model.

Figures 2.2A and 2.2B illustrate a typical image of the AFM bubble probe captured by the equipped top-view camera and the geometrical condition of the bubble-substrate interaction process.
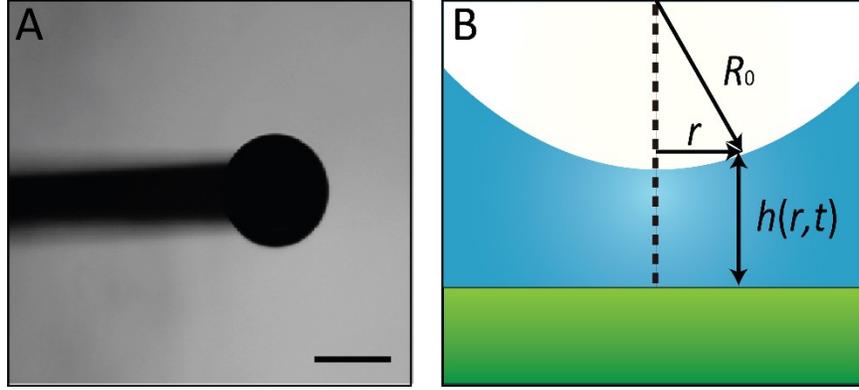
Figure 2.2. (A). A typical image of the AFM bubble probe (radius ~ 70 μm) of the bubble probe AFM technique in which the scale bar is 100 μm. (B). Geometrical condition of the bubble-substrate interaction process.

A theoretical model based on Reynolds lubrication and augmented Young-Laplace equation incorporating the effect of disjoining pressure, the Stokes-Reynolds-Young-Laplace model, was applied to analyze the interaction forces between air bubbles and hydrophobic solid surfaces measured by AFM.[3, 9, 12-13] Assuming the tangentially immobile boundary condition imposed at the air/water and solid/water interfaces, the drainage process of the thin water film confined by the bubble and the substrate can be described by Reynolds lubrication theory as shown in Equation 2.1,[9, 14-15]

$$\frac{\partial h(r,t)}{\partial t} = \frac{1}{12\mu r}\frac{\partial}{\partial r}\left(rh^3\frac{\partial p(r,t)}{\partial r}\right) \tag{3.1}$$

where r is the radial coordinate, $h(r,t)$ is the local thickness of the confined thin water film, μ is the viscosity of water and $p(r,t)$ is the excessive hydrodynamic pressure relative to the bulk solution.

The deformation of the bubble probe in response to external force can be calculated by the augmented Young-Laplace equation (Equation 3.2),[13]

$$\frac{\gamma}{r}\frac{\partial}{\partial r}\left(r\frac{\partial h(r,t)}{\partial r}\right)=\frac{2\gamma}{R_0}-p(r,\text{t})-\Pi\left[h(r,t)\right] \tag{3.2}$$

where γ is the air/water interfacial tension, R_0 is the bubble radius and $\Pi[(h(r,t)]$ is the disjoining pressure due to surface interactions, including VDW, EDL and HB interactions which can be quantified using Equations 3.3, 3.4 and 3.5, respectively, the derivatives of the surface interaction energies per unit area (Equations 1.1, 1.3 and 1.7) with respective to distance.[3, 8, 16-17]

$$\Pi_{VDW}[h(r,t)]=-\frac{A_H}{6\pi h^3(r,t)} \tag{3.3}$$

$$\Pi_{EDL}[h(r,t)]=\frac{2\varepsilon_0\varepsilon\kappa^2\left[\left(e^{+\kappa h(r,t)}+e^{-\kappa h(r,t)}\right)\psi_1\psi_2-\left(\psi_1^2+\psi_2^2\right)\right]}{\left(e^{+\kappa h(r,t)}-e^{-\kappa h(r,t)}\right)^2} \tag{3.4}$$

$$\Pi_{HB}[h(r,t)]=-\frac{\gamma(1-\cos\theta_c)}{D_0}\exp\left(-\frac{h(r,t)}{D_0}\right) \tag{3.5}$$

According to the spherical geometry of the bubble probe, the initial film thickness can be expressed as Equation 3.6.[9, 13]

$$h(r,t_0)=h(0,t_0)+\frac{r^2}{2R_0} \tag{3.6}$$

Due to axial symmetry of the bubble, $\partial h(r,t)/\partial r=0$ and $\partial p(r,t)/\partial r=0$ at r=0, and $r(\partial p/\partial r)+4p=0$ at $r=r_{max}$ because $p(r,t)$ decays with an inverse four power of r as $r\rightarrow\infty$. By incorporating the cantilever velocity V and assuming the bubble volume is constant during the interaction process, the boundary condition regarding the movement and deformation of the bubble probe is illustrated in Equation 3.7,

$$\frac{\partial h(r_{max}, t)}{\partial t} = V - \frac{1}{2\pi\gamma}\frac{dF(t)}{dt}\left\{\log\left(\frac{r_{max}}{2R_0}\right) + B(\theta) - \frac{2\pi\gamma}{K}\right\}$$

$$B(\theta) = 1 + \frac{1}{2}\log\left(\frac{1+\cos\theta}{1-\cos\theta}\right)$$

(3.7)

where r_{max} is radius of the region where most contribution to the interaction force is included, V is the interaction velocity, K is the spring constant of the tipless cantilever, and $B(\theta)$ is a function of the bubble's contact angle on the cantilever θ that can be calculated using equation $\sin(180-\theta) = r_{gold}/R_0$ in which r_{gold} is the known radius of the hydrophobized circular gold patch at the front end of cantilever.[9, 13]

The overall interaction force $F(t)$ can be calculated by integrating the sum of hydrodynamic pressure and disjoining pressure via Derjaguin approximation shown in Equation 3.8.

$$F(t) = 2\pi\int_0^\infty \left\{p(r,t) + \Pi\left[h(r,t)\right]\right\}r\,dr$$

(3.8)

The equations mentioned above are rescaled with $h_c = R_0 C_a^{1/2}$, $r_c = R_0 C_a^{1/4}$, $P_c = \gamma/R_0$ and $t_c = \mu C_a^{-1/2}/P_c$, where $C_a = \mu V/\gamma$ is the capillary number, and then solved numerically using MATLAB software.

2.4. References.

1.   Hutter, J. L.; Bechhoefer, J., Calibration of Atomic-Force Microscope Tips. *Rev. Sci. Instrum.* **1993**, *64*, 1868-1873.

2.   Shi, C.; Chan, D. Y.; Liu, Q.; Zeng, H., Probing the Hydrophobic Interaction between Air Bubbles and Partially Hydrophobic Surfaces Using Atomic Force Microscopy. *J. Phys. Chem. C* **2014**, *118*, 25000-25008.

3.   Shi, C.; Cui, X.; Xie, L.; Liu, Q.; Chan, D. Y.; Israelachvili, J. N.; Zeng, H., Measuring Forces and Spatiotemporal Evolution of Thin Water Films between an Air Bubble and Solid Surfaces of Different Hydrophobicity. *ACS Nano* **2014**, *9*, 95-104.

4.   Xue, Y.; Li, X.; Li, H.; Zhang, W., Quantifying Thiol-Gold Interactions Towards the Efficient Strength Control. *Nat. Commun.* **2014**, *5*, 4348.

5.   Tabor, R. F.; Manica, R.; Chan, D. Y.; Grieser, F.; Dagastine, R. R., Repulsive Van Der Waals Forces in Soft Matter: Why Bubbles Do Not Stick to Walls. *Phys. Rev. Lett.* **2011**, *106*, 064501.

6.   Vakarelski, I. U.; Manica, R.; Tang, X.; O'Shea, S. J.; Stevens, G. W.; Grieser, F.; Dagastine, R. R.; Chan, D. Y., Dynamic Interactions between Microbubbles in Water. *Proc. Natl. Acad. Sci.* **2010**, *107*, 11177-11182.

7.   Cui, X.; Shi, C.; Xie, L.; Liu, J.; Zeng, H., Probing Interactions between Air Bubble and Hydrophobic Polymer Surface: Impact of Solution Salinity and Interfacial Nanobubbles. *Langmuir* **2016**, *32*, 11236-11244.

8.   Cui, X.; Shi, C.; Zhang, S.; Xie, L.; Liu, J.; Jiang, D.; Zeng, H., Probing the Effect of Salinity and Ph on Surface Interactions between Air Bubbles and Hydrophobic Solids: Implications for Colloidal Assembly at Air/Water Interfaces. *Chem. - Asian J.* **2017**, 12, 1568-1577.

9.   Xie, L.; Shi, C.; Cui, X.; Zeng, H., Surface Forces and Interaction Mechanisms of Emulsion Drops and Gas Bubbles in Complex Fluids. *Langmuir* **2017**, *33*, 3911-3925.

10.   Xie, L.; Shi, C.; Wang, J.; Huang, J.; Lu, Q.; Liu, Q.; Zeng, H., Probing the Interaction between Air Bubble and Sphalerite Mineral Surface Using Atomic Force Microscope. *Langmuir* **2015**, *31*, 2438-2446.

11.   Tabor, R. F.; Chan, D. Y.; Grieser, F.; Dagastine, R. R., Anomalous Stability of Carbon Dioxide in Ph-Controlled Bubble Coalescence. *Angew. Chem. Int. Ed.* **2011**, *50*, 3454-3456.

12.   Hendrix, M. H.; Manica, R.; Klaseboer, E.; Chan, D. Y.; Ohl, C.-D., Spatiotemporal Evolution of Thin Liquid Films During Impact of Water Bubbles on Glass on a Micrometer to Nanometer Scale. *Phys. Rev. Lett.* **2012**, *108*, 247803.

13.   Chan, D. Y.; Klaseboer, E.; Manica, R., Film Drainage and Coalescence between Deformable Drops and Bubbles. *Soft Matter* **2011**, *7*, 2235-2264.

14.   Manor, O.; Vakarelski, I. U.; Stevens, G. W.; Grieser, F.; Dagastine, R. R.; Chan, D. Y., Dynamic Forces between Bubbles and Surfaces and Hydrodynamic Boundary Conditions. *Langmuir* **2008**, *24*, 11533-11543.

15.   Manica, R.; Chan, D. Y., Drainage of the Air–Water–Quartz Film: Experiments and Theory. *Phys. Chem. Chem. Phys.* **2011**, *13*, 1434-1439.

16.   Israelachvili, J. N., *Intermolecular and Surface Forces*; Academic press, 2011.

17.   Hogg, R.; Healy, T. W.; Fuerstenau, D., Mutual Coagulation of Colloidal Dispersions. *Trans. Faraday Soc.* **1966**, *62*, 1638-1651.

Chapter 3   Probing Effect of Salinity and pH on Surface Interactions between Air Bubbles and Hydrophobic Solids: Implications on Colloidal Assembly at Air/Water Interface

3.1. Introduction.

As a ubiquitous and essential component, gas bubbles play a crucial role in a variety of engineering and technological applications such as air flotation,[1] microfluidic devices,[2-3] to and food production.[4] Over the last two decades, micro/nanoparticle-loaded bubbles have received much research attention due to their great potential in fabrication of advanced materials and structures for a wide range of applications, such as bimodal contrast agents for ultrasound imaging and drug delivery,[5-6] stimuli-responsive aqueous foams,[7] thermal and acoustic light-weight insulators,[8] hollow spheres with enhanced performance in catalysis,[9-11] sensing[12-13] and lithium batteries.[14] In most of these applications, achieving the targeted properties and functionalities is extensively determined by the assembly and aggregation of hydrophobic colloidal particles at gas/water interface which can be modulated by their surface interactions such as van der Waals (VDW), electrical double-layer (EDL) and hydrophobic (HB) interactions.[15-16] Generally, the VDW interaction between gas bubble and solid particle in aqueous medium is repulsive according to the Lifshitz theory, and the EDL interactions can be repulsive or attractive depending on surface charges and aqueous solution condition.[17-18] HB interaction is one of the most important nonspecific interactions in many engineering and biological systems, which is generally beilieved to originate from the rearrangement of vicinal water molecules as two hydrophobic species come close to each other.[19-21] HB interaction plays a

critical role in the stable particle-bubble attachment and immobilization.[22-23] A systematic and quantitative understanding of the surface interaction mechanism between gas bubbles and hydrophobic particles is of both fundamental and practical importance, allowing the precise prediction of assembly behaviors of solid particles onto surfaces of gas bubbles and cost-effective preparation of novel functional materials for related practical applications.

The early attempts to experimentally quantify the surface interactions between gas bubbles and colloidal particles were conducted mainly using atomic force microscope (AFM) colloidal probe technique, in which a micrometer-sized solid sphere was glued on a tipless cantilever and driven to interact with a sessile bubble immobilized on a substrate. The results identified the important roles of the involved surface interactions (e.g. VDW, EDL and HB interactions) in particle attachment onto bubble surface. However, the interpretation of bubble deformation, and precise correlation between the interaction forces and surface separation still remained challenging.[24-27] The more recently developed bubble probe AFM technique was capable of directly measuring the interaction forces between a gas bubble and a variety of solid surfaces (or two bubbles) and precisely quantifying the contribution from different surface interactions to the overall disjoining pressure.[28-35] A theoretical model based on Reynolds lubrication theory and augmented Young-Laplace equation could successfully interpretate the measured force results. The validity of this technique has been demonstrated using AFM coupled with refraction interference contrast microscope (RICM).[31] The bubble/drop probe AFM-RICM technique allows the synchronous measurements of interaction forces and visualization of the spatiotemporal evolution of the confined thin liquid film at the nanoscale between bubbles/drops, colloids and solid substrates.[31, 34]

In this work, a facile methodology based on the bubble probe AFM technique and theoretical calculations has been applied to quantitatively study the interactions between gas bubbles and hydrophobic solid particles. The principal parameters of the surface interactions involved in the bubble-particle interaction, such as surface potentials and decay length of HB interaction under different aqueous conditions (e.g., salinity and pH), were obtained by theoretical analysis of the measured interaction forces between bubbles and flat substrates (with same surface chemistry as solid particles) using a theoretical model based on Reynolds lubrication theory and augmented Young-Laplace equation by including the effect of disjoining pressure.[36-39] These parameters, in turn, were applied to predict the bubble-particle interaction behaviors and the critical forces required for the particle-bubble attachment under various aqueous conditions. Here, air bubble and mica substrate hydrophobized with octadecyltrichlorosilane (OTS) were applied as the model bubble-hydrophobic solid system. The results in this work have improved the fundamental understanding of interactions between bubbles and solid particles under different solution conditions, and provided useful implications for the assembly mechanism of solid particles at gas/water interface in a wide range of engineering processes. This methodology can be readily extended to the interactions of diverse solid particles, bubbles or oil droplets in aqueous media.

3.2. Experimental section.

3.2.1. Materials.

Octadecyltrichlorosilane (OTS, 95%), sodium chloride (NaCl, Crystalline/Certified ACS), sodium hydroxide (NaOH, Pellets/Certified ACS), hydrochloric acid (HCl, TraceMetal[TM] grade), cyclohexane (HPLC grade) and ethanol (HPLC grade) were purchased from Fisher Scientific,

Canada. 1-decanethiol (96%) and silica particles (1-5 μm in diameter) were purchased from Sigma-Aldrich, Canada. All the chemicals were used as received without any further purification.

3.2.2. Preparation of OTS-hydrophbized solid substrate.

A freshly cleaved mica substrate (1×1 cm^2) was hydrophobized by OTS through a vapor deposition process under vacuum for 48 hours at room temperature. After being annealed at 80 ^{o}C under vacuum for 12 hours, the substrate washed with cyclohexane, dried with N$_2$ and kept in a vacuum desiccator for further use.[31] The morphology of the prepared OTS-mica substrate was characterized by AFM tapping mode imaging and the static water contact angle was measured to be 90° (Figure 3.1).
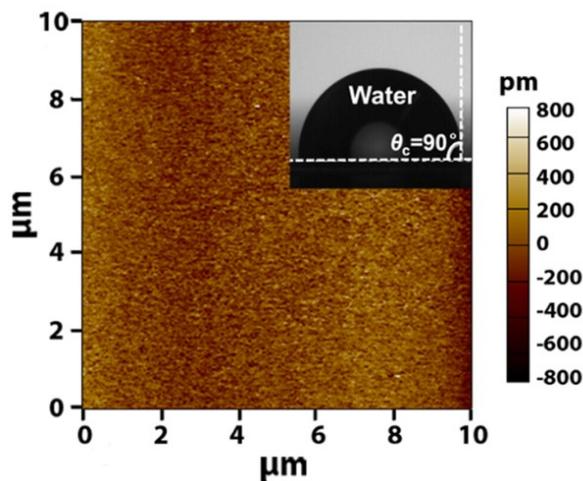
Figure 3.1. Topographic image of the prepared OTS-mica substrate characterized by AFM in tappling mode. The root-mean-square (RMS) is ~ 0.2 nm and static water contact angle is ~ 90°.

3.2.3. Preparation of OTS-hydrophobized silica particles

OTS-hydrophobized colloidal particles were prepared through a silanation process in cyclohexane containing 5 mM OTS.[40-41] 0.2 g silica particles (1-5 μm in diameter) were pre-

cleaned through UV/Ozone treatment and then dispersed in the solution for 20 mins under

magnetic stirring. The suspension was then centrifuged at a speed of 400 rpm. The obtained

particles were washed by cyclohexane for 3 to 4 times and then dried under vacuum at 80°C

overnight. The contact angle of the OTS-hydrophobized colloidal particles was ~90°.[42-43]

3.2.4. Force measurements using bubble probe AFM.

An MPF-3D AFM system (Asylum Research, Santa Barbara, CA) was applied to measure

the interaction between two air bubbles and between an air bubble and a hydrophobic OTS-mica

substrate under various aqueous conditions, and the experimental setup of the AFM force

measurement is illustrated in Figure 3.2. The AFM cantilever applied in this work was a

customized rectangular silicon cantilever (400 × 70 × 2 μm) with a circular gold patch (diameter

~ 65 μm) which had been previously hydrophobized in 10 mM 1-decanethiol in ethanol

overnight to make it energetically favorable to immobilize air bubble.[31] The cantilever's spring

constant was obtained using Hutter and Bechhoefer method,[44] ranging from 0.3 to 0.4 nN/nm.

Air bubbles were generated on the glass slide of the AFM fluid cell filled with aqueous solution

by carefully injecting air through an ultra-sharp glass pipet. Then, the hydrophobized tipless

cantilever was lowered down slowly to anchor an air bubble with radiius 50-100 μm, and then

elevated carefully to detach the bubble from the glass slide. Afterwards, the bubble probe was

driven to approach and retract from a sessile air bubble with similar size or an OTS-mica

substrate at a nominal velocity. The cantilever displacement and interaction force were measured

and recorded by the AFM software.
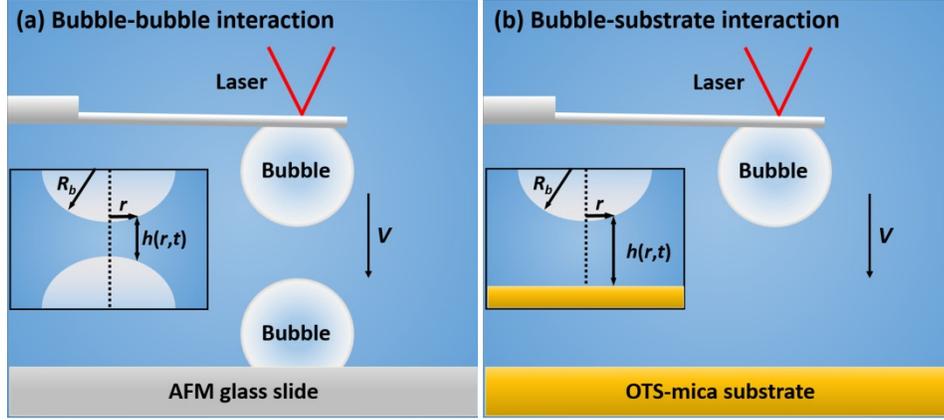
Figure 3.2. Experimental setup for measuring the interaction forces (a) between two bubbles and (b) between an air bubble and an OTS-mica substrate by using the bubble probe AFM technique. The insets illustrate the geometric parameters in the corresponding interaction processes.

3.2.5 Theoretical model for analyzing the measured interaction force.

The theoretical model applied to analyze the measured interaction force is based on Reynolds lubrication theory and augmented Young-Laplace equation taking the effect of disjoining pressure into consideration.[45-47] The drainage behavior of the thin water film is described by the Reynolds lubrication theory (equation 3.1), assuming tangentially immobile hydrodynamic boundary condition at air/water and solid/water interfaces,[36, 48-49]

$$\frac{\partial h(r,t)}{\partial t} = \frac{1}{12\mu r}\frac{\partial}{\partial r}\left(rh^3\frac{\partial p(r,t)}{\partial r}\right) \tag{3.1}$$

where $h(r,t)$ is the thickness of the thin water film, μ is the viscosity of water and $p(r,t)$ is the excessive hydrodynamic pressure relative to the bulk solution.

The deformation of air bubble is described by the augmented Young-Laplace equation in three forms corresponding to bubble-bubble, bubble-substrate, and bubble-particle interactions,

respectively, as shown in equation 3.2,[30, 49] where γ is the air-water interfacial tension, R_b and R_p are the radii of air bubble and solid particle respectively, and $\Pi[(h(r,t)]$ is the overall disjoining pressure originating from various surface interactions, including VDW, EDL and HB interactions.

$$\frac{1}{2}\frac{\gamma}{r}\frac{\partial}{\partial r}\left(r\frac{\partial h(r,t)}{\partial r}\right)=\frac{2\gamma}{R_b}-p(r,\mathrm{t})-\Pi\left[h(r,t)\right]\text{(bubble-bubble)}$$

$$\frac{\gamma}{r}\frac{\partial}{\partial r}\left(r\frac{\partial h(r,t)}{\partial r}\right)=\frac{2\gamma}{R_b}-p(r,\mathrm{t})-\Pi\left[h(r,t)\right]\text{(bubble-susbtrate)}$$

$$\frac{\gamma}{r}\frac{\partial}{\partial r}\left(r\frac{\partial h(r,t)}{\partial r}\right)=\frac{2\gamma}{R_{bp}}-p(r,\mathrm{t})-\Pi\left[h(r,t)\right]\text{(bubble-particle)} \qquad (3.2)$$

$$\overline{R}_b\equiv\frac{1}{2}(1/R_{b1}+1/R_{b2})^{-1},\quad \overline{R}_{bp}\equiv(1/R_b+1/R_p)^{-1}$$

Equation 3.3 is applied to calculate the contribution from VDW interaction to the overall disjoining pressure based on the Lifshitz theory. For air/water/air system A_H is positive indicating attractive VDW interaction. In contrast, A_H for bubble-solid interaction is calculated to be negative which leads to repulsive VDW interaction.[17, 31]

$$\Pi_{VDW}[h(r,t)]=-\frac{A_H}{6\pi h^3(r,t)} \qquad (3.3)$$

The EDL interaction between two air bubbles can be calculated by equation 3.4, where κ^{-1} denotes Debye length, Ψ_{Bub} is the surface potential of air bubble, ρ_∞ is the number density of ion in bulk solution, z is the valency of the ion, $\varepsilon_0\varepsilon$ is the dielectric permittivity of the aqueous medium.[17] For asymmetric bubble-substrate and bubble-particle systems, "Hogg-Healy-Fuerstenau" equation is given in equation 3.5 to model the EDL interaction between air bubble and OTS surface, where Ψ_{OTS} is the surface potential of OTS.[50-51]

$$\Pi_{EDL}[h(r,t)] = 64 k_B T \rho_\infty \tanh^2 (\frac{ze\psi_{Bub}}{4k_B T}) \exp[-\kappa h(r,t)]$$

(3.4)

$$\kappa^{-1} = \left(\sum_i \rho_{\infty i} e^2 z_i^2 / \varepsilon_0 \varepsilon kT \right)^{-\frac{1}{2}}$$

$$\Pi_{EDL}[h(r,t)] = \frac{2\varepsilon_0 \varepsilon \kappa^2 \left[\left(e^{+\kappa h(r,t)} + e^{-\kappa h(r,t)} \right) \psi_{Bub} \psi_{OTS} - \left(\psi_{Bub}^2 + \psi_{OTS}^2 \right) \right]}{\left(e^{+\kappa h(r,t)} - e^{-\kappa h(r,t)} \right)^2}$$

(3.5)

The HB interaction between air bubble and OTS-mica substrate was reported to follow an exponential relation, as described in equation 3.6, where D_0 is the decay length of HB interaction, γ_{AW} is the air/water interfacial tension, and θ_c is static the water contact angle on the OTS-mica substrate.[31, 33, 52-53]

$$\Pi_{HB}[h(r,t)] = -\frac{C_0}{D_0} \exp\left(-\frac{h(r,t)}{D_0} \right) = -\frac{\gamma_{AW}(1-\cos\theta_c)}{D_0} \exp\left(-\frac{h(r,t)}{D_0} \right)$$

(3.6)

The overall force $F(t)$ experienced by the AFM cantilever is calculated by equation 3.7 as the integration of the sum of hydrodynamic pressure and disjoining pressure based on Derjaguin approximation.[37, 49, 54]

$$F(t) = 2\pi \int_0^\infty \left\{ p(r,t) + \Pi\left[h(r,t) \right] \right\} r dr$$

(7)

3.2.6. Surface tension measurement.

The dynamic surface tension of the NaCl aqueous solution containing OTS-hydrophobized colloidal particles (0.5 g/L) was measured by Contact Angle Tensiometer (Ramé-hart Instrument Company, USA) through pendent drop shape method. The sample was loaded into the glass syringe which was connected with a straight stainless steel needle. The testing program was triggered immediately when the aqueous droplet was generated at the end of the straight needle

hanging in air. The light resource provided light through the droplet so that the camera was able to capture the drop profiles and then to fit the dynamic surface tension with time.

3.3. Results and discussion.

Figure 3.3a shows the bubble-bubble interaction at the velocity of 1 μm/s in 1 mM NaCl with natural pH ~ 5.6. A strong repulsion was observed and increased gradually as the two bubbles approached each other, and afterwards the repulsion decreased during the retraction of the bubble probe and a tiny attraction was measured due to the hydrodynamic suction effect.[31, 37-38] No jump-in behavior occurred in the interaction force curve, indicating the thin water film confined between the two bubbles prevented the bubble coalescence. In this case, the VDW interaction between two air bubbles kept attractive at any separation (A_H ~ 3.73 × 10^{-20} J) which was favorable for bubble coalescence.[17] Given that the air/water interface was negatively charged at pH ~ 5.6 and the Debye length κ^{-1} was calculated to be 9.6 nm in 1 mM NaCl, it was the strong EDL repulsion that overcame the VDW attraction, resulting in a repulsive disjoining pressure that sustained the confined thin water film. The measured interaction forces (open symbols) agreed well with the theoretical fitting results (red curve) with the surface potential of air bubble Ψ_{Bub} ~ -33 ± 4 mV, which was consistent with the previously reported value.[48-49] The disjoining pressures arising from the involved surface interactions (e.g., VDW and EDL interactions) are shown in Figure 3.3b, which clearly demonstrates the dominant role of EDL repulsion in the bubble-bubble interaction in 1 mM NaCl at pH ~ 5.6. The thin water film was stabilized at a critical separation of 17.8 nm where the repulsive overall disjoining pressure $\prod_{Overall}$ balanced the Laplace pressure $\Delta P_{Laplace}$ inside the bubble (note here the hydrodynamc pressure was negligible at 1 μm/s). The evolution of the bubble profile during the interaction was

also calculated based on the theoretical model and shown in Figure 3.3c, which clearly shows that the opposing interaction regions of the bubbles were notably flattened and the thin water film was sustained due to the repulsive overall disjoining pressure.
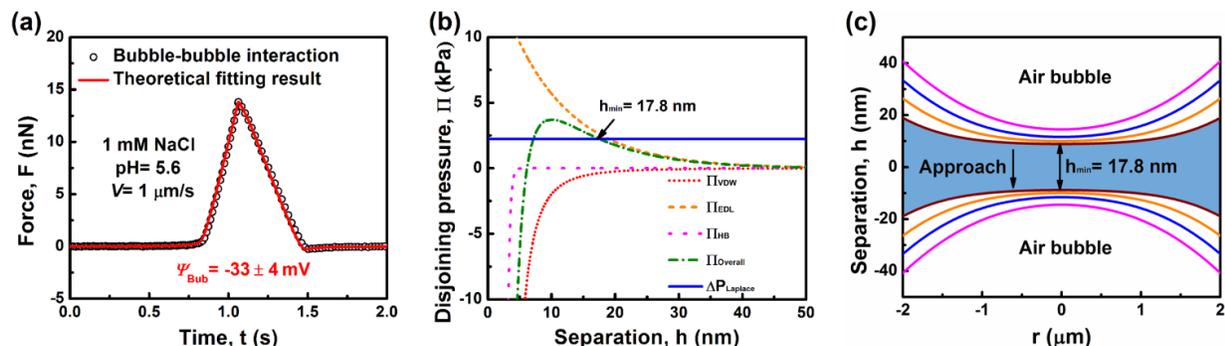
Figure 3.3. Interaction between two air bubbles (radius ~ 65 μm) at an interaction velocity 1 μm/s in 1 mM NaCl of pH ~ 5.6. (a) Measured interaction force (open symbols) and theoretical fitting results (solid curve). (b) Disjoining pressure profiles of the involved surface interactions. (c) Evolution of the calculated bubble profiles during approaching process and the brown curve denotes the bubble profile at the minimal separation.

It has been reported that the air/water interface is negatively charged due to the preferential adsorption of hydroxide ions, and therefore the surface potential of air bubble in water is sensitive to the variation of aqueous pH.[55-56] Employing the above method, the bubble-bubble interactions in 1 mM NaCl of different pH (i.e., 3.0, 8.0 and 10.0) were measured and analyzed through the theoretical model (Figure 3.4). The interactions exhibit similar force curves to that in the case of pH ~ 5.6, with no jump-in behavior observed and no bubble coalescence occured during the interaction processes. The surface potentials of air bubbles under the these aqueous solution conditions were determined and listed in Table 3.1, which coincide with the measured

44

zeta potentials in previous studies, indicating that the air bubbles become more negatively charged with increasing solution pH.[57-58]
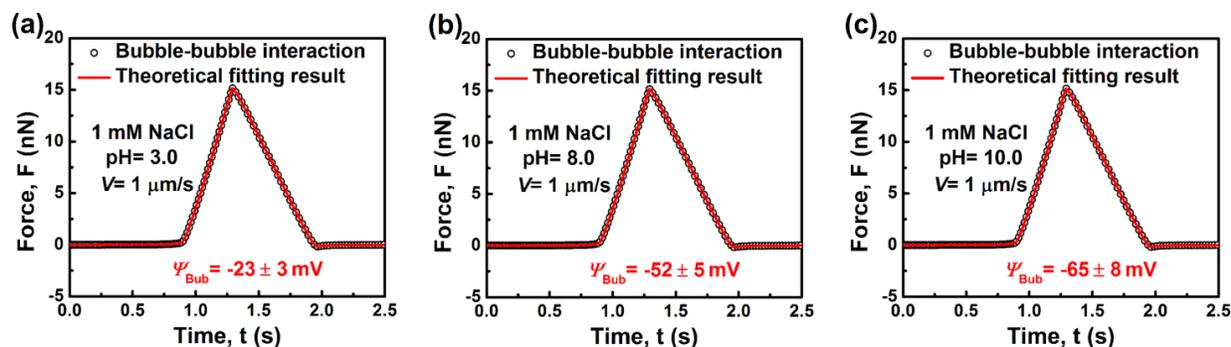
Figure 3.4. Interaction force profiles between two air bubbles (radius $\sim$ 65 $\pm$ 5 μm) at an interaction velocity 1 μm/s in 1 mM NaCl of different aqueous pH. (a) pH $\sim$ 3.0. (b) pH $\sim$ 8.0. (c) pH $\sim$ 10.0.

Applying the obtained Ψ_{Bub} value under a specific aqueous condition, the surface potential of OTS-mica substrate Ψ_{OTS} can be further determined by theoretically analyzing the measured interaction forces between an air bubble and the OTS-mica substrate. Figure 3.5a displays the measured force profile of the bubble-OTS-mica substrate (with water contact angle $\sim$ 90°) interaction at 1 μm/s in 1 mM NaCl of pH $\sim$ 5.6 and the corresponding fitting result based on the theoretical model incorporating the effect of HB interaction. Similar to the bubble-bubble interaction under the same aqueous condition, the relatively long-range EDL repulsion made the major contribution so that the air bubble was inhibited from attaching onto the hydropohobic OTS-mica substrate with no jump-in behavior detected in the force curve. With Ψ_{Bub} $\sim$ -33 $\pm$ 4 mV, Ψ_{OTS} was determined to be -50 $\pm$ 5 mV in 1 mM NaCl of pH $\sim$ 5.6 which was in good agreement with the previously reported value.[59] The disjoining pressures of different surface interactions involved in the bubble-substrate interaction are shown in Figure 3b, which

demonstrates the strong EDL repulsion (Debye length $\kappa^{-1} \sim 9.6$ nm) dominated the bubble-substrate interaction in this case, while the VDW repulsion ($A_H \sim -2.21 \times 10^{-20}$ J) and HB attraction ($C_0 \sim 0.0725$ J/m^2 calculated based on equation 3.6 in Experimental section, decay length of HB interaction $D_0 \sim 1.0 \pm 0.1$ nm) contributed less significantly to the overall disjoining pressure.[17, 31] The confined thin water film was stabilized at a separation of 21.8 nm (Figure 3.5c) where the Laplace pressure inside the bubble was balanced by the overall repulsive disjoining pressure and the air bubble was prevented from further approaching the hydrophobic substrate.
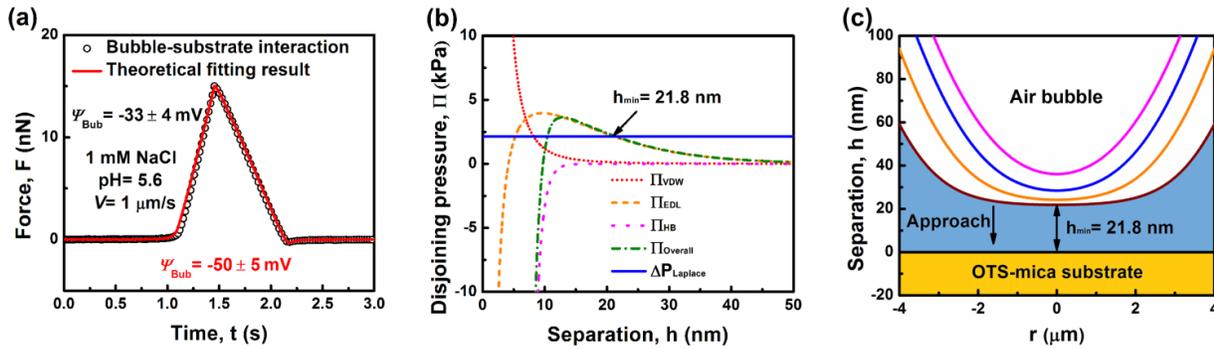
Figure 3.5. Interaction between an air bubble (radius ~ 68 μm) and an OTS-mica substrate at the interaction velocity 1 μm/s in 1 mM NaCl of pH ~ 5.6. (a) Measured interaction force (open symbols) and theoretical fitting (solid curve) results. (b) Disjoining pressure profiles of the involved surface interactions. (c) Evolution of the calculated bubble profiles during approaching process and the brown curve denotes the bubble profile at the minimal separation.

Similarly, by theoretically analyzing the bubble-substrate interactions in 1 mM NaCl of pH 3.0, 8.0 and 10.0 (Figure 3.6), the corresponding Ψ_{OTS} values were determined and listed in Table 3.1, showing that OTS-mica surface becomes more negatively charged with increasing solution pH.[60-62] It is noticeable that a distinct jump-in behavior was observed in the interaction

force curve for the case of 1 mM NaCl of pH ~ 3.0, indicating that the bubble attached onto the hydrophobic substrate during the approaching process. This phenomenon could arise from the fact that the weak EDL repulsion in this case was not able to resist the strong HB attraction (with a decay length of D_0 ~ 1.0 nm here). The bubble attachment behavior and the HB interaction are further discussed in a late section of this work.
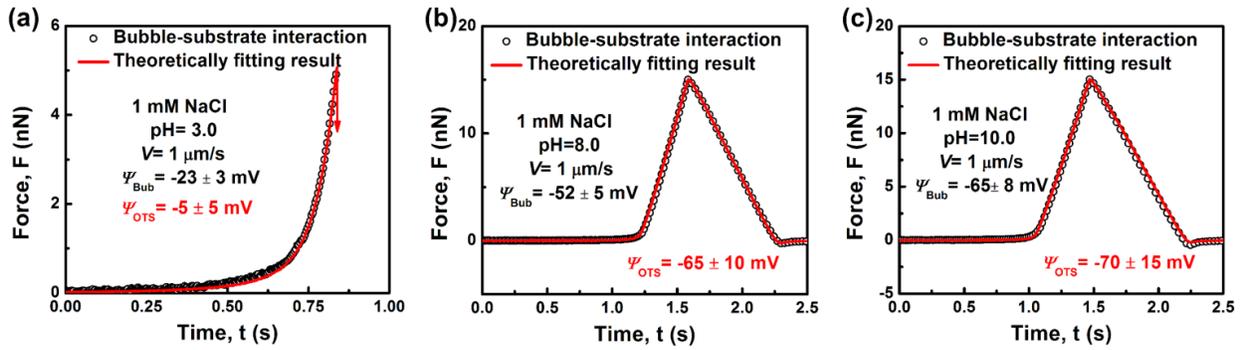
Figure 3.6. Interaction force profiles between an air bubble and an OTS-mica substrate at an interaction velocity 1 μm/s in 1 mM NaCl of different aqueous pH: (a) pH ~ 3.0, (b) pH ~ 8.0, and (c) pH ~ 10.0.

Table 3.1. Theoretically fitted surface potentials of air bubble and OTS-mica substrate in 1 mM NaCl with various aqueous pH conditions.

Aqueous pH	Ψ_{Bub} (mV)	Ψ_{OTS} (mV)
3.0	-23 ± 3	-5 ± 5
5.6	-33 ± 4	-50 ± 8
8.0	-52 ± 5	-65 ± 10

Based on the Ψ_{Bub} and Ψ_{OTS} values in Table 1, the bubble-bubble and bubble-substrate interactions under different hydrodynamic conditions (i.e., different interaction velocities) and the corresponding aqueous conditions could be theoretically predicted. Taking the case in 1 mM NaCl of pH ~ 5.6 as an example, Figures 3.7a and 3.7b display the interaction force profiles of bubble-bubble and bubble-OTS-mica substrate interactions at different velocities (i.e., 20, 10 and 5 μm/s) calculated using Ψ_{Bub} ~ -33 ± 4 mV and Ψ_{OTS} ~ -50 ± 8 mV, which clearly show that these theoretical predictions (solid curves) are in good agreement with the experimentally measured forces (open symbols), further validating the fitted Ψ_{Bub} and Ψ_{OTS} values and demonstrating that these parameters could not be affected by the hydrodynamic conditions.
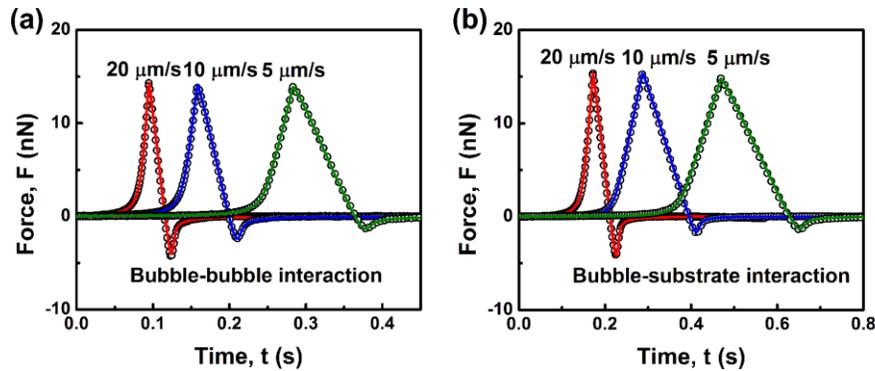
Figure 3.7. Interaction force profiles (a) between two air bubbles (radius ~ 70 μm) and (b) between an air bubble (radius~70 μm) and an OTS-mica substrate at different interaction velocities in 1 mM NaCl of pH ~ 5.6. The red, blue and green curves denote the theoretically predicted interaction forces at the interaction velocity of 20 μm/s, 10 μm/s 5 μm/s, respectively, and the open symbols represent the experimentally measured results.

With the NaCl concentration increasing to 500 mM, very different interaction behavior (i.e. force profile) was measured as shown in Figure 3.8a. Following a relatively small repulsion, a distinct "jump-in" behavior appeared which corresponded to the bubble attachment onto the

hydrophobic OTS-mica substrate during the AFM force measurement as also confirmed using the optical microscope coupled with AFM. In 500 mM NaCl, the EDL repulsion was signficantly suppressed with a Debye length $\kappa^{-1} \sim 0.43$ nm, which, hence, could be considered insignificant and negligible as compared to the VDW and HB interactions. Therefore, the bubble probe would be able to further approach the substrate till a critical separation was reached where the HB attraction could conquer the repulsive VDW interaction and trigger the bubble attachment. The decay length of the HB attraction D_0 was theoretically fitted to be 1.0 ± 0.1 nm, which was validated under different interaction velocities, consistent with the value in previous studies[31, 63] Figure 3.8b shows the disjoining pressure profiles of the involved surface interactions which demonstrates the critical role of HB interaction in bubble attachment for this case. The critical separation was determined to be ~ 10.0 nm where the attractive overall disjoining pressure just exceeded the Laplace pressure inside the bubble, leading to bubble attachment. The evolution of the bubble profile during the interaction was calculated and shown in Figure 3.8c, which depicted a pimple shape, indicating that the center region of the bubble was strongly attracted towards the hydrophobic substrate in 500 mM NaCl of pH 5.6.
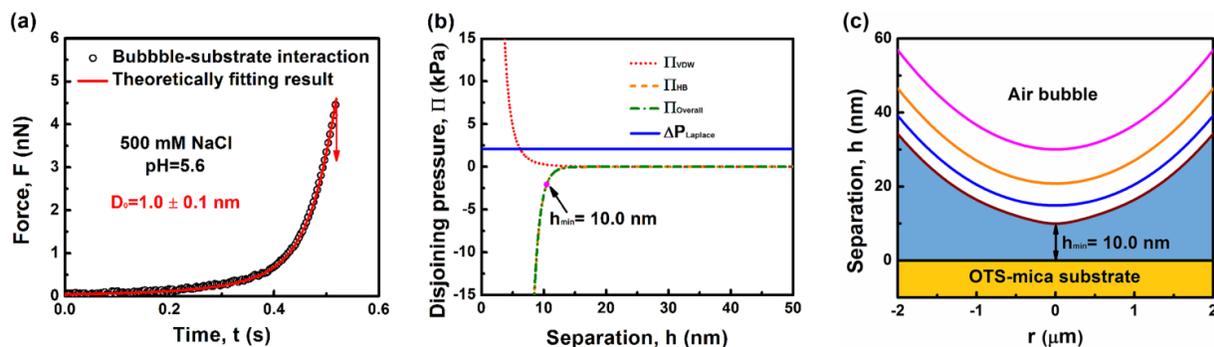
Figure 3.8. Interaction profile between an air bubble (radius ~ 65 μm) and an OTS-mica substrate (with water contact angle 90°) at the interaction velocity 1 μm/s in 500 mM NaCl of pH ~ 5.6. (a) Measured interaction force profile (open symbols) and theoretical fitting results (solid curve). (b) Disjoining pressure profiles of the involved surface interactions. (c) Evolution of the calculated bubble profiles during approaching process and the brown curve denotes the bubble profile at the minimal separation before "jump-in".

The interactions between air bubbles and OTS-mica substrates in aqueous solutions of different NaCl concentrations (i.e. 100 mM, 1 M and 2 M) and pH conditions (i.e., 500 mM NaCl of pH ~ 3.0, 8.0 and 10.0) have been also investiaged and shown in Figure 3.9. It has been found that the measured interaction forces agree well with the theoretical calculations based on $D_0 = 1.0 \pm 0.1$ nm, demonstrating that the HB attraction between air bubble and hydrophobic OTS-mica substrate was independent of the aqueous salinity and pH condition.
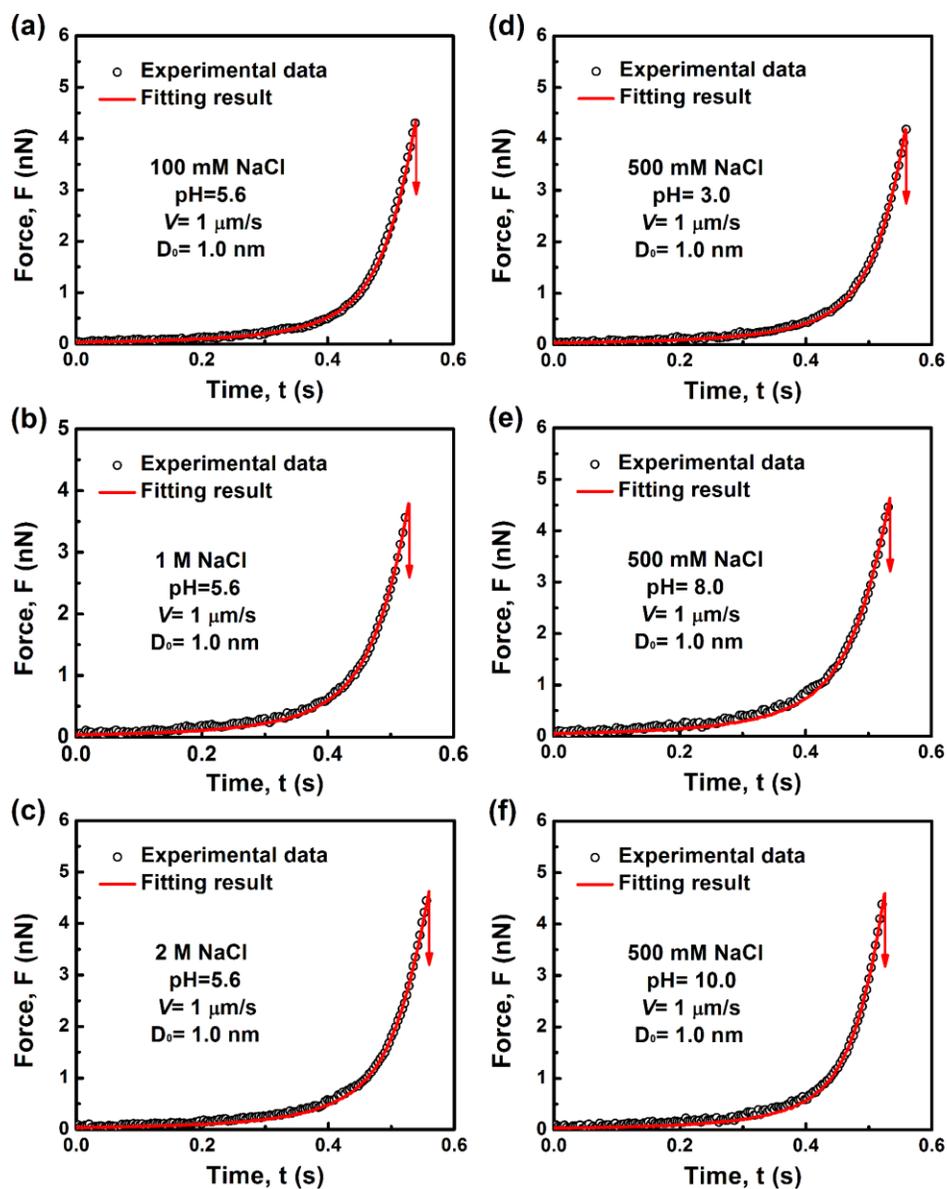
Figure 3.9. Interaction force profiles between an air bubble (radius ~ 65 ± 5 μm) and an OTS-mica substrate at the interaction velocity 1 μm/s in (a) 100 mM NaCl of pH ~ 5.6, (b) 1 M NaCl of pH ~ 5.6, (c) 2 M NaCl of pH ~ 5.6, (d) 500 mM NaCl of pH ~ 3.0, (e) 500 mM NaCl of pH ~ 8.0, and (f) 500 mM NaCl of pH ~ 10.0, respectively.

The assembly of colloidal particles at air/water interfaces in complex fluids is a ubiquitous and important process involved in a variety of engineering systems. The bubble-particle

interaction associated with such assembly processes can be quantitatively simulated based on the theoretical model, by applying the quantified parameters obtained through direct force measurements between air bubble and flat hydrophobic substrate (with the same surface properties as the colloidal particles). A schematic diagram of bubble-particle interaction is shown in Figure 3.10a. Here, the radii of OTS-hydrophobized particle and air bubble were fixed as 3 μm and 50 μm, respectively, and the interaction velocity was set as 1 μm/s to reduce the hydrodynamic effect and highlight the effect of surface forces. As the particle moves towards the bubble surface, a thin water film would be stabilized if the overall repulsive disjoining pressure balances the Laplace pressure inside the bubble, impeding the further drainage of the confined water and preventing the particle from further approaching the bubble surface. As a result, a critical force is required to overcome the overall repulsive disjoining pressure barrier, driving the particle to a critical separation where the HB attraction is strong enough to trigger the particle attachment. It is evident from Figure 3.10b that increasing the solution pH (from 3.0 to 10.0) of 1 mM NaCl makes both the air bubble and the hydrophobic particle more negatively charged, thus substantially enhancing the EDL repulsion and leading to an increasingly repulsive overall disjoining pressure. The normalized critical forces for particle attachment in 1 mM NaCl of different pH have been quantitatively predicted using the theoretical model and displayed in Figure 3.10c, showing a higher repulsion should be overcome (from 0.11 mN/m to 7.78 mN/m) with the pH increasing from 3.0 to 10.0. A smaller critical force indicates that the hydrophobic particle tends to attach to the bubble surface more easily.
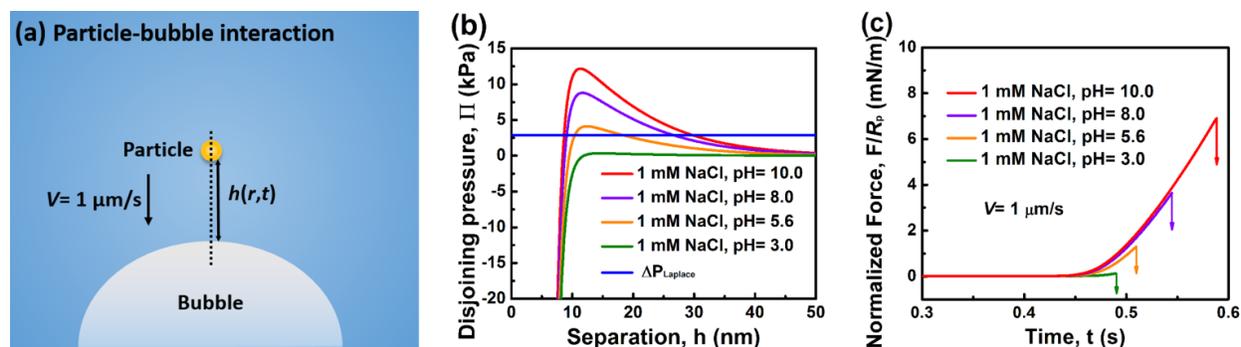
Figure 3.10. Interaction between a model OTS-hydrophobized particle ($R_p \sim 3$ μm) and an air bubble ($R_b \sim 50$ μm) at 1 μm/s in 1 mM NaCl of different aqueous pH conditions. (a) Schematic diagram of the particle-bubble interaction. (b) Theoretically calculated profiles of the overall disjoining pressure for the four different pH cases. (c) Theoretically predicted interaction forces between the particle and air bubble before attachment (arrows indicate "jump-in").

The attachment behaviors of the hydrophobic particle to air/water interface under different solution conditions have been also analyzed. Figure 3.11 shows that if the hydrophobic particle is continuously driven towards the air bubble (by overcoming the repulsive disjoining pressure), "jump-in" behavior can occur at some critical separation ($h_{cr} \sim 9.9, 9.3, 9.0$ and 8.7 nm for the cases in 1 mM NaCl of pH $\sim 3.0, 5.6, 8.0$ and 10.0, respectively), leading to bubble-particle attachment. More importantly, Figure 3.11 manifests that the air bubble experiences distinct deformations under different pH conditions when the hydrophobic particle is driven close to the bubble surface, pimpling at pH ~ 3.0, flattening at pH ~ 5.6 and dimpling at pH ~ 8.0 and 10.0, respectively. Such phenomena imply that under relatively low salinity condition, increasing aqueous pH strengthens repulsive disjoining pressure between the hydrophobic particles and air bubbles, leading to higher energy barrier for particle-bubble attachment.
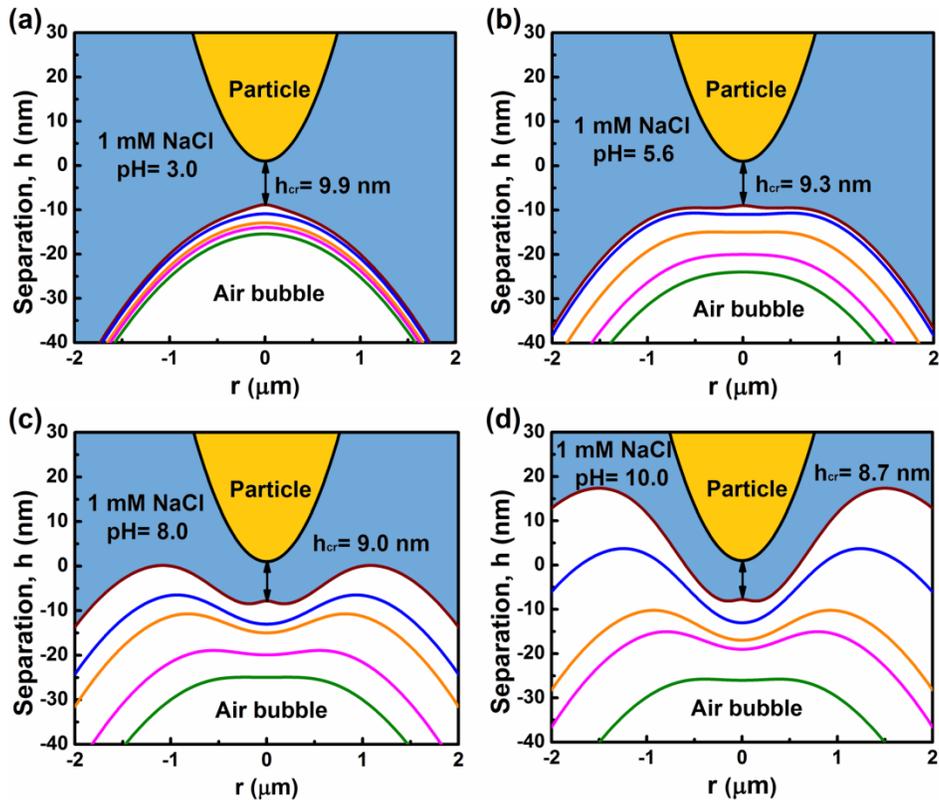
Figure 3.11. Evolution of the calculated bubble profile during the approaching of an OTS-hydrophobized particle ($R_p \sim 3$ μm) to an air bubble ($R_b \sim 50$ μm) at the velocity of 1 μm/s in 1 mM NaCl of (a) pH 3.0, (b) pH 5.6, (c) pH 8.0, and (d) pH 10.0, respectively.

The influence of aqueous salinity on the attachment behavior of the hydrophobic solid particle to air bubble has also been investigated by theoretically predicting the particle-bubble interaction in 500 mM NaCl of pH ~ 5.6 (Figure 3.12). In this case, the EDL was highly screened and can be considered negligible, and the strong HB attraction dominated the overall disjoining pressure, facilitating the particle attachment onto the bubble surface. Accordingly, the normalized critical force for the particle attachment is quite weak (~ 0.10 mN/m) and pimple shape can be also developed before the bubble-particle attachment (occurring at a critical separation of 10.0 nm), similar to the case in 1 mM NaCl of pH ~ 3.0.
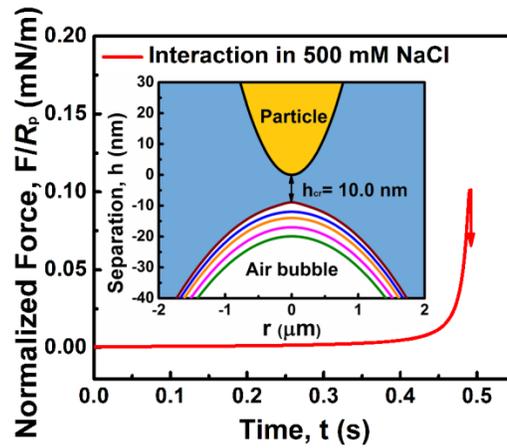
Figure 3.12. Theoretically predicted interaction force profile between a model OTS-hydrophobized particle ($R_p \sim 3$ μm) and an air bubble ($R_b \sim 50$ μm) at 1 μm/s in 500 mM NaCl aqueous solution (pH 5.6). The inset shows the evolution of the calculated bubble deformation during the interaction.

Theoretical analysis has also been conducted for the case that the hydrophobic particle interacts with a much larger bubble. Here, the particle radius was kept as 3 μm, while the bubble radius was changed to 1000 μm so that it could be considered approximately as a colloidal particle interacting with a flat air/water interface. Figure 3.13a illustrates the normalized critical forces for particle attachment as predicted by the theoretical model, showing that only 0.03 mN/m would be required for particle attachment at pH ~ 3.0 (due to the highly suppressed EDL repulsion) but much larger forces would be needed at higher pH (i.e., 5.6, 8.0 and 10.0). Similarly, as shown in Figure 3.13b, much lower force (~ 0.03 mN/m) would be required for particle-bubble attachment at high salinity condition (i.e., 500 mM NaCl) as compared to the 1 mM NaCl case with fixed pH ~ 5.6. To experimentally verify these results surface tension measurements were conducted on NaCl aqueous solutions containing OTS-hydrophobized silica particles (with diameter 1-5 μm, water contact angle 90°) using a pendent drop shape method. As

shown in Figure 3.13c, the surface tension remained constant during the measurement ($\sim$ 2400 s) for 1 mM NaCl of pH $\sim$ 5.6, 8.0 and 10.0, implying that the hydrophobic particles could have much less probability to attach and assemble onto the air/water interface at higher pH. In contrast, for 1 mM NaCl of pH $\sim$ 3.0 the surface tension was observed to decrease gradually with time which indicates the continuous particle attachment, and then reached a plateau (at $\sim$1500 s) suggesting equilibrium assembly of the hydrophobic particles at the air/water interface.[64-66] The apparent decline of surface tension was also observed for the case of 500 mM NaCl with pH $\sim$5.6 (Figure 3.13d). The surface tension results and theoretical prediction demonstrates that lowering the aqueous pH or increasing the solution salinity can suppress the EDL repulsion and facilitate the attachment and assembly of hydrophobic particles onto the air/water interface driven by the strong HB attraction.
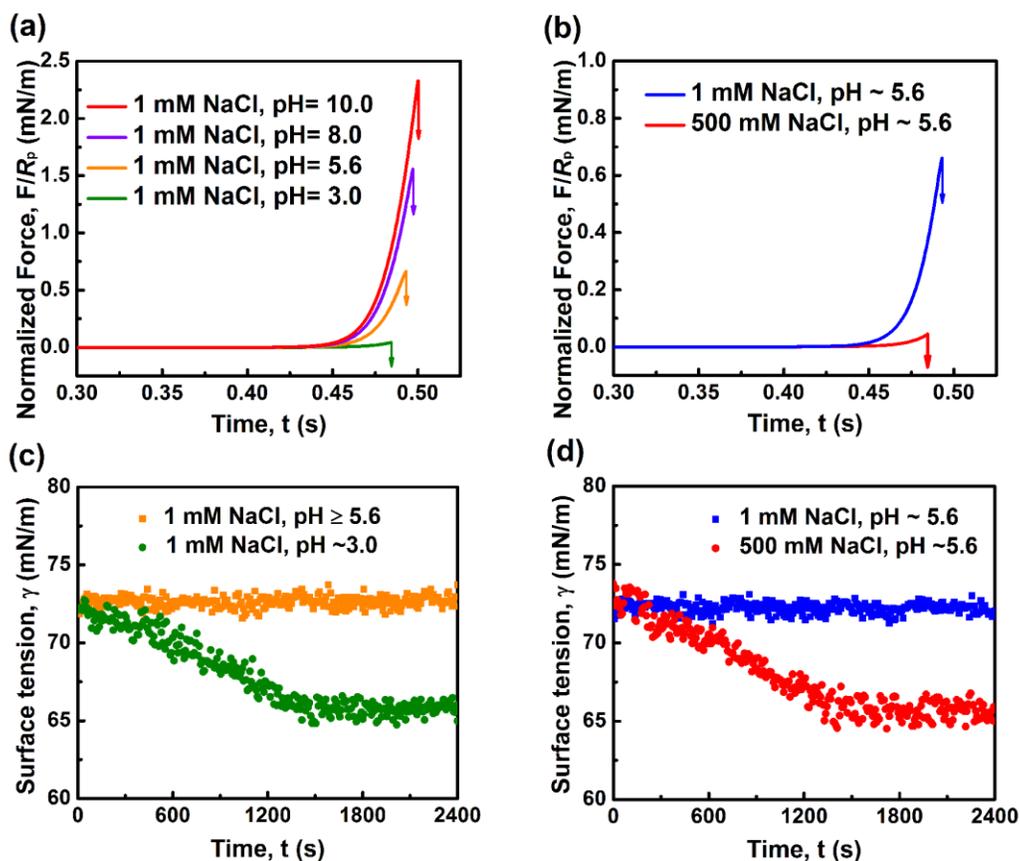
Figure 3.13. Theoretically predicted interaction force between a model OTS-hydrophobized particle ($R_p \sim 3$ μm) and an air bubble ($R_b \sim 1000$ μm) at 1 μm/s under different aqueous conditions: (a) 1 mM NaCl of pH 3.0, 5.6, 8.0, 10.0, and (b) 1 and 500 mM NaCl with fixed pH 5.6. Surface tensions of NaCl aqueous solutions containing OTS-hydrophobized colloidal particles (1-5 μm in diameter), measured using a pendent drop shape method: (c) 1 mM NaCl of different pH, and (d) 1 and 500 mM NaCl with fixed pH 5.6.

Similar theoretical analysis has been conducted to evaluate the influence of particle size on the particle-bubble interactions. Figure 3.14 shows the normalized critical forces required for particle-bubble attachment during the interactions between OTS-hydrophobized particles of different sizes (radii 5-50 μm) and an air bubble with fixed radius (i.e., 50 μm or 1000 μm) in 1

mM NaCl of different pH conditions. It was found that for a given bubble size, the critical normalized force F/R_p required for the particle-bubble attachment would not be significantly affected by the particle size, but would depend on the specific aqueous condition.
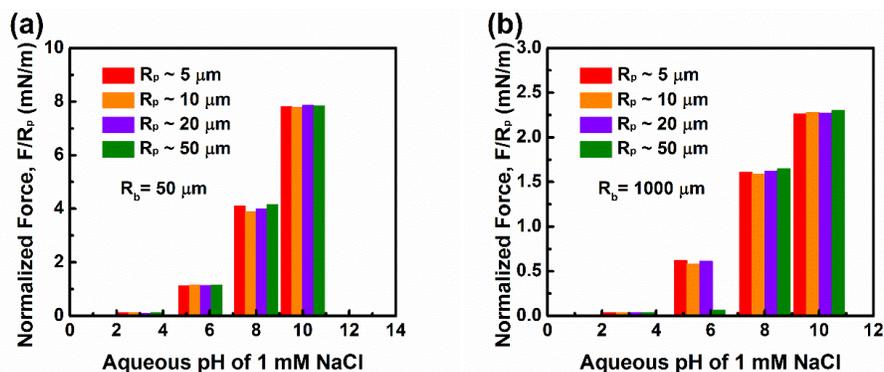
Figure 3.14. Theoretically predicted interaction forces between OTS-hydrophobized colloidal particles of different radii (5 μm, 10 μm, 20 μm, 50 μm, respectively) and an air bubble with radius of (a) 50 μm and (b) 1000 μm.

3.4. Conclusions.

In this work, air bubble and OTS-hydrophobized mica substrate (with water contact angle 90°) have been used as a model bubble-hydrophobic solid system to investigate their surface interaction mechanism and attachment behaviors under different solution conditions (of varying salinity and pH). Bubble probe AFM technique was employed to quantitatively measure the forces for both bubble-bubble and bubble-substrate under various aqueous conditions. The experimental force results were analyzed using a theoretical model based on the Reynolds lubrication theory and augmented Young-Laplace equation by including the influence of disjoining pressure, and several principal parameters (e.g. surface potential, decay length of hydrophobic interaction) involved in bubble-OTS interactions were further determined. It was

found that both air bubble and OTS-hydrophobized surface became less negatively charged by lowering the aqueous pH (pH 10.0 to 3.0) or increasing the solution salinity (NaCl concentration 1 mM to 2 M), and the HB attraction between air bubble and the hydrophobic OTS-mica substrate was independent of the aqueous salinity and pH, showing a decay length of 1.0 ± 0.1 nm.

These parameters (e.g. surface potential, decay length of HB interaction) obtained from AFM force measurements were further applied to predict the interaction and attachment behaviors of the OTS-hydrophobized colloidal particles and air bubbles in aqueous media. Surface tension measurements were also conducted on aqueous solutions containing OTS-hydrophobized particles. The AFM force measurements, theoretical calculations and surface tension results agreed with each other excellently, which have verified the theoretical prediction based on force measurements and demonstrated that lowering the solution pH or increasing the solution salinity would suppress the EDL repulsion and facilitate the attachment of hydrophobic particles to air bubble surfaces under the chosen aqueous solution condition driven by the strong HB attraction.

Our results have improved the fundamental understanding of the surface interaction mechanism between hydrophobic colloidal particles and air bubbles, by quantifying the surface forces and drainage behaviors of the confined thin water film between the bubble and hydrophobic solid. This useful and facile methodology can be readily extended to quantitatively probe the interactions of many other colloidal particles with gas/water and oil/water interfaces in aqueous media, with implications on the colloidal assembly at gas/water and oil/water interfaces in a wide range of engineering applications.

3.5. References.

1.   Ralston, J.; Fornasiero, D.; Hayes, R., Bubble–Particle Attachment and Detachment in Flotation. *Int. J. Miner. Process.* **1999**, *56*, 133-164.

2.   Park, J. I.; Nie, Z.; Kumachev, A.; Abdelrahman, A. I.; Binks, B. P.; Stone, H. A.; Kumacheva, E., A Microfluidic Approach to Chemically Driven Assembly of Colloidal Particles at Gas–Liquid Interfaces. *Angew. Chem.* **2009**, *121*, 5404-5408.

3.   Zhang, X.; Lohse, D., Perspectives on Surface Nanobubbles. *Biomicrofluidics* **2014**, *8*, 041301.

4.   Dickinson, E., Food Emulsions and Foams: Stabilization by Particles. *Curr. Opin. Colloid Interface Sci.* **2010**, *15*, 40-49.

5.   Park, J. I.; Jagadeesan, D.; Williams, R.; Oakden, W.; Chung, S.; Stanisz, G. J.; Kumacheva, E., Microbubbles Loaded with Nanoparticles: A Route to Multiple Imaging Modalities. *ACS Nano* **2010**, *4*, 6579-6586.

6.   Klibanov, A. L., Microbubble Contrast Agents: Targeted Ultrasound Imaging and Ultrasound-Assisted Drug-Delivery Applications. *Invest. Radiol.* **2006**, *41*, 354-362.

7.   Fameau, A. L.; Carl, A.; Saint-Jalmes, A.; Von Klitzing, R., Responsive Aqueous Foams. *ChemPhysChem* **2015**, *16*, 66-75.

8.   Binks, B. P.; Murakami, R., Phase Inversion of Particle-Stabilized Materials from Foams to Dry Water. *Nat. Mater.* **2006**, *5*, 865-869.

9.   Zhou, C.; Zhao, Y.; Bian, T.; Shang, L.; Yu, H.; Wu, L.-Z.; Tung, C.-H.; Zhang, T., Bubble Template Synthesis of Sn 2 Nb 2 O 7 Hollow Spheres for Enhanced Visible-Light-Driven Photocatalytic Hydrogen Production. *Chem. Commun.* **2013**, *49*, 9872-9874.

10.   Mao, Z.; Xu, H.; Wang, D., Molecular Mimetic Self-Assembly of Colloidal Particles. *Adv. Funct. Mater.* **2010**, *20*, 1053-1074.

11.   Xu, J.; Li, X.; Wu, X.; Wang, W.; Fan, R.; Liu, X.; Xu, H., Hierarchical Cuo Colloidosomes and Their Structure Enhanced Photothermal Catalytic Activity. *J. Phys. Chem. C* **2016**, *120*, 12666-12672.

12.   Lou, X. W. D.; Archer, L. A.; Yang, Z., Hollow Micro-/Nanostructures: Synthesis and Applications. *Adv. Mater.* **2008**, *20*, 3987-4019.

13.   Zhang, L.; Zheng, M.; Liu, X.; Sun, J., Layer-by-Layer Assembly of Salt-Containing Polyelectrolyte Complexes for the Fabrication of Dewetting-Induced Porous Coatings. *Langmuir* **2010**, *27*, 1346-1352.

14.   Wu, C.; Xie, Y.; Lei, L.; Hu, S.; OuYang, C., Synthesis of New-Phased Vooh Hollow "Dandelions" and Their Application in Lithium-Ion Batteries. *Adv. Mater.* **2006**, *18*, 1727-1732.

15.   Fan, X.; Zhang, Z.; Li, G.; Rowson, N., Attachment of Solid Particles to Air Bubbles in Surfactant-Free Aqueous Solutions. *Chem. Eng. Sci.* **2004**, *59*, 2639-2645.

16.   Wang, X.; Feng, J.; Bai, Y.; Zhang, Q.; Yin, Y., Synthesis, Properties, and Applications of Hollow Micro-/Nanostructures. *Chem. Rev.* **2016**, *116*, 10983-11060.

17.   Israelachvili, J. N., *Intermolecular and Surface Forces: Revised Third Edition*; Academic press, 2011.

18.   Butt, H.-J.; Graf, K.; Kappl, M., *Physics and Chemistry of Interfaces*; John Wiley & Sons, 2006.

19.   Hammer, M. U.; Anderson, T. H.; Chaimovich, A.; Shell, M. S.; Israelachvili, J., The Search for the Hydrophobic Force Law. *Faraday Discuss.* **2010**, *146*, 299-308.

20.   Chandler, D., Interfaces and the Driving Force of Hydrophobic Assembly. *Nature* **2005**, *437*, 640-647.

21.   Davis, J. G.; Gierszal, K. P.; Wang, P.; Ben-Amotz, D., Water Structural Transformation at Molecular Hydrophobic Interfaces. *Nature* **2012**, *491*, 582-585.

22.   Lam, S.; Velikov, K. P.; Velev, O. D., Pickering Stabilization of Foams and Emulsions with Particles of Biological Origin. *Curr. Opin. Colloid Interface Sci.* **2014**, *19*, 490-500.

23.   Bournival, G.; Ata, S.; Wanless, E. J., The Roles of Particles in Multiphase Processes: Particles on Bubble Surfaces. *Adv. Colloid Interface Sci.* **2015**, *225*, 114-133.

24.   Zeng, H.; Shi, C.; Huang, J.; Li, L.; Liu, G.; Zhong, H., Recent Experimental Advances on Hydrophobic Interactions at Solid/Water and Fluid/Water Interfaces. *Biointerphases* **2016**, *11*, 018903.

25.   Butt, H.-J., A Technique for Measuring the Force between a Colloidal Particle in Water and a Bubble. *J. Colloid Interface Sci.* **1994**, *166*, 109-117.

26.   Ducker, W. A.; Xu, Z.; Israelachvili, J. N., Measurements of Hydrophobic and DLVO Forces in Bubble-Surface Interactions in Aqueous Solutions. *Langmuir* **1994**, *10*, 3279-3289.

27.   Ishida, N., Direct Measurement of Hydrophobic Particle–Bubble Interactions in Aqueous Solutions by Atomic Force Microscopy: Effect of Particle Hydrophobicity. *Colloids Surf., A* **2007**, *300*, 293-299.

28.   Vakarelski, I. U.; Lee, J.; Dagastine, R. R.; Chan, D. Y.; Stevens, G. W.; Grieser, F., Bubble Colloidal Afm Probes Formed from Ultrasonically Generated Bubbles. *Langmuir* **2008**, *24*, 603-605.

29. Tabor, R. F.; Manica, R.; Chan, D. Y.; Grieser, F.; Dagastine, R. R., Repulsive Van Der Waals Forces in Soft Matter: Why Bubbles Do Not Stick to Walls. *Phys. Rev. Lett.* **2011**, *106*, 064501.

30. Chan, D. Y.; Klaseboer, E.; Manica, R., Film Drainage and Coalescence between Deformable Drops and Bubbles. *Soft Matter* **2011**, *7*, 2235-2264.

31. Shi, C.; Cui, X.; Xie, L.; Liu, Q.; Chan, D. Y.; Israelachvili, J. N.; Zeng, H., Measuring Forces and Spatiotemporal Evolution of Thin Water Films between an Air Bubble and Solid Surfaces of Different Hydrophobicity. *ACS Nano* **2014**, *9*, 95-104.

32. Xie, L.; Shi, C.; Wang, J.; Huang, J.; Lu, Q.; Liu, Q.; Zeng, H., Probing the Interaction between Air Bubble and Sphalerite Mineral Surface Using Atomic Force Microscope. *Langmuir* **2015**, *31*, 2438-2446.

33. Cui, X.; Shi, C.; Xie, L.; Liu, J.; Zeng, H., Probing Interactions between Air Bubble and Hydrophobic Polymer Surface: Impact of Solution Salinity and Interfacial Nanobubbles. *Langmuir* **2016**.

34. Xie, L.; Wang, J.; Yuan, D.; Shi, C.; Cui, X.; Zhang, H.; Liu, Q.; Liu, Q.; Zeng, H., Interaction Mechanisms between Air Bubble and Molybdenite Surface: Impact of Solution Salinity and Polymer Adsorption. *Langmuir* **2017**.

35. Xie, L.; Shi, C.; Cui, X.; Zeng, H., Surface Forces and Interaction Mechanisms of Emulsion Drops and Gas Bubbles in Complex Fluids. *Langmuir* **2017**.

36. Webber, G. B.; Manica, R.; Edwards, S. A.; Carnie, S. L.; Stevens, G. W.; Grieser, F.; Dagastine, R. R.; Chan, D. Y., Dynamic Forces between a Moving Particle and a Deformable Drop. *J. Phys. Chem. C* **2008**, *112*, 567-574.

37.   Tabor, R. F.; Grieser, F.; Dagastine, R. R.; Chan, D. Y., Measurement and Analysis of Forces in Bubble and Droplet Systems Using Afm. *J. Colloid Interface Sci.* **2012**, *371*, 1-14.

38.   Tabor, R. F.; Wu, C.; Grieser, F.; Dagastine, R. R.; Chan, D. Y., Measurement of the Hydrophobic Force in a Soft Matter System. *J. Phys. Chem. Lett.* **2013**, *4*, 3872-3877.

39.   Tabor, R. F.; Morfa, A. J.; Grieser, F.; Chan, D. Y.; Dagastine, R. R., Effect of Gold Oxide in Measurements of Colloidal Force. *Langmuir* **2011**, *27*, 6026-6030.

40.   Horozov, T. S.; Aveyard, R.; Clint, J. H.; Binks, B. P., Order− Disorder Transition in Monolayers of Modified Monodisperse Silica Particles at the Octane− Water Interface. *Langmuir* **2003**, *19*, 2822-2829.

41.   Wang, J.; Li, J.; Xie, L.; Shi, C.; Liu, Q.; Zeng, H., Interactions between Elemental Selenium and Hydrophilic/Hydrophobic Surfaces: Direct Force Measurements Using Afm. *Chem. Eng. J.* **2016**, *303*, 646–654.

42.   Paunov, V. N., Novel Method for Determining the Three-Phase Contact Angle of Colloid Particles Adsorbed at Air− Water and Oil− Water Interfaces. *Langmuir* **2003**, *19*, 7970-7976.

43.   Fielden, M. L.; Hayes, R. A.; Ralston, J., Surface and Capillary Forces Affecting Air Bubble− Particle Interactions in Aqueous Electrolyte. *Langmuir* **1996**, *12*, 3721-3727.

44.   Hutter, J. L.; Bechhoefer, J., Calibration of Atomic-Force Microscope Tips. *Rev. Sci. Instrum.* **1993**, *64*, 1868-1873.

45.   Klaseboer, E.; Chevaillier, J. P.; Gourdon, C.; Masbernat, O., Film Drainage between Colliding Drops at Constant Approach Velocity: Experiments and Modeling. *J. Colloid Interface Sci.* **2000**, *229*, 274-285.

46.   Hendrix, M. H.; Manica, R.; Klaseboer, E.; Chan, D. Y.; Ohl, C.-D., Spatiotemporal Evolution of Thin Liquid Films During Impact of Water Bubbles on Glass on a Micrometer to Nanometer Scale. *Phys. Rev. Lett.* **2012**, *108*, 247803.

47.   Yiantsios, S. G.; Davis, R. H., Close Approach and Deformation of Two Viscous Drops Due to Gravity and Van Der Waals Forces. *J. Colloid Interface Sci.* **1991**, *144*, 412-433.

48.   Manor, O.; Vakarelski, I. U.; Stevens, G. W.; Grieser, F.; Dagastine, R. R.; Chan, D. Y., Dynamic Forces between Bubbles and Surfaces and Hydrodynamic Boundary Conditions. *Langmuir* **2008**, *24*, 11533-11543.

49.   Manica, R.; Chan, D. Y., Drainage of the Air–Water–Quartz Film: Experiments and Theory. *Phys. Chem. Chem. Phys.* **2011**, *13*, 1434-1439.

50.   Hogg, R.; Healy, T. W.; Fuerstenau, D., Mutual Coagulation of Colloidal Dispersions. *Trans. Faraday Soc.* **1966**, *62*, 1638-1651.

51.   Stankovich, J.; Carnie, S. L., Electrical Double Layer Interaction between Dissimilar Spherical Colloidal Particles and between a Sphere and a Plate: Nonlinear Poisson− Boltzmann Theory. *Langmuir* **1996**, *12*, 1453-1461.

52.   Donaldson Jr, S. H.; Røyne, A.; Kristiansen, K.; Rapp, M. V.; Das, S.; Gebbie, M. A.; Lee, D. W.; Stock, P.; Valtiner, M.; Israelachvili, J., Developing a General Interaction Potential for Hydrophobic and Hydrophilic Interactions. *Langmuir* **2014**, *31*, 2051-2064.

53.   Donaldson Jr, S. H.; Das, S.; Gebbie, M. A.; Rapp, M.; Jones, L. C.; Roiter, Y.; Koenig, P. H.; Gizaw, Y.; Israelachvili, J. N., Asymmetric Electrostatic and Hydrophobic–Hydrophilic Interaction Forces between Mica Surfaces and Silicone Polymer Thin Films. *ACS Nano* **2013**, *7*, 10094-10104.

54.   Manica, R.; Connor, J. N.; Dagastine, R. R.; Carnie, S. L.; Horn, R. G.; Chan, D. Y., Hydrodynamic Forces Involving Deformable Interfaces at Nanometer Separations. *Phys. Fluids* **2008**, *20*, 032101.

55.   Creux, P.; Lachaise, J.; Graciaa, A.; Beattie, J. K.; Djerdjev, A. M., Strong Specific Hydroxide Ion Binding at the Pristine Oil/Water and Air/Water Interfaces. *J. Phys. Chem. B* **2009**, *113*, 14146-14150.

56.   Tabor, R. F.; Chan, D. Y.; Grieser, F.; Dagastine, R. R., Anomalous Stability of Carbon Dioxide in Ph-Controlled Bubble Coalescence. *Angew. Chem.* **2011**, *123*, 3516-3518.

57.   Takahashi, M., Z Potential of Microbubbles in Aqueous Solutions: Electrical Properties of the Gas-Water Interface. *J. Phys. Chem. B* **2005**, *109*, 21858-21864.

58.   Yang, C.; Dabros, T.; Li, D.; Czarnecki, J.; Masliyah, J. H., Measurement of the Zeta Potential of Gas Bubbles in Aqueous Solutions by Microelectrophoresis Method. *J. Colloid Interface Sci.* **2001**, *243*, 128-135.

59.   Lützenkirchen, J.; Richter, C., Zeta-Potential Measurements of Ots-Covered Silica Samples. *Adsorption* **2013**, *19*, 217-224.

60.   Hozumi, A.; Sugimura, H.; Yokogawa, Y.; Kameyama, T.; Takai, O., Z-Potentials of Planar Silicon Plates Covered with Alkyl-and Fluoroalkylsilane Self-Assembled Monolayers. *Colloids Surf., A* **2001**, *182*, 257-261.

61.   Schweiss, R.; Welzel, P. B.; Werner, C.; Knoll, W., Dissociation of Surface Functional Groups and Preferential Adsorption of Ions on Self-Assembled Monolayers Assessed by Streaming Potential and Streaming Current Measurements. *Langmuir* **2001**, *17*, 4304-4311.

62.   Chen, K.; Shan, L.; He, S.; Hu, G.; Meng, Y.; Tian, Y., Biphasic Resistive Pulses and Ion Concentration Modulation During Particle Translocation through Cylindrical Nanopores. *J. Phys. Chem. C* **2015**, *119*, 8329-8335.

63.   Shi, C.; Chan, D. Y.; Liu, Q.; Zeng, H., Probing the Hydrophobic Interaction between Air Bubbles and Partially Hydrophobic Surfaces Using Atomic Force Microscopy. *J. Phys. Chem. C* **2014**, *118*, 25000-25008.

64.   Gonzenbach, U. T.; Studart, A. R.; Tervoort, E.; Gauckler, L. J., Stabilization of Foams with Inorganic Colloidal Particles. *Langmuir* **2006**, *22*, 10983-10988.

65.   Stocco, A.; Rio, E.; Binks, B. P.; Langevin, D., Aqueous Foams Stabilized Solely by Particles. *Soft Matter* **2011**, *7*, 1260-1267.

66.   Gonzenbach, U. T.; Studart, A. R.; Tervoort, E.; Gauckler, L. J., Ultrastable Particle-Stabilized Foams. *Angew. Chem. Int. Ed.* **2006**, *45*, 3526-3530.

Chapter 4   Probing Interactions between Air Bubble and Hydrophobic Polymer Surface: Impact of Solution Salinity and Interfacial Nanobubbles

4.1. Introduction.

Hydrophobic polymers are widely used in many industrial and engineering applications, such as microfluidic devices,[1] bioengineering,[2] and food industry.[3] In most of these systems, the interactions between air bubbles and hydrophobic polymers in aqueous media play an important role in achieving desired characteristics and functionalities such as stabilization of foams and self-assembly driven by hydrophobic effects.[4] Much effort has been devoted over the past two decades to quantify the interactions between air bubbles and hydrophobic solid surfaces, although very limited work was available on hydrophobic polymer surfaces. Early studies applied a hydrophobic solid sphere glued on an atomic force microscope (AFM) tipless cantilever, so-called colloidal probe, to directly measure its interaction force with an air bubble immobilized on a solid substrate.[5-8] The effects of hydrodynamics, water chemistry (e.g., pH, surfactant, ion type and strength), particle hydrophobicity and surface chemistry, were investigated.[7, 9-12] However, the colloidal probe AFM technique showed some restrictions such as relatively high roughness of the colloidal particle and limited choices of particle materials. These limitations have been conquered by a bubble probe AFM technique, in which a gas bubble anchored on a tipless cantilever was used as a force probe to measure the interaction forces between the bubble and apposing substrates.[13-17] A theoretical model based on Reynolds lubrication theory and augmented Young-Laplace equation was developed to quantitatively analyze the surface interactions and drainage process of confined thin liquid films between

bubbles and substrates.[16-19] The evolution of thin water film confined between air bubble and solid substrate surface was also synchronously determined and visualized by incorporating the bubble probe AFM with reflection interference contrast microscope (RICM).[20] These previous studies revealed the important roles of various surface forces in the interactions between air bubbles and hydrophobic solid surfaces: repulsive electrical double-layer (EDL) and van der Waals (VDW) interactions are prone to stabilize the confined thin water film, while the strong attraction arising from hydrophobic (HB) interaction can lead to the film rupture and bubble attachment.[16, 17, 20]

Interfacial nanobubbles (INBs) can spontaneously form on hydrophobic solid surfaces upon immersion in an aqueous solution, which can affect the interaction between an air bubble and an apposing hydrophobic substrate. A number of experimental and theoretical studies were conducted to characterize the physical properties (e.g., morphology and distribution) of the INBs on various hydrophobic solid surfaces such as highly oriented pyrolytic graphite (HOPG) and hydrophobic polymers (e.g., polystyrene).[21-28] Several models have been proposed to explain the remarkable stability of INBs, such as line tension,[29, 30] contamination on the air/water interface,[31] and a dynamic equilibrium theory.[32, 33] The presence of INBs was also reported to be an important factor influencing the interaction between hydrophobic solid surfaces in water. INBs were shown to cause stepwise jump-in behavior in force-distance curves between two hydrophobic solid surfaces measured by AFM,[34-35] which could be responsible for the observed long-range "hydrophobic attraction".[4, 36, 37] When two hydrophobic solid surfaces approach each other, the nanobubbles on the solid surfaces can interact and coalesce, resulting in the formation of capillary bridges that drive the two surfaces to abruptly jump into contact. The range and magnitude of this nanobubble-induced bridging attraction between two solid surfaces was found

to be greatly affected by the formation and stability of INBs depending on ion specificity, ion concentration and degassing conditions.[36, 38, 39] Therefore, the INBs on hydrophobic solids are expected to also influence the interactions between air bubbles and hydrophobic substrates, which, however, has been rarely reported.

In this work, the interactions between air bubbles and surfaces of a model hydrophobic polymer (i.e., polystyrene, PS) were directly measured in aqueous solutions using the bubble probe AFM technique, and the measured forces were analyzed by the theoretical model based on Reynolds lubrication theory and augmented Young-Laplace equation including the influence of disjoining pressure. PeakForce quantitative nano-mechanics (PF-QNM) and tapping mode (TM) AFM imaging was applied to characterize the INBs on the PS surfaces under different solution conditions, which was correlated to the surface forces measured.

4.2. Experiments and methods.

4.2.1. Preparation of polystyrene surfaces.

PS surfaces were prepared by spin-coating 2-3 drops of PS solution on a silica substrate (1×1 cm^2) at 2000 rpm and then the surfaces were dried under vacuum overnight (> 10 hours) to completely remove the residual solvent. PS solution was prepared by dissolving PS with Mw = 1,050,000 and $M_w/M_n \approx 1.09$ (Polymer Source Inc., Canada) in toluene (HPLC grade, Fishier Scientific, Canada) at a concentration of 0.5 wt%. The thickness of the prepared PS film was determined to be 30.0 ± 3.0 nm by ellipsometry. Figure 4.1A shows the morphology of the prepared PS surface with a root-mean-square (RMS) roughness ~ 0.3 nm, characterized by TM imaging using Dimension Icon AFM equipped with Nanoscope Analysis software (Bruker, USA), and the inset shows a water contact angle (WCA) of $90 \pm 2°$ on the PS surface measured

by goniometry. The NaCl aqueous solutions were prepared by dissolving suitable amount of highest-purity anhydrous NaCl (Sigma-Aldrich, 99.999+ %) in Milli-Q water with a resistance of ≥ 18.2 MΩ cm.
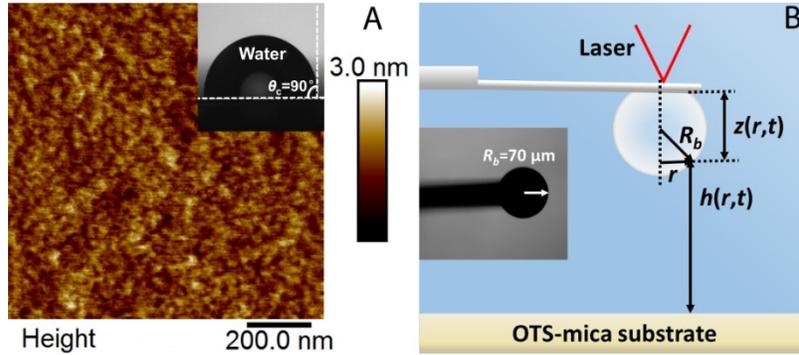
Figure 4.1. (A) Topographic image of prepared hydrophobic PS surface by tapping mode (TM) AFM in air (with a root-mean-square roughness of RMS ~ 0.3 nm), and the inset shows a water contact angle (WCA) of 90° on the PS surface; (B) schematic for experimental setup of the AFM force measurement between an air bubble and a PS surface, and the inset shows a typical AFM bubble probe with radius R_b ~ 70 μm.

4.2.2. Force measurement between air bubble and PS surface.

The bubble probe AFM technique based on an MPF-3D AFM system (Asylum Research, Santa Barbara, USA) was applied to measure the interaction force between air bubbles and PS surfaces in NaCl solutions. The schematic of experimental setup for the AFM force measurement of bubble-PS interaction is shown in Figure 4.1B, and a picture of a typical AFM bubble probe with bubble radius R_b ~ 70 μm is shown in the inset. The theoretical model based on Reynolds lubrication theory and augmented Young-Laplace equation including the influence of disjoining pressure was used to analyze the measured force data. The detailed information on the experimental setup and the theoretical model could be found in previous studies.[16-20, 40-42] The

Reynolds lubrication theory (Equation 4.1) describes the drainage behavior of the thin water film confined between air bubble and PS surface, assuming tangentially immobile hydrodynamic boundary condition at air/water and PS/water interfaces,[16, 17, 20, 42]

$$\frac{\partial h(r,t)}{\partial t} = \frac{1}{12\mu r}\frac{\partial}{\partial r}\left(rh^3\frac{\partial p(r,t)}{\partial r}\right) \tag{4.1}$$

where $h(r,t)$ is the thickness of the thin water film, μ is the viscosity of water, r is the radical coordinate and $p(r,t)$ is the excessive hydrodynamic pressure relative to the bulk solution.

The deformation of air bubble during the interaction can be described by the augmented Young-Laplace equation (Equation 4.2),[20-24, 46-48]

$$\frac{\gamma}{r}\frac{\partial}{\partial r}\left(r\frac{\partial h(r,t)}{\partial r}\right) = \frac{2\gamma}{R_b} - p(r,\mathrm{t}) - \Pi\big[h(r,t)\big] \tag{4.2}$$

where γ is the air/water interfacial tension, R_b is the radius of air bubble and $\Pi[(h(r,t)]$ is the disjoining pressure arising from the sum of various surface interactions, including VDW, EDL and HB interactions. The contributions from VDW, EDL and HB interactions[20] to the overall disjoining pressure are given by Equations 4.3 to 4.5, respectively, where A_H is the Hamaker constant for air-water-PS system, κ is Debye-Huckel parameter, ψ_b and ψ_s are the surface potentials of bubble and PS surface, respectively, D_0 is the decay length of HB interaction, and θ_c is the water contact angle on the PS surface.[16, 17, 20]

$$\Pi_{VDW}[h(r,t)] = -\frac{A_H}{6\pi h^3(r,t)} \tag{4.3}$$

$$\Pi_{EDL}[h(r,t)] = \frac{2\varepsilon_0\varepsilon\kappa^2\left[\left(e^{+\kappa h(r,t)} + e^{-\kappa h(r,t)}\right)\psi_b\psi_s - \left(\psi_b^2 + \psi_s^2\right)\right]}{\left(e^{+\kappa h(r,t)} - e^{-\kappa h(r,t)}\right)^2} \tag{4.4}$$

$$\Pi_{HB}[h(r,t)] = -\frac{\gamma(1-\cos\theta_c)}{D_0}\exp\left(-\frac{h(r,t)}{D_0}\right) \tag{4.5}$$

The overall force $F(t)$ can be calculated by integrating hydrodynamic pressure and disjoining pressure based on Derjaguin approximation as shown in Equation 4.6 .[16-17, 20]

$$F(t) = 2\pi \int_0^\infty \{p(r,t) + \Pi[h(r,t)]\} r dr \qquad (4.6)$$

4.2.3. Imaging of INB on PS surface in NaCl.

Both PF-QNM imaging and TM imaging were applied to characterize the morphology of the hydrophobic PS surface in NaCl solutions using Dimension Icon AFM equipped with Nanoscope Analysis software (Bruker, USA). PF-QNM imaging is capable of simultaneously mapping the morphology and mechanical properties across a surface, which can verify the presence of INBs on PS surfaces. TM imaging was also applied to study the evolution of morphology and distribution of INBs on PS surfaces in various NaCl solutions. During TM imaging, minimum force was applied from the cantilever tip, its disturbance on the properties of INBs could be less than PF-QNM imaging.

4.3. Results and discussion.

4.3.1. Interactions between Air Bubbles and PS Surfaces in NaCl Solutions.

The interactions between air bubbles and hydrophobic PS surfaces in NaCl solutions were directly measured using the bubble probe AFM technique. Figures 4.2A, 4.2B and 4.2C show the measured interaction forces between an air bubble (with radius R_b ~70, 68 and 60 μm, respectively) and a hydrophobic PS surface in 1, 500 and 1000 mM NaCl at natural pH (~ 5.6) at 1 μm/s, respectively, denoted by the open blue symbols. As shown in Figure 4.2A, strong repulsion was measured when the air bubble approached the PS surface and no bubble-PS attachment was observed. Both air bubble and PS surfaces were reported to be negatively

charged at the natural pH (~ 5.6),[43-45] therefore the relatively long-range repulsive EDL interaction between bubble and PS could inhibit bubble attachment onto the PS surface in 1 mM NaCl (with a Debye length of κ^{-1} ~ 9.6 nm). During the retraction of the bubble probe, the measured repulsive force gradually decreased and a small (negative) attractive force was measured which was attributed to the hydrodynamic suction effect.[16, 17, 20] In 1 mM NaCl (pH ~ 5.6), the surface potential of air bubble is -35 ± 5 mV and the Hamaker constant for air/water/PS system is -2.18×10^{-20} J.[17, 19, 46] Figure 4.2A shows that the measured force data could be well fitted by the aforementioned theoretical model as denoted by the solid red curve, with the surface potential of the PS surface fitted to be -85±10 mV that falls within the previously reported values.[45, 47, 48] The corresponding disjoining pressure profiles were also calculated and shown in Figure 4.2D, which clearly demonstrates that the EDL interaction was the dominant component among the different surface interactions. The minimum thickness of thin water film confined between the bubble and the PS surface was calculated to be h_{min} ~ 27.5 nm where the overall repulsive disjoining pressure was balanced by the Laplace pressure inside the bubble, and the bubble was prevented from further approaching the PS surface (viz. furthering increasing the applied load only flattened the bubble surface without decreasing the thickness of confined water film under the selected experimental condition). At this critical separation, the attractive HB interaction was too weak to trigger the bubble attachment onto the hydrophobic PS surface.

In contrast, as shown in Figure 4.2B, bubble attachment onto the PS surface was observed in 500 mM NaCl, indicated by "jump-in" behavior (denoted as the red arrow) on the force curve. In this case, the EDL repulsion was significantly screened (with a Debye length less than 1 nm) and the VDW interaction was repulsive at any separation for air/water/PS system. By neglecting the contribution of EDL interaction to the overall disjoining pressure, the measured force data

could be well fitted by the theoretical model using Equations 3-6 with a decay length of the HB interaction $D_0 = 0.75 \pm 0.05$ nm, denoted as the red curve in Figure 4.2B. The theoretically calculated disjoining pressure profiles are shown in Figure 4.2E, which clearly indicates that the hydrophobic attraction was the driving interaction for the bubble-PS attachment observed. The bubble attachment was calculated to occur at a critical separation of 7.4 nm where the overall attractive disjoining pressure just exceeded the Laplace pressure inside the bubble (Figure 4.2E). Similar results were obtained for the bubble-PS interaction in 1000 mM NaCl, as shown in Figures 4.2C and 4.2F, and the theoretical fitting denoted as red curve also showed a decay length of the HB interaction $D_0 = 0.75 \pm 0.05$ nm, and the critical separation for bubble attachment was 7.3 nm. It should be noted that all the above theoretical calculations assumed that the PS surfaces were pristine and free of INBs in the aqueous solution conditions studied, which will be further discussed later in this section.
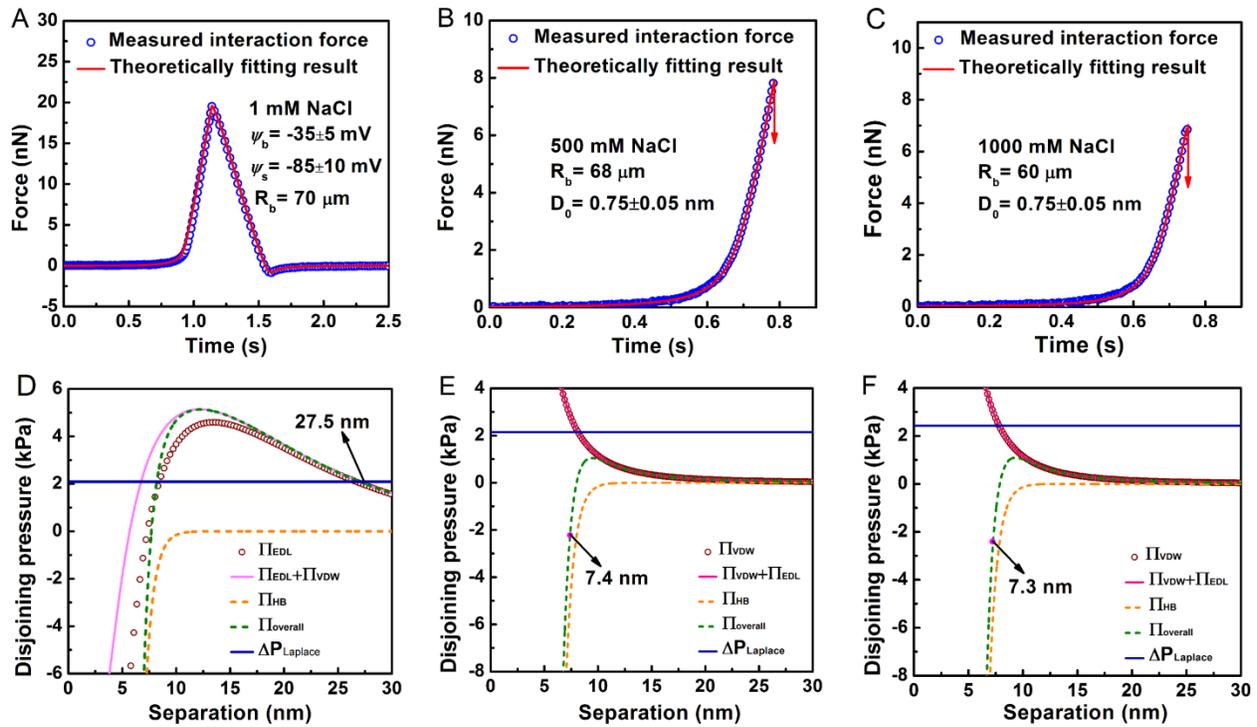
Figure 4.2. (A, B and C) Interactions between air bubbles (radius R_b ~70 μm, 68 μm and 60 μm, respectively) and hydrophobic PS surfaces in 1 mM, 500 mM and 1000 mM NaCl aqueous solutions at 1 μm/s, respectively. The open blue symbols represent the measured interaction forces while the solid red curves are the theoretically calculated results based on the theoretical model (Equations 3-6) and red arrows indicate attachment of bubble probe to the PS surface. (D, E and F) Theoretically calculated disjoining pressure profiles as a function separation, including van der Waals (VDW), electric double layer (EDL) and hydrophobic (HB) interactions, involved in the bubble-PS interactions in 1, 500 and 1000 mM NaCl aqueous solutions, respectively.

The bubble-PS interaction was also measured in 100 mM NaCl. Surprisingly, the theoretical model failed to describe the interaction between air bubble and PS surface in 100 mM NaCl (shown in Figure 4.3A). In this case, the EDL repulsion was very short-ranged with a Debye length of only 0.96 nm, which could be considered negligible as compared to VDW repulsion

and HB attraction. Thus, using the decay length of HB interaction of $D_0 = 0.75 \pm 0.05$ nm and

Hamaker constant for air/water/PS system of -2.18×10^{-20} J, bubble-PS attachment was expected

to occur in 100 mM NaCl according to the theoretical calculation (denoted by the red curve and

arrow in Figure 3A), similarly to that in 500 and 1000 mM NaCl. However, the measured force

curve showed that no bubble attachment occurred during the force measurement, and the air

bubble remained stable on the cantilever, indicating that a thin water film was confined between

the air bubble and the PS surface in 100 mM NaCl, that could be stabilized by some additional

repulsion. The above discrepancy between experimental results and theoretical calculations

could not be interpreted by the classical Derjaguin-Landau-Verwey-Overbeek (DLVO) theory

even including the effects of hydrophobic interaction. It should be noted that in the theoretical

calculations, the PS surface was assumed to a pristine and bare PS surface, while interfacial

nanobubbles have been reported to exist on PS surface in water.[24, 49] Therefore, the INBs on the

PS surface are likely to contribute to the repulsion measured in 100 mM NaCl (Figure 4.3A). To

verify this mechanism, the interaction force between two air bubbles (radius $R_{b,1} = R_{b,2} = 50$ μm)

was measured under the same solution condition (i.e., 100 mM NaCl), and no bubble attachment

and coalescence was observed, as shown in Figure 4.3B. The two stable air bubbles against

coalescence in 100 mM NaCl agree with previous results by Craig *et al.* that bulk bubble

coalescence could be inhibited in solutions with high concentration of NaCl (typically around or

above 0.1 M).[50, 51] Previous study also proposed that the hydroxyl ions could spontaneously

adsorb onto the oil/water interfaces and attract hydrated cations inducing water bound structures

and thus inhibiting the coalescence of oil droplets due to the additional hydration force.[52]

Therefore, it is reasonable to speculate that interfacial nanobbles could exist on the hydrophobic

PS surface that prevented the attachment of bubble probe (on the AFM cantilever) onto the PS

surface in 100 mM NaCl, while INBs may also influence the interactions between air bubble probe and PS substrates under other salt concentration conditions. Therefore, the PS surfaces were imaged in aqueous solutions of varying NaCl concentration using both PF-QNM and TM AFM imaging techniques to verify the possible INBs formed on the PS surfaces.
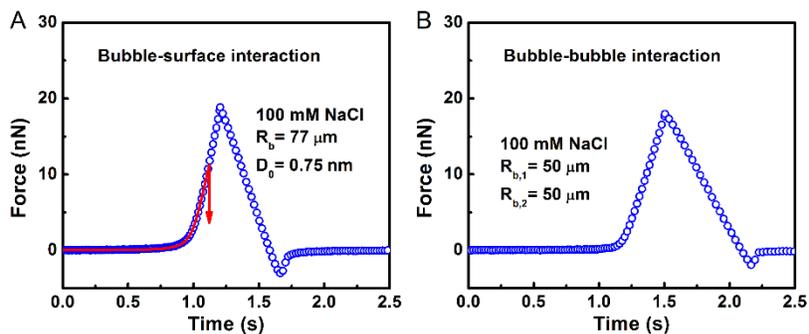
Figure 4.3. (A) Interaction between an air bubble (radius ~ 77 μm) and a hydrophobic PS surface in 100 mM NaCl. (B) Measured interaction force between two air bubbles (radius $R_{b,1} = R_{b,2} = 50$ μm) in 100 mM NaCl. Open blue symbols represent the measured interaction forces and solid red curve represents the theoretical calculation results using a decay length of HB interaction of 0.75 ± 0.05 nm and Hamaker constant for air/water/PS system of -2.18×10^{-20} J.

4.3.2. Characterization of INBs on hydrophobic PS surface.

PF-QNM imaging enables simultaneous topographic imaging and mapping of nano-mechanical properties (e.g., Derjaguin-Muller-Toporov, (DMT) modulus) of a substrate surface. Here, the morphology of the hydrophobic PS surface was first imaged in 100 mM NaCl using PF-QNM imaging to verify the presence of INBs on the PS surface. As shown in Figures 4.4A and 4.4B, the morphology of the PS surface in 100 mM NaCl was notably different from that in air (Figure 4.1A). A large number of spherical nanostructure regimes were densely distributed on the PS surface in 100 mM NaCl, rendering the RMS surface roughness to be ~1.5 nm, much higher than that measured in air. Moreover, these nanostructure regimes exhibited much lower

DMT modulus than the other regimes on the PS surface, as shown in Figures 4.4C and 4.4D, which indicate that these distinct nanostructure regimes could be composed of much softer substance (instead of PS) and were speculated to be the INBs. It is noted that although the absolute values of the DMT moduli were not provided in Figures 4.4C and 4.4D, the apparent contrast in the moduli of the different regimes clearly indicated that the nanostructure regimes would not be PS material, as further confirmed from the force-distance curves (Figure 4.5) and TM-AFM imaging (Figure 4.6).
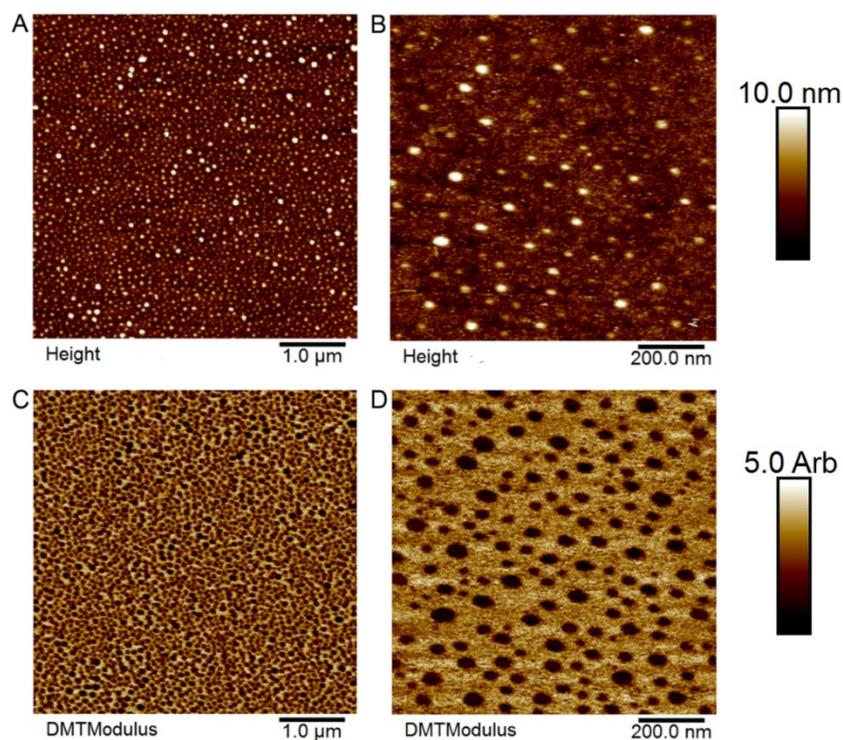
Figure 4.4. PF-QNM AFM images of hydrophobic PS surface in 100 mM NaCl aqueous solution. (A and B) Height images and (C and D) DMT modulus images with scale of 5 μm ×5 μm, and 1 μm ×1 μm, respectively.

The force curves of the tip-PS regime and tip-nanostructure regime interactions were also captured during the PF-QNM imaging process, and were shown in Figures 4.5A and 4.5B,

respectively. In Figure 4.5A, the attraction force was not detected during approach until at some

critical and small separation where jump-in phenomenon occurred which could be attributed to

the VDW attraction the AFM tip and the PS surface. After jump-in, further lowering the AFM tip

led to a drastically increased repulsion. When the AFM tip was retracted from the PS surface,

jump-out occurred at a small separation (Figure 4.5A). The interaction force before the jump-out

point followed an almost linear relation with the separation with a steep slope, indicating a hard

contact of the AFM tip with the relatively rigid PS surface. In comparison, for the tip-

nanostructure regime interaction, jump-in was observed at a much larger separation, and the

force-separation curve before jump-out showed much smaller slope, implying that the

nanostructure regimes experienced large deformations during the interaction process.

Interestingly, the force curve of the tip-nanostructure interaction is similar to that between a tip

and a nanobubble reported previously.[22, 53-55] Therefore, these soft nanostructure regimes on the

hydrophobic PS surface (Figure 4.4A and 4.4B) are believed to be the INBs.
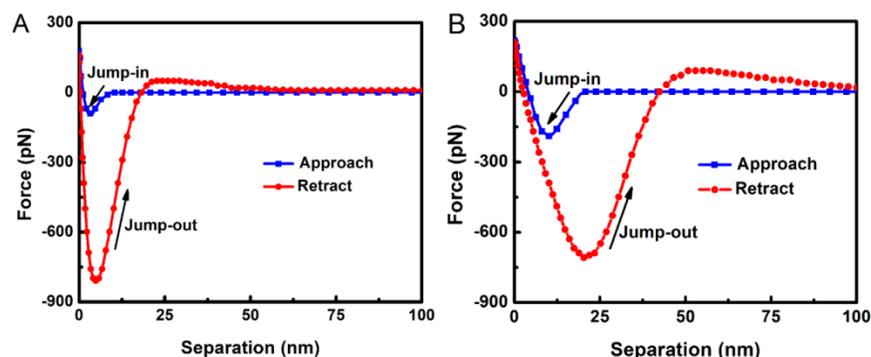
Figure 4.5. Force curves for interactions of (A) AFM tip-PS surface and (B) AFM tip-nanostructure regime (INB) interactions, respectively, captured during the PF-QNM imaging process. Square blue symbols represent the approach process and circular red symbols represent the retraction process.

In PF-QNM imaging process, a relatively high load in the magnitude of pN is generally excreted on the AFM tip, which may lead to significant deformations of the INBs and thereby influence the INB morphology. Therefore, it is generally difficult to accurately determine the morphology of INBs using PF-QNM.[21, 22, 56, 57] Here, TM imaging with much smaller disturbance to INBs was applied to characterize the morphology of INBs on PS surface in NaCl solutions of different concentrations. A very close approximation to the actual size of INBs could be obtained due to the intermittent contact of the tip with the air/water interface in TM imaging. Meanwhile, the apparent phase difference can also help distinguish the INBs from the PS domains. Figures 4.6A, 4.6B, C and 4.6D show the morphology and distribution of the INBs on PS surfaces in 1, 100, 500 and 1000 mM NaCl solutions. The parameters for characterizing the INBs could be obtained based on a spherical cap model shown in Figure 4.7. The height (H), width (W), and surface coverage of INBs were obtained through Nanoscope software analysis, and the effective radius of curvature (R) and nanoscopic contact angle (θ_n) were calculated using equation $R = (H^2 + W^2)/2H$ and $\theta_n = 180° - \arcsin(W/R)$, respectively.
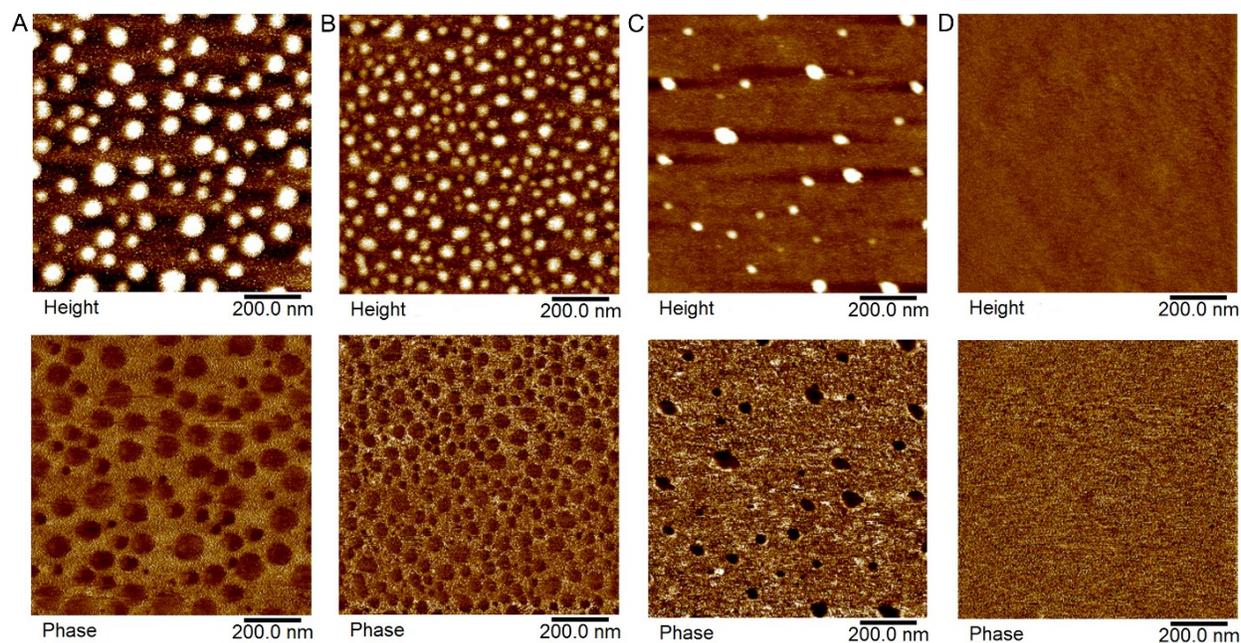
Figure 4.6. TM AFM imaging results of the morphology and distribution of the INBs on the hydrophobic PS surface in NaCl solutions: (A) 1 mM, (B) 100 mM, (C) 500 mM, and (D) 1000 mM. The upper and lower images are the height and phases images, respectively.
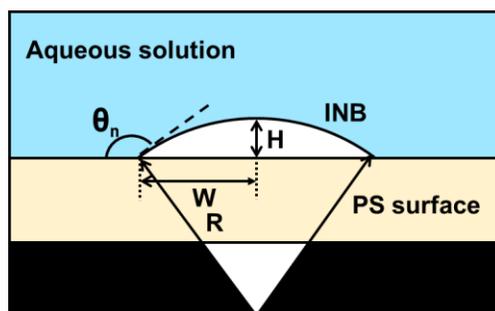
Figure 4.7. Schematic diagram of the spherical cap model for the INB morphology on the PS surface in NaCl aqueous solution.

Figure 4.8 illustrates the height and width histograms of the INBs on the PS surface in various NaCl solutions with various concentrations. In 1 mM and 100 mM NaCl, the size of INBs shrank in average height (~ 7.2 to ~ 4.5 nm), average width (45 to 33 nm) and effective

radius of curvature (144 to 123 nm), resulting in a decreased surface coverage of INBs on the PS surface (41.3% to 34.5% show in Figure 4.6A and 4.6B, respectively). When the NaCl concentration further increased to 500 mM, the surface coverage of INBs drastically reduced to ~ 7.1% (shown in Figure 4.6C). In 1000 mM NaCl, no INBs were observed on the hydrophobic PS surface. The calculated nanoscopic contact angle θ_n is between 160° and 170°, consistent with the values in previous studies.[26-32] The INBs on hydrophobic PS surface in this work exhibited smaller size and lower surface coverage as compared to the results in pure water reported previously,[24] which could be due to the presence of NaCl in the aqueous environment. The above results also agree well with previous work by Faghihnejad and Zeng that increasing NaCl concentration could suppress the formation and stability of nanobubbles on the PS surfaces, leading to shorter-ranged bridging attraction under high NaCl concentration conditions using a surface forces apparatus.[36]
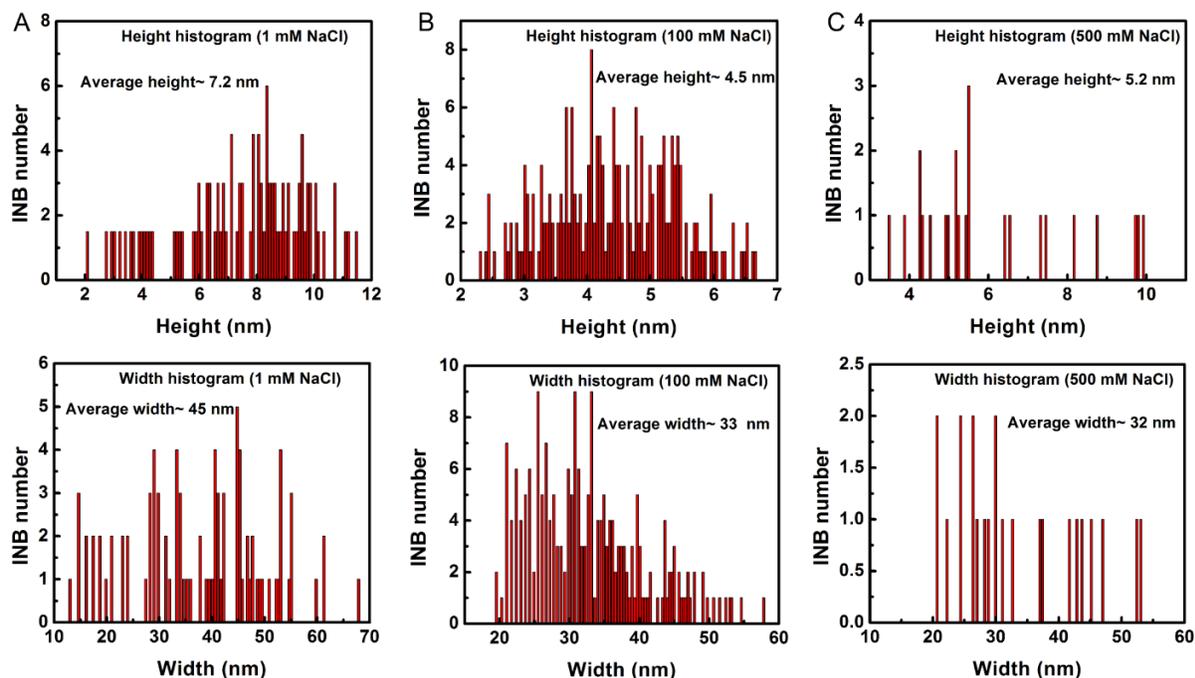
Figure 4.8. Height and width histograms of the INBs on the PS surface in NaCl solutions: (A) 1 mM, (B) 100 mM, and (C) 500 mM, respectively. The upper and lower images are the height and width histograms, respectively.

Although the quantitative formation mechanism of nanobubbles spontaneously attached on hydrophobic polymer surfaces is not fully understood, it is highly likely that the hydrophobic interaction between air bubbles and hydrophobic substrates plays a crucial role. From the perspective of thermodynamics, the air dissolution in water is entropically unfavorable, because the water molecules reorient around the dissolved air to preserve the hydrogen-bonding network. In the presence of a hydrophobic polymer surface, the dissolved air has a strong potential to adsorb onto the surface to minimize the disruption of the hydrogen-bonding network and reduce the entropy of the system,[46, 58] inducing the formation of INBs on the hydrophobic polymer surface. High-charge-density ion Na^+ has high affinity to water molecules and can significantly reduce the number of water molecules as the building unit for the cages for the dissolved air. As

a result, high NaCl concentration (e.g., 500 mM) would not only lower the air solubility in water, but also suppress the formation of the INBs on hydrophobic polymer surface, leading to an evident decrease in the size and number density of the INBs on PS surface.[36]

4.3.3. Effect of INBs on the interaction between air bubble and PS surface.

By correlating the AFM imaging results of the INBs and force measurements between air bubble probe and PS surface in various NaCl solutions, the effect of INBs on the bubble-PS interaction could be illustrated as shown in Figure 4.9. In 1 mM NaCl, the INBs covered ~ 41% of the PS surface (Figure 4.6A). Therefore, the bubble probe did not directly interact with the real PS but with the INBs formed on the PS surface. In 1 mM NaCl, the strong EDL repulsion with a Debye length of 9.6 nm dominated the interaction between the bubble probe and INBs on PS surface, which sustained a thin water film and inhibited the bubble probe attachment on PS. It is noted that the PS surface was found to be covered with INBs in 1 mM NaCl, thus the theoretically fitted surface potential value -85 ± 10 mV of PS in Figure 4.2A was the apparent surface potential of the PS surface with ~ 41% covered with INBs, not the pristine/bare PS. When the NaCl concentration increased to 100 mM, the number density of INBs increased while their size decreased (Figure 4.6B and Figure 4.9B), maintaining a surface coverage of INBs ~ 35% on PS. Although the EDL repulsion was suppressed in 100 mM NaCl, additional non-DLVO repulsion possibly arising from hydration interaction between the air bubble and the densely distributed INBs on the PS could stabilize the confined thin water film and prevent the bubble probe attachment on PS. With NaCl concentration further increased to 500 mM and 1000 mM, the formation of INBs on the PS surface was dramatically suppressed by the high salinity condition, leading to a much reduced surface coverage of the INBs ~ 7% (Figure 4.6C and

Figure 4.9C) and 0% (Figure 4.6D and Figure 4.9D) on the PS, respectively. Consequentially, the effect of INBs on the bubble-PS interaction could be almost neglected in 500 mM and 1000 mM NaCl, and thus the HB attraction with a decay length of 0.75 nm could overcome the repulsive VDW interaction, leading to the bubble attachment on the PS surface.
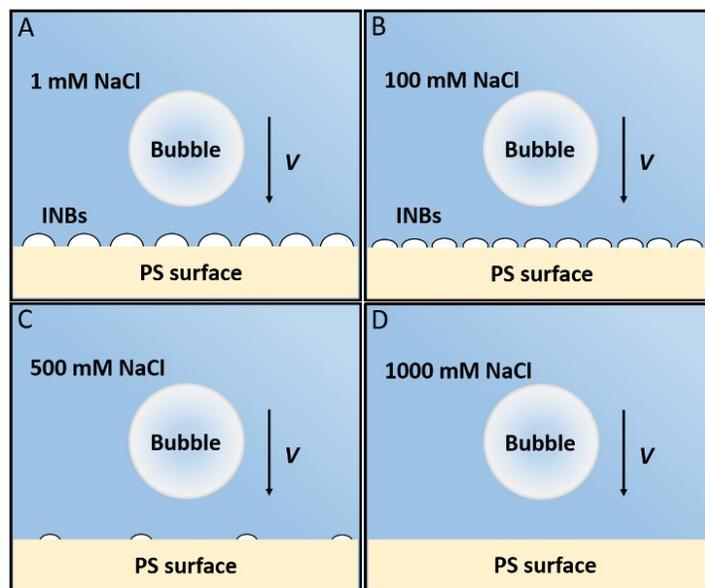
Figure 4.9. Schematic of the interactions between an air bubble probe and PS surface in aqueous solutions of different NaCl concentrations: (A) 1 mM, (B) 100 mM, (C) 500 mM, and (D) 1000 mM, repsectively.

4.4. Conclusions.

In this work, the interaction forces between air bubbles and hydrophobic PS surfaces in NaCl solutions were directly measured using a bubble probe AFM technique, and the measured forces were analyzed by a theoretical model based on Reynolds lubrication theory and augmented Young-Laplace equation including the influence of disjoining pressure. Although the measured force profiles could be reasonably described by the theoretical model in solutions of

both low (i.e., 1 mM NaCl) and high (i.e., 500 and 1000 mM Naco) salinity by assuming that the PS surface was a pristine/bare polymer surface, discrepancy was found between experiments and theoretical calculations in 100 mM NaCl which could not be described by the classical DLVO theory even including the effects of non-DLVO interactions (e.g., hydrophobic interaction). PeakForce quantitative nano-mechanics and tapping mode AFM imaging demonstrated that the above discrepancy was caused by the presence of interfacial nanobubbles on the hydrophobic PS surface. AFM imaging results further indicated that solution salinity could significantly affect the size and surface coverage of INBs on the PS surface, which were correlated to the surface force measurements. At low NaCl concentration (e.g., 1 mM), the strong EDL repulsion between air bubble probe and PS surface covered with INBs sustained a thin water film and inhibited the bubble probe attachment onto the PS surface. At medium NaCl concentration (e.g., 100 mM), although the EDL repulsion was much suppressed, a layer of INBs still existed on the PS surface that caused additional non-DLVO repulsion against the air bubble probe which stabilized the confined thin water film and inhibited bubble attachment. The origin of this non-DLVO repulsion remains to be further explored. At high NaCl concentration (e.g., 500 and 1000 mM) the INB formation (and its impact on the surface forces) and EDL repulsion were highly suppressed, and the bubble-PS attachment was attributed to the HB attraction with a decay length of $\sim 0.75 \pm 0.05$ nm between the air bubble probe and the PS surface. The results agree with our previous surface force measurements between two PS surfaces using a surface forces apparatus.[36] This work provides useful information regarding the interaction mechanism between air bubbles and hydrophobic polymer surfaces, as well as the influence of solution salinity and interfacial nanobubbles on the bubble-polymer interaction, with implications in related industrial and bioengineering applications.

4.5. References.

1.   Park, J. I.; Nie, Z.; Kumachev, A.; Abdelrahman, A. I.; Binks, B. P.; Stone, H. A.; Kumacheva, E. A microfluidic approach to chemically driven assembly of colloidal particles at gas–liquid interfaces. *Angew. Chem.* **2009,** *121*, 5404-5408.

2.   Khademhosseini, A.; Langer, R.; Borenstein, J.; Vacanti, J. P. Microscale technologies for tissue engineering and biology. *Proc. Natl. Acad. Sci. U. S. A.* **2006,** *103*, 2480-2487.

3.   Sanguansri, P.; Augustin, M. A. Nanoscale materials development–a food industry perspective. *Trends Food Sci. Technol.* **2006,** *17*, 547-556.

4.   Meyer, E. E.; Rosenberg, K. J.; Israelachvili, J. Recent progress in understanding hydrophobic interactions. *Proc. Natl. Acad. Sci. U. S. A.* **2006,** *103*, 15739-15746.

5.   Butt, H.-J. A technique for measuring the force between a colloidal particle in water and a bubble. *J. Colloid Interface Sci.* **1994,** *166*, 109-117.

6.   Fielden, M. L.; Hayes, R. A.; Ralston, J. Surface and capillary forces affecting air bubble-particle interactions in aqueous electrolyte. *Langmuir* **1996,** *12*, 3721-3727.

7.   Nguyen, A.; Nalaskowski, J.; Miller, J. A study of bubble–particle interaction using atomic force microscopy. *Miner. Eng.* **2003,** *16*, 1173-1181.

8.   Ducker, W. A.; Xu, Z.; Israelachvili, J. N. Measurements of hydrophobic and DLVO forces in bubble-surface interactions in aqueous solutions. *Langmuir* **1994,** *10*, 3279-3289.

9.   Wangsa-Wirawan, N.; Ikai, A.; O'Neill, B.; Middelberg, A. Measuring the interaction forces between protein inclusion bodies and an air bubble using an atomic force microscope. *Biotechnol. Prog.* **2001,** *17*, 963-969.

10.   Preuss, M.; Butt, H.-J. Direct measurement of particle-bubble interactions in aqueous electrolyte: Dependence on surfactant. *Langmuir* **1998,** *14*, 3164-3174.

11.   Ishida, N. Direct measurement of hydrophobic particle–bubble interactions in aqueous solutions by atomic force microscopy: effect of particle hydrophobicity. *Colloids Surf., A* **2007,** *300*, 293-299.

12.   Preuss, M.; Butt, H.-J. Measuring the contact angle of individual colloidal particles. *J. Colloid Interface Sci.* **1998,** *208*, 468-477.

13.   Vakarelski, I. U.; Lee, J.; Dagastine, R. R.; Chan, D. Y.; Stevens, G. W.; Grieser, F. Bubble colloidal AFM probes formed from ultrasonically generated bubbles. *Langmuir* **2008,** *24*, 603-605.

14.   Tabor, R. F.; Morfa, A. J.; Grieser, F.; Chan, D. Y.; Dagastine, R. R. Effect of gold oxide in measurements of colloidal force. *Langmuir* **2011,** *27*, 6026-6030.

15.   Tabor, R. F.; Manica, R.; Chan, D. Y.; Grieser, F.; Dagastine, R. R. Repulsive van der Waals forces in soft matter: why bubbles do not stick to walls. *Phys. Rev. Lett.* **2011,** *106*, 064501.

16.   Shi, C.; Chan, D. Y.; Liu, Q.; Zeng, H. Probing the hydrophobic interaction between air bubbles and partially hydrophobic surfaces using atomic force microscopy. *J. Phys. Chem. C* **2014,** *118*, 25000-25008.

17.   Xie, L.; Shi, C.; Wang, J.; Huang, J.; Lu, Q.; Liu, Q.; Zeng, H. Probing the Interaction between Air Bubble and Sphalerite Mineral Surface Using Atomic Force Microscope. *Langmuir* **2015,** *31*, 2438-2446.

18.   Chan, D. Y.; Klaseboer, E.; Manica, R. Film drainage and coalescence between deformable drops and bubbles. *Soft Matter* **2011,** *7*, 2235-2264.

19.   Manica, R.; Chan, D. Y. Drainage of the air–water–quartz film: experiments and theory. *Phys. Chem. Chem. Phys.* **2011,** *13*, 1434-1439.

20.   Shi, C.; Cui, X.; Xie, L.; Liu, Q.; Chan, D. Y.; Israelachvili, J. N.; Zeng, H. Measuring forces and spatiotemporal evolution of thin water films between an air bubble and solid surfaces of different hydrophobicity. *ACS Nano* **2014,** *9*, 95-104.

21.   Walczyk, W.; Schön, P. M.; Schönherr, H. The effect of PeakForce tapping mode AFM imaging on the apparent shape of surface nanobubbles. *J. Phys.: Condens. Matter* **2013,** *25*, 184005.

22.   Zhao, B.; Song, Y.; Wang, S.; Dai, B.; Zhang, L.; Dong, Y.; Lü, J.; Hu, J. Mechanical mapping of nanobubbles by PeakForce atomic force microscopy. *Soft Matter* **2013,** *9*, 8837-8843.

23.   Wang, X.; Zhao, B.; Ma, W.; Wang, Y.; Gao, X.; Tai, R.; Zhou, X.; Zhang, L. Interfacial Nanobubbles on Atomically Flat Substrates with Different Hydrophobicities. *ChemPhysChem* **2015,** *16*, 1003-1007.

24.   Simonsen, A. C.; Hansen, P. L.; Klösgen, B. Nanobubbles give evidence of incomplete wetting at a hydrophobic interface. *J. Colloid Interface Sci.* **2004,** *273*, 291-299.

25.   Hampton, M.; Nguyen, A. Nanobubbles and the nanobubble bridging capillary force. *Adv. Colloid Interface Sci.* **2010,** *154*, 30-55.

26.   Lohse, D.; Zhang, X. Surface nanobubbles and nanodroplets. *Rev. Mod. Phys.* **2015,** *87*, 981.

27.   Zhang, X. H.; Quinn, A.; Ducker, W. A. Nanobubbles at the interface between water and a hydrophobic solid. *Langmuir* **2008,** *24*, 4756-4764.

28.   Bhushan, B.; Jung, Y. C. Natural and biomimetic artificial surfaces for superhydrophobicity, self-cleaning, low adhesion, and drag reduction. *Prog. Mater Sci.* **2011,** *56*, 1-108.

29.   Weijs, J. H.; Lohse, D. Why surface nanobubbles live for hours. *Phys. Rev. Lett.* **2013,** *110*, 054501.

30.   Yang, J.; Duan, J.; Fornasiero, D.; Ralston, J. Very small bubble formation at the solid-water interface. *J. Phys. Chem. B* **2003,** *107*, 6139-6147.

31.   Ducker, W. A. Contact angle and stability of interfacial nanobubbles. *Langmuir* **2009,** *25*, 8907-8910.

32.   Brenner, M. P.; Lohse, D. Dynamic equilibrium mechanism for surface nanobubble stabilization. *Phys. Rev. Lett.* **2008,** *101*, 214505.

33.   Seddon, J. R.; Zandvliet, H. J.; Lohse, D. Knudsen gas provides nanobubble stability. *Phys. Rev. Lett.* **2011,** *107*, 116101.

34.   Attard, P. Bridging bubbles between hydrophobic surfaces. *Langmuir* **1996,** *12*, 1693-1695.

35.   Carambassis, A.; Jonker, L. C.; Attard, P.; Rutland, M. W. Forces measured between hydrophobic surfaces due to a submicroscopic bridging bubble. *Phys. Rev. Lett.* **1998,** *80*, 5357.

36.   Faghihnejad, A.; Zeng, H. Hydrophobic interactions between polymer surfaces: using polystyrene as a model system. *Soft Matter* **2012,** *8*, 2746-2759.

37.   Tyrrell, J. W.; Attard, P. Images of nanobubbles on hydrophobic surfaces and their interactions. *Phys. Rev. Lett.* **2001,** *87*, 176104.

38.   Ishida, N.; Sakamoto, M.; Miyahara, M.; Higashitani, K. Attraction between hydrophobic surfaces with and without gas phase. *Langmuir* **2000,** *16*, 5681-5687.

39.   Azadi, M.; Nguyen, A. V.; Yakubov, G. E. Attractive forces between hydrophobic solid surfaces measured by AFM on the first approach in salt solutions and in the presence of dissolved gases. *Langmuir* **2015,** *31*, 1941-1949.

40.   Carnie, S. L.; Chan, D. Y.; Lewis, C.; Manica, R.; Dagastine, R. R. Measurement of dynamical forces between deformable drops using the atomic force microscope. I. Theory. *Langmuir* **2005,** *21*, 2912-2922.

41.   Manor, O.; Vakarelski, I. U.; Stevens, G. W.; Grieser, F.; Dagastine, R. R.; Chan, D. Y. Dynamic forces between bubbles and surfaces and hydrodynamic boundary conditions. *Langmuir* **2008,** *24*, 11533-11543.

42.   Manor, O.; Vakarelski, I. U.; Tang, X.; O'Shea, S. J.; Stevens, G. W.; Grieser, F.; Dagastine, R. R.; Chan, D. Y. Hydrodynamic boundary conditions and dynamic forces between bubbles and surfaces. *Phys. Rev. Lett.* **2008,** *101*, 024501.

43.   Creux, P.; Lachaise, J.; Graciaa, A.; Beattie, J. K.; Djerdjev, A. M. Strong specific hydroxide ion binding at the pristine oil/water and air/water interfaces. *J. Phys. Chem. B* **2009,** *113*, 14146-14150.

44.   Tabor, R. F.; Chan, D. Y.; Grieser, F.; Dagastine, R. R. Anomalous Stability of Carbon Dioxide in pH-Controlled Bubble Coalescence. *Angew. Chem., Int. Ed.* **2011,** *50*, 3454-3456.

45.   Xu, R. Progress in nanoparticles characterization: Sizing and zeta potential measurement. *Particuology* **2008,** *6*, 112-115.

46.   Israelachvili, J. N. *Intermolecular and surface forces: revised third edition*; Academic press, 2011.

47.   Carrique, F.; Zurita, L.; Delgado, A. Dielectric relaxation in polystyrene suspensions. Effect of ionic strength. *Colloids Surf., A* **1994,** *92*, 9-21.

48. Carrique, F.; Zurita, L.; Delgado, A. Correlation of the dielectric and conductivity properties of polystyrene suspensions with zeta potential and electrolyte concentration. *J. Colloid Interface Sci.* **1994,** *166*, 128-132.

49. Wang, Y.; Bhushan, B.; Zhao, X. Nanoindents produced by nanobubbles on ultrathin polystyrene films in water. *Nanotechnology* **2008,** *20* , 045301.

50. Craig, V.; Ninham, B.; Pashley, R. Effect of electrolytes on bubble coalescence. *Nature* **1993,** *364*, 317-319.

51. Craig, V. S.; Ninham, B. W.; Pashley, R. M. The effect of electrolytes on bubble coalescence in water. *J. Phys. Chem.* **1993,** *97*, 10192-10197.

52. Clasohm, L. Y.; Vakarelski, I. U.; Dagastine, R. R.; Chan, D. Y.; Stevens, G. W.; Grieser, F. Anomalous pH dependent stability behavior of surfactant-free nonpolar oil drops in aqueous electrolyte solutions. *Langmuir* **2007,** *23*, 9335-9340.

53. Walczyk, W.; Schönherr, H. Characterization of the interaction between AFM tips and surface nanobubbles. *Langmuir* **2014,** *30*, 7112-7126.

54. Song, Y.; Zhao, B.; Zhang, L.; Lü, J.; Wang, S.; Dong, Y.; Hu, J. The Origin of the "Snap-In" in the Force Curve between AFM Probe and the Water/Gas Interface of Nanobubbles. *ChemPhysChem* **2014,** *15*, 492-499.

55. Li, D.; Jing, D.; Pan, Y.; Wang, W.; Zhao, X. Coalescence and stability analysis of surface nanobubbles on the polystyrene/water interface. *Langmuir* **2014,** *30*, 6079-6088.

56. Zhao, B.; Wang, X.; Song, Y.; Hu, J.; Lü, J.; Zhou, X.; Tai, R.; Zhang, X.; Zhang, L. Stiffness and evolution of interfacial micropancakes revealed by AFM quantitative nanomechanical imaging. *Phys. Chem. Chem. Phys.* **2015,** *17*, 13598-13605.

57.   Walczyk, W.; Schönherr, H. Dimensions and the Profile of Surface Nanobubbles: Tip–Nanobubble Interactions and Nanobubble Deformation in Atomic Force Microscopy. *Langmuir* **2014,** *30*, 11955-11965.

58.   Chandler, D. Interfaces and the driving force of hydrophobic assembly. *Nature* **2005,** *437*, 640-647.

Chapter 5   Probing Effect of Ion Specificity on Hydrophobic Interactions between Air Bubbles and Hydrophobic Polymers Using Bubble Probe AFM

5.1. Introduction

Hydrophobic polymers have been widely used in a variety of industrial and engineering applications, such as water-repellent protective coatings,[1] oil/water separation,[2] controlled gas transport,[3] and microfluidic devices,[4] owing to their unique interfacial properties including wettability and hydrophobicity. In most of these applications, hydrophobic (HB) interaction can be a decisive factor for achieving the targeted features and functionalities. It has been generally accepted that the intrinsic HB interaction could originate from the structuring effect of the water molecules at the hydrophobic interfaces.[5-6] Because of their weak interactions with the apposing hydrophobic surfaces, the interfacial water molecules are driven to rearrange into a more ordered hydrogen-bonding network as compared to those in the bulk, leading to a significant increase in the configurational entropy which is unfavorable in terms of thermodynamics. As a result, the hydrophobic substances in aqueous media have a strong tendency to aggregate together to minimize their surface area exposed to water, manifested as the attractive HB interaction.

Since the pioneering attempt by Israelachvili and Parsley who claimed that HB interaction decayed exponentially with separation,[7] considerable efforts, mainly through nano-mechanical techniques such as surface forces apparatus (SFA) and atomic force microscopy (AFM), have been devoted to experimentally quantifying the HB interactions of various material systems under different aqueous conditions.[8-12] However, up to date, only a few studies have been focused on the HB interactions involving hydrophobic polymers despite their extensive

application and great importance. For instance, the HB interactions between two chemisorbed poly (dimethylsiloxane) (PDMS) monolayers have been quantified using SFA and the measured interaction forces could be well interpreted by a general interaction potential model incorporating a non-dimensional Hydra parameter.[12] The interactions between two polystyrene (PS) surfaces in different electrolyte solutions have also been measured by SFA, which elucidated that ion specificity and concentration could change the gas solubility in water and thus affect the formation of interfacial nanobubbles and the force measurement results.[13] This result was supported by the following research in investigating the bubble-PS interactions in aqueous media via a bubble probe AFM technique, demonstrating that high salinity (i.e., 1000 mM) could effectively prevent the formation of nanobubbles and simplify the quantification of the intrinsic HB interactions between air bubbles and pristine PS surfaces.[14]

According to the previous reports, different ions can exhibit distinctive behaviors when interacting with some proteins and macromolecules carrying some special moieties such as aromatic components, charged groups or strong dipole moments, affecting the solubility and aggregation of these protein and macromolecules in aqueous environment.[15-17] Besides, a series of experimental and theoretical studies using simple hydrophobic self-assembled monolayers (SAMs) have revealed that some ions could be selectively adsorbed onto or repelled from neutral hydrophobic surfaces in aqueous media, depending on their inherent properties, which would interfere in the structuring of the interfacial water molecules and thus influence the range and magnitude of the intrinsic HB interactions.[18-21] Despite these insightful studies, further effort is still required to deeply and systematically probe the effects of ion specificity on the HB interactions involving hydrophobic polymers, which is of vital importance in improving the

fundamental understanding of the physical mechanism of HB interaction and providing theoretical guidance for practical applications.

In this work, a bubble probe AFM technique was applied to directly measure the interactions between air bubbles and three hydrophobic polymer surfaces with distinctive chemical compositions, i.e., polystyrene (PS), poly (methyl methacrylate) (PMMA), and polydimethylsiloxane (PDMS), in aqueous solutions containing different ions, aiming to illuminate how the ion specificity impacts the involved HB interactions. Air bubble was applied as the AFM probe not only because the bubble surface is atomically smooth and intrinsically hydrophobic,[22-24] which would facilitate the precise measurement and quantification of the involved HB interactions, but also because the hydrophobic interactions between air bubbles and hydrophobic polymers are of great importance in many bioengineering and industrial applications, such as controlled drug delivery,[25] ultrasound imaging contrast agent,[26] gas evolution reaction[27] and drag reduction.[28] By virtue of a theoretical model based on Reynolds lubrication theory and augmented Young-Laplace equation incorporating the effects of disjoining pressure, the measured interaction forces were analyzed and the bubble-polymer HB interactions in different electrolyte solutions were precisely quantified, shedding novel light on the effects of ion specificity on the HB interactions involving hydrophobic polymers.

5.2. Experimental section.

5.2.1. Materials.

Polystyrene (PS, $M_n \sim 112,500$ g/mol, $M_w/M_n \approx 1.05$) and poly (methyl methacrylate) (PMMA, $M_n \sim 110,000$ g/mol, $M_w/M_n \approx 1.09$) were purchased from Polymer Source Inc., Canada. monoglycidyl ether-terminated poly (dimethylsiloxane) (PDMS, $M_n \sim 1,000$ g/mol) was

purchased from Gelest Inc., USA. (3-aminopropyl) triethoxysilane (APTES, 99%), 1-decanethiol (96%), reagent alcohol (anhydrous, $\leq$ 0.005% water), and sodium iodide (NaI, $\geq$ 99.5%) were purchased from Sigma-Aldrich, Canada. Sodium chloride (NaCl, $\geq$ 99.0%), potassium chloride (KCl, $\geq$ 99.0%), lithium chloride (LiCl, $\geq$ 98.5%), ammonium chloride (NH$_4$Cl, $\geq$ 99.5%), sodium fluoride (NaF, 99.99%), magnesium chloride (MgCl$_2$, $\geq$ 99.0%), calcium chloride dihydrate (CaCl$_2$·2H$_2$O, $\geq$ 99.5%), and toluene (HPLC grade, $\geq$ 99.8%) were purchased from Fisher Scientific, Canada. All the chemicals were used as received. The PS and PMMA solutions were prepared by dissolving the corresponding polymers in toluene at concentration of 1 wt%. All the electrolyte solutions were prepared by dissolving the corresponding electrolytes in Milli-Q water with a resistance of $\geq$ 18.2 MΩ cm at a concentration of 1000 mM.

5.2.2. Preparation of hydrophobic polymer surfaces.

The PS and PMMA surfaces were prepared by spin-coating 3 drops ($\sim$ 0.15 ml) of the corresponding polymer solutions on pre-cleaned silica wafers (1 $\times$ 1 cm^2) at a speed of 2000 rpm. Afterwards, the prepared polymer surfaces were placed in a vacuum oven at room temperature overnight ($\sim$ 12 h) to eliminate the residual solvent. The PDMS surface was prepared via a click reaction which have been elaborated in the previous study.[12, 29] The silica wafer (1 $\times$ 1 cm^2) was first treated by UV/Ozone plasma for 30 min and then modified by APTES through a vapor deposition process under vacuum at room temperature for $\sim$ 48 h. After being annealed at 60 ^{o}C for $\sim$ 12 h, rinsed with toluene, and dried with nitrogen stream, the amine-terminated wafer was immediately immersed in pure monoglycidyl ether-terminated PDMS liquid and placed in a vacuum oven at 80 ^{o}C for 60 h. Then, the PDMS-silica wafer was rinsed with toluene thoroughly to remove the physisorbed PDMS molecules and dried with nitrogen completely. After the

preparation procedures, all the polymer surfaces were kept under vacuum for further use. The morphology of the polymer surfaces in 1000 mM electrolyte solution was characterized by AFM tapping model imaging through an MPF-3D AFM system (Asylum Research, Santa Barbara, USA). The surface hydrophobicity was evaluated by a contact angle tensiometer (Ramé-hart Instrument Company, USA), and the thickness of the polymer layers was measured by ellipsometry (Sopra GESP-5 spectroscopic ellipsometer, France).

5.2.3. Force measurement using bubble probe AFM.

The interactions between air bubbles and these three hydrophobic polymer surfaces in 1000 mM solutions containing different ions were directly measured via a bubble probe AFM based on the MPF-3D AFM system equipped with an inverted microscope (Nikon Ti-U). The experimental setup, typical image of a bubble probe and the involved geometric conditions are shown in Figures 5.1A, 5.1B and 5.1C, respectively, and the detailed information on the bubble probe AFM technique have been elaborated in the previous studies.[8, 30-32] A customized rectangular silicon tipless cantilever (400 × 70 ×2 μm) was applied in this work, which has a circular gold patch (diameter ~ 65 μm, thickness ~ 30 nm) at its front end. The cantilever's spring constant was determined using Hutter-Bechhoefer method.[33] Prior to the AFM force measurement, the gold patch was strongly hydrophobized by immersing the tipless cantilever in an ethanoic solution containing 10 mM 1-decanethiol overnight, in order to make it favorable to anchor the air bubble.[34-35] Air bubbles were generated through an ultra-sharp glass pipet and immobilized on the mildly hydrophobic glass slide of the AFM fluid cell which was filled with the aqueous solution. Afterwards, the cantilever was lowered down slowly to pick up an applicable air bubble (radius ~ 40-100 nm), and then lifted carefully to detach the bubble from

the glass slide. Subsequently, the bubble probe was manipulated to interact with the polymer surface which had been previously placed in the fluid cell. The interaction velocity was fixed as 1 μm/s to minimize the hydrodynamic force and highlight the effects of surface interactions. The interaction force and cantilever deformation were recorded simultaneously by the AFM software.
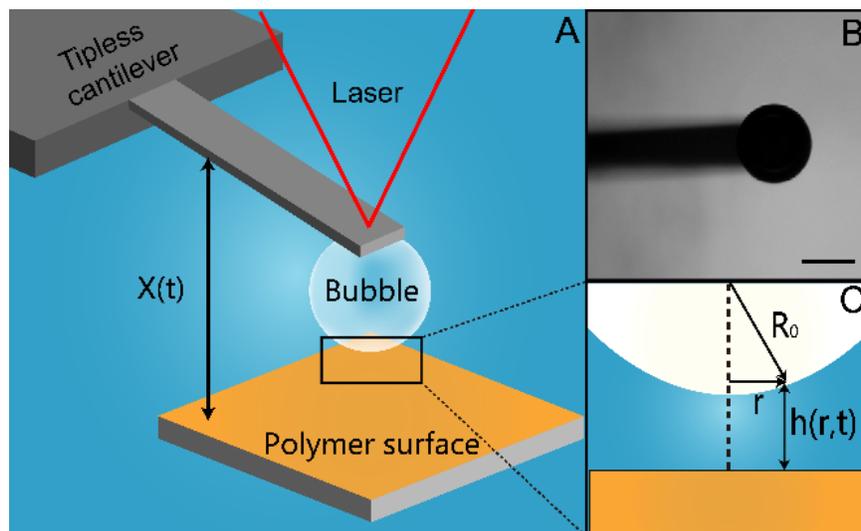
Figure 5.1. AFM force measurement using bubble probe technique. (A) Schematic illustration of the experimental setup. (B) Typical image of an air bubble anchored on a hydrophobized tipless cantilever. The scale bare is 100 μm. (C) The geometric conditions during the interaction process.

5.2.4 Theoretical model

A Stokes-Reynolds-Young-Laplace model incorporating the effect of disjoining pressure arising from surface interactions was applied to quantitatively analyze the measured interaction forces under the corresponding aqueous conditions. Assuming tangentially immobile boundary conditions at air/water and solid/water interfaces, the drainage process of the thin water film confined between the bubble and the surface is described by Reynolds lubrication theory (equation 5.1),[36-38]

$$\frac{\partial h(r,t)}{\partial t} = \frac{1}{12\mu r}\frac{\partial}{\partial r}\left(rh^3\frac{\partial p(r,t)}{\partial r}\right) \tag{5.1}$$

where μ is the viscosity of the aqueous solution, $p(r,t)$ is the excessive hydrodynamic pressure relative to the bulk solution, $h(r,t)$ denotes the thickness of the thin water film, and r is the radical coordinate.

Different from rigid solids, the bubble probe would change its shape in response to external forces, and the deformation during the AFM measurement process could be calculated by the augmented Young-Laplace equation shown in equation 5.2,[8-9, 32, 34, 38]

$$\frac{\gamma}{r}\frac{\partial}{\partial r}\left(r\frac{\partial h(r,t)}{\partial r}\right) = \frac{2\gamma}{R_0} - p(r,t) - \Pi\left[h(r,t)\right] \tag{5.2}$$

where γ is the air/solution interfacial tension, R_0 is the bubble radius, and $\Pi[(h(r,t)]$ is the overall disjoining pressure of surface interactions. In this work, electrical double-layer (EDL) interaction was almost screened due to the high salinity and could be considered negligible during the interaction process, and the van der Waals (VDW) and hydrophobic (HB) interactions made major contributions to the overall disjoining pressure, which are quantified using equations 5.3 and 5.4, respectively, where A_H is the Hamaker constant for the air-water-polymer system, D_0 is the decay length of HB interaction, and θ_c is the static water contact angle (WCA) on the polymer surface.[8-9, 14, 32, 39]

$$\Pi_{VDW}[h(r,t)] = -\frac{A_H}{6\pi h^3(r,t)} \tag{5.3}$$

$$\Pi_{HB}[h(r,t)] = -\frac{\gamma(1-\cos\theta_c)}{D_0}\exp\left(-\frac{h(r,t)}{D_0}\right) \tag{5.4}$$

The overall interaction force $F(t)$ experienced by the AFM tipless cantilever is described by Equation 5.5,

$$F(t) = 2\pi \int_0^{r_{max}} \left\{ p(r,t) + \Pi \left[h(r,t) \right] \right\} r dr \tag{5.5}$$

in which r_{max} denotes the range where most contribution to the overall force is included.

5.3. Results and discussion.

5.3.1. Characterization of the prepared polymer surfaces.

In an effort to confirm that the prepared polymer surfaces were applicable for the AFM force measurement, the topography of the prepared PS, PMMA, and PDMS surfaces in 1000 mM electrolyte solution was characterized by AFM tapping mode imaging and presented in Figures5.2A, 5.2B and 5.2C, respectively. It is clear that all the polymer surfaces were fairly smooth with root-mean-square (RMS) roughness of $\sim 0.30 \pm 0.05$ nm. More importantly, they were pristine and free of interfacial nanobubbles in aqueous solution at 1000 mM salinity, which would contribute to precise quantification of the involved surface interactions, especially the intrinsic HB interactions between the air bubbles and the polymer surfaces. The AFM imaging results are in good consistence with our previous work which verified that high salinity could sufficiently suppress the formation of interfacial nanobubbles.[13-14] The static WCA θ_c on the polymer surfaces was also measured and displayed in Figures 5.2D, 5.2E and 5.2F, showing $\sim$ 90°, 75° and 103° for PS, PMMA and PDMS surfaces, respectively. The thickness of the PS, PMMA and PDMS surfaces was measured to be ~ 20.0 nm, 20.0 nm and 1.5 nm, respectively.
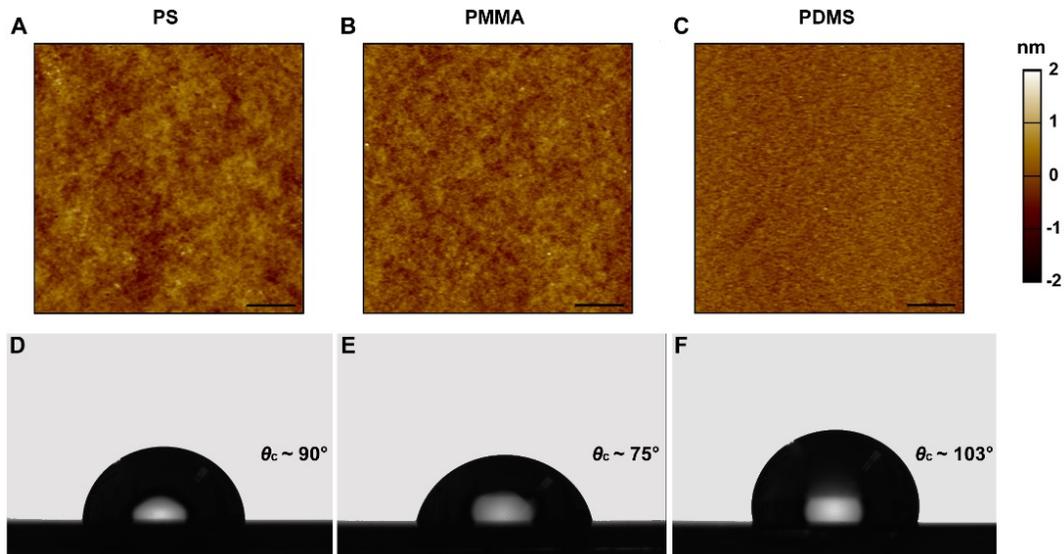
Figure 5.2. (A, B and C) AFM topographic images of the prepared PS, PMMA, and PDMS surfaces in 1000 M electrolyte solution, respectively. The scale bar is 1 μm. (D, E and F) Images of static WCA on the PS, PMMA and PDMS surfaces in air, respectively. The volume of the water droplet is ~ 5 μl.

5.3.2. Interactions between air bubbles and polymer surfaces in presence of various cations.

To begin with, the interactions between air bubbles and PS surfaces in aqueous solutions containing various cations (salinity ~ 1000 mM) were investigated. Figure 5.3A illustrates the measured interaction force (blue symbols) and theoretically fitting result (red curve) in 1000 mM NaCl. As the bubble probe moved towards the polymer surface, a repulsive feature appeared in the force curve, which could arise from the hydrodynamic and VDW repulsions. The following sudden "jump-in" behavior indicated that the air bubble attached onto the PS surface with the bubble further approaching, which was also observed from the integrated top-view camera. Considering that in 1000 mM NaCl the VDW interaction between air bubble and PS kept repulsive (A_H ~ -2.18×10^{-20} J), it is the attractive HB interaction that was strong enough to

conquer the VDW repulsion, rupture the thin water film and trigger the bubble attachment eventually. According to the theoretically modeling result, the HB interaction between air bubble and PS surface in 1000 mM NaCl was found to decay exponentially with a characteristic decay length $D_0 \sim 0.75 \pm 0.05$ nm, equal to the previously reported value.[14] Figure 5.3B displays the theoretically reconstructed disjoining pressure curves of the involved surface interactions, illustrating that the strong HB attraction dominated the bubble-PS interaction. The bubble attachment should occur at a critical separation ~ 7.3 nm (consistent with the minimal separation before bubble attachment calculated through the theoretical model) where the attractive overall disjoining pressure just exceeded the Laplace pressure inside the bubble. The bubble profile at the minimal separation was also calculated and shown in Figure 5.3C, and the "pimple" shape suggested that the central part of the air bubble was strongly attracted towards the hydrophobic PS surface. Besides, the air bubble could not be picked up by retracting the tipless cantilever, which indicated a strong adhesion between the air bubble and the PS surface.
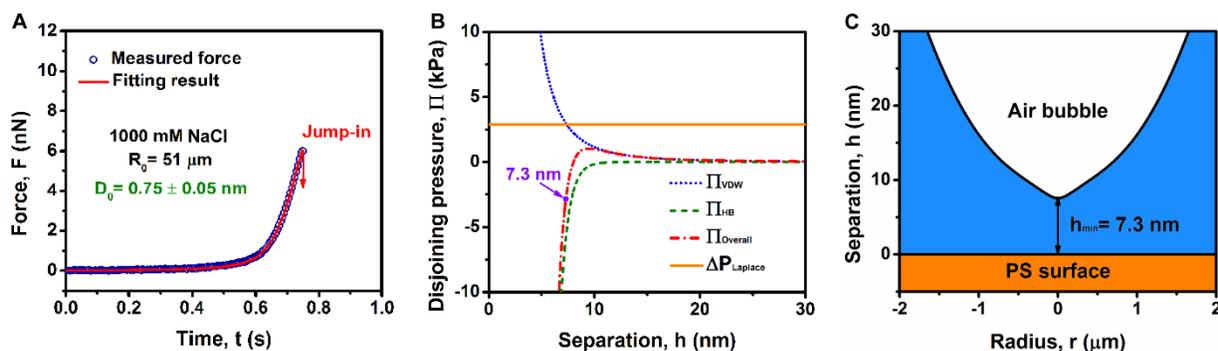
Figure 5.3. Interaction between an air bubble (radius ~ 51 μm) and a hydrophobic PS surface at velocity of 1 μm/s in 1000 mM NaCl. (A) Measured interaction force (blue symbols) and theoretically fitting result (red curve), respectively. (B) Theoretically reconstructed disjoining pressure curves of the involved surface interactions. (C) Calculated bubble profile at the minimal separation before bubble attachment.

Applying the similar method, the bubble-PS interactions in aqueous solutions containing 1000 mM various cations were also quantitatively investigated. It was found that the force curve of the bubble-PS interaction in 1000 mM LiCl (Figure 5.4A) was similar to that in the case of NaCl, and more importantly, the theoretically fitting result could also be in excellent agreement with the measured interaction force with $D_0 \sim 0.75 \pm 0.05$ nm which was equal to that in NaCl. However, when the cation was changed to K^+ and NH_4^+, the fitted value of D_0 was found to decline to $\sim 0.60 \pm 0.05$ nm (Figures 5.4B and 5.4C), suggesting an apparent decrease in the range of the HB interaction between the air bubble and the PS surface. On the basis of these results, it can be inferred that the cation specificity should play an important role in modulating the HB interactions between air bubbles and PS surfaces in electrolyte solutions. To further confirm this specific cation effect, the force measurement of the bubble-PS interactions in aqueous solutions containing other cations, including $N(CH_3)_4^+$, Mg^{2+} and Ca^{2+}, were also conducted using bubble probe AFM technique. The involved HB interactions in all the cases were quantified based on the theoretical model, and the corresponding values of D_0 along with some principal parameters of all the applied cations, including ionic radius (r), width of hydration shell (Δr), and molar hydration energy ($\Delta_{hyd}G^*$) are listed in Table 5.1.[40] Interestingly, for the cases of Mg^{2+} and Ca^{2+} with relatively higher charge density, D_0 was theoretically fitted to be $\sim 0.75 \pm 0.05$ nm, consistent with that in the case of Li^+ or Na^+; whereas the fitted D_0 was $\sim 0.60 \pm 0.05$ nm for the bubble-PS HB interaction in solution of $N(CH_3)_4^+$ whose charge density is relatively lower. To gain more insight, a solution containing a mixture of NH_4^+ and Na^+ (molar ratio $\sim 1: 4$) was applied as the aqueous environment, and the theoretical fitting result could agree well with the experimentally measured force applying $D_0 \sim 0.60 \pm 0.05$ nm, suggesting that

the introduction of the cation with low charge density could effectively reduce the range of the HB interactions between air bubbles and PS surfaces in aqueous media.
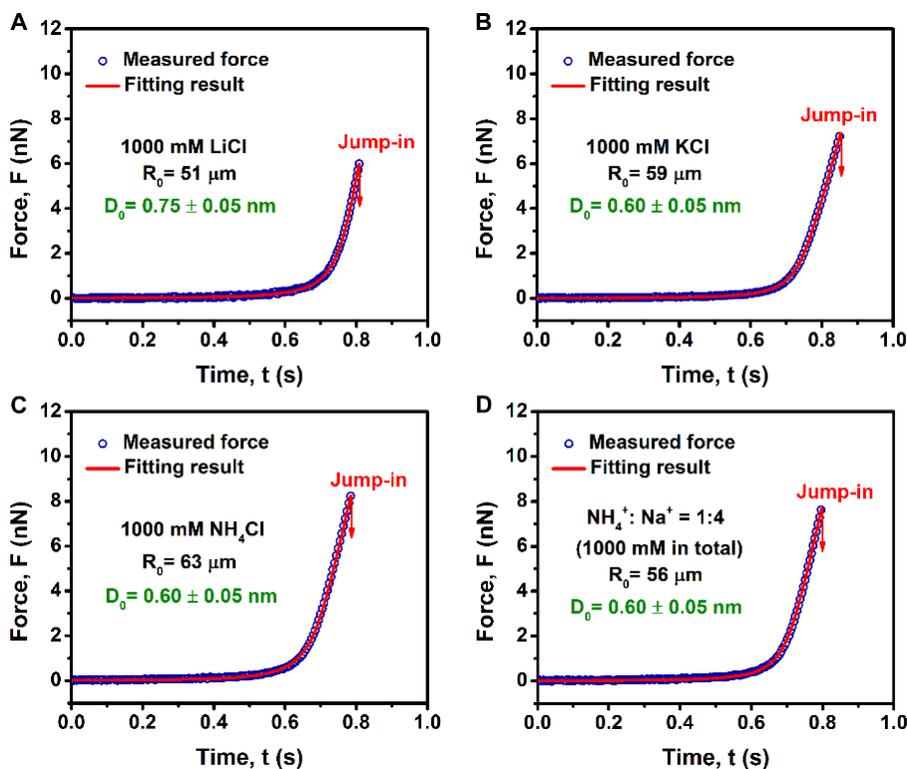
Figure 5.4. Interactions between air bubbles (radius ~ 51 μm, 59 μm, 63 μm and 56 μm, respectively) and PS surfaces at velocity of 1 μm/s in 1000 mM electrolyte solutions containing various cations: (A) LiCl, (B) KCl, (C) NH₄Cl, and (D) NH₄Cl/NaCl (1:4), respectively.

It has been previously reported that the water molecules in proximity to the hydrophobic surface would reorient and reorganize into a more ordered hydrogen bonding network as compared to those in the bulk, and the degree of this ordering effect could significantly influence the range of the HB interaction.[5, 12, 22, 41-42] As a deduction, this striking cation-dependence of the bubble-PS HB interactions should be highly associated with the specific interactions between the electron-rich pendant aromatic groups (i.e., benzene rings in this work) and the adjacent cations, the so-called "cation-π interactions", and the selective adsorption of the cations to the PS surface

would give rise to the difference in the degree of the water structuring effects and the range of the bubble-PS HB interactions. The cations are well hydrated by neighbouring water molecules in aqueous environment, leading to a desolvation penalty for cation-π interactions. As a consequence, the cations in aqueous media would selectively bind to the aromatic benzene pendant groups of the PS surface depending on their hydration degree, as illustrated in Figure 5. Therefore, even though the smaller cations (e.g. Li^+ and Na^+) have stronger charge-quadrupole interactions in gas phase due to their higher charge density,[43-44] they possess larger hydration shells which build up higher desolvation energy barriers and screen the cation-π interactions. On the contrary, the larger cations with relatively lower charge density such as NH_4^+ and K^+ bear smaller hydration shells, pay lower desolvation energy cost for the cation-π interactions and hence show higher affinity for the aromatic benzene groups.[45-46] As reported in the previous experimental force measurement and theoretical simulation studies, the cation-π binding capacities in aqueous media follow the order: $N(CH_3)_4^+$, NH_4^+, K^+ >> Na^+, Li^+,[47-48] which provides convincing explanation for the results of the quantification of the HB interactions between air bubbles and PS surfaces. Because the smaller cations (i.e., Na^+, Li^+ Mg^{2+} and Ca^+) cannot be adsorbed onto the aromatic benzene pendant groups, their presence in the aqueous media have little effect on the water structuring effect in proximity to the hydrophobic PS surfaces, which could be responsible for the relatively longer-ranged bubble-PS HB interactions ($D_0 \sim 0.75$ nm); in contrast, the spontaneous adsorption of the larger hydrated cations (i.e., K^+, NH_4^+ and $N(CH_3)_4^+$) onto the PS surfaces due to the cation-π interactions could disrupt the original ordered structure of the interfacial water molecules and shorten the range of the bubble-PS HB interactions ($D_0 \sim 0.60$ nm), as described in Figure 5.5.
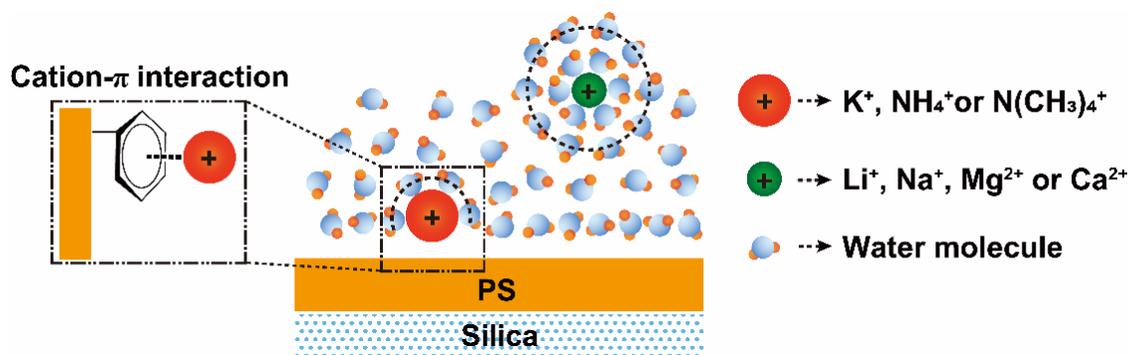
Figure 5.5. Schematic diagram of the interactions between different hydrated cations and the aromatic PS surface in aqueous environment and the effect of cation-π interactions on the structure of the interfacial water molecules.

Table 5.1. Parameters of the Applied Cations and the Decay length of the Bubble-PS HB Interactions under the Corresponding Aqueous Environment.

Cation	r (nm)	Δr (nm)	$\Delta_{hyd}G^*$ (kJ/mol)	D_0 (nm)
$N(CH_3)_4^+$	0.280	0.014	-160	0.60
NH_4^+	0.148	0.065	-285	0.60
K^+	0.138	0.074	-295	0.60
Na^+	0.102	0.116	-365	0.75
Li^+	0.069	0.172	-475	0.75
Mg^{2+}	0.072	0.227	-1830	0.75
Ca^{2+}	0.100	0.171	-1505	0.75

To further probe the effect of cation specificity on the HB interactions between air bubbles and polymer surfaces, another two types of polymers, the acrylate PMMA and silicone PDMS surfaces, were also applied as the model hydrophobic materials in this work. Figures 5.6A and 5.6B show the measured force curves and the theoretically fitting results of the bubble-PMMA and bubble-PDMS interactions in 1000 mM NaCl, respectively, and the decay length of the HB interaction D_0 was determined to be ~ 0.63 ± 0.03 nm and ~ 0.72 ± 0.03 nm, respectively. More importantly, it was found that the cation specificity appeared to have no obvious effect on the HB interactions between air bubbles and these two hydrophobic polymers, which was totally different from the cases of the aromatic PS surfaces. The measured interaction forces in 1000 mM LiCl, KCl and NH_4Cl aqueous solutions exhibited similar behaviors, and notably, the fitted D_0 remained almost constant for the bubble-PMMA and bubble-PDMS HB interactions in these three solutions. On the basis of these results, it could be implied that no specific interactions exist between the cations and the PMMA and PDMS surfaces, and the original ordered structure of the interfacial water molecules would not suffer from the disruption caused by the presence of different hydrated cations. This result agreed well with the previous research in the quantification of the HB interaction between two alkanethiol SAMs which demonstrated that the cation specificity could hardly impact the the involved HB interactions if there is no selective binding of cations to the hydrocarbon chains that would disturb the water structuring effect at the hydrophobic interfaces.[21]
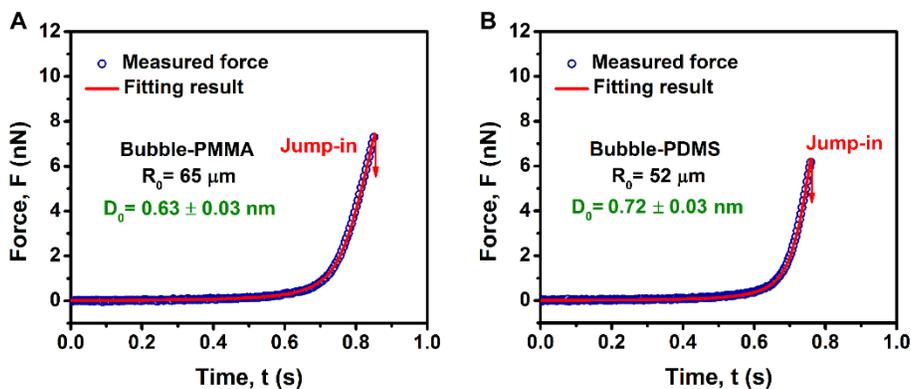
Figure 5.6. Interaction between air bubbles (radius ~ 65 μm and 52 μm, respectively) and polymer surfaces at velocity of 1 μm/s in 1000 mM NaCl: (A) bubble-PMMA and (B) bubble-PDMS interactions, respectively.

It should be noted that, the decay length of the HB interactions between the air bubble and the polymer surface was not completely identical for the cases involving PS, PMMA and PDMS surfaces, ranging from ~ 0.60 nm to ~ 0.75 nm. Such a discrepancy in the range of HB interactions, small but cannot be neglected, may reflect that the degree of the water structuring effect may vary at different polymer/water interfaces, which could root in the difference in the intensity of the interactions between interfacial water molecules and different pendant groups of the polymers. Furthermore, the obtained D_0 values of the HB interactions between air bubbles and polymer surfaces were found to be relatively lower than those between air bubbles and hydrophobic octadecyltrichlorosilane (OTS) monolayers (~ 0.8 nm - 1.0 nm),[8, 14, 49] but higher than that between two perfluoronated oil droplets. (~ 0.3 nm).[11] This remarkable divergence could also be attributed to the variation in the ordering degree of the water molecules at different hydrophobic interfaces. Being incapable of forming hydrogen bonds or electrostatically interact with the interfacial water molecules, the hydrophobic surface would impose a physical restriction which forces the apposing water molecules to change their configuration and rearrange into an

ordered hydrogen bonding network. Such physical restriction could be more intensive at a rigid, thermodynamically immobile hydrophobic interface, so that the interfacial water molecules tend to form a more ordered structure as compared to those at a soft, thermodynamically flexible interface which with a relaxed physical restriction.[5, 12] Several relevant sum frequency generation (SFG) studies have also demonstrated that the degree of water structuring effect is indispensable to the rigidity of the hydrophobic surfaces, reporting that the water molecules would exhibit a more ordered ice-like structure when facing a rigid monolayer composed of an array of densely packed and highly oriented hydrocarbon chains, whereas the water structure would be less ordered at a deformable interface oil/water interface.[22, 42, 50] In this work, the applied amorphous polymer thin films can exhibit enhanced mobility at the interfaces,[51-54] and thus the surface-induced physical restriction that orderly reorganizes the interfacial water molecules would be relaxed to an intermediate degree between that of the rigid closely-packed hydrocarbon monolayer and that of the deformable pure liquid surface. As mentioned before, the degree of the water structuring effect at hydrophobic interfaces could be a crucial factor in determining the range of HB interactions, and consequently, the HB interactions between air bubbles and amorphous polymer surfaces would decay exponentially with a moderate D_0.

5.3.3. Interactions between air bubbles and polymer surfaces in presence of various anions.

It has been claimed that the anions could also be preferentially adsorbed onto hydrophobic SAM surfaces in aqueous environment, which would substantially vary the strength of the HB interactions. Aiming to get a comprehensive understanding of the specific ion effects, the interactions between air bubbles and hydrophobic polymers in aqueous solutions containing different anions were also measured using bubble probe AFM and analyzed through the

theoretical model. The principal parameters of the anions applied in this work are summarized in Table 5.2.[40] Figures 5.7A and 5.7B present the AFM force measurement and theoretically fitting results of the bubble-PS interactions at velocity of 1 μm/s in 1000 mM NaF and NaI, respectively, showing no obvious difference in these force curves which could be well fitted by the theoretical model applying a constant $D_0 \sim 0.75 \pm 0.05$ nm equal to that in 1000 mM NaCl. This uniformity in the range of the bubble-PS HB interactions in the presence of various anions may indicate that the anions could not be selectively adsorbed onto the aromatic PS surface owing to the possible repulsion between the hydrated anions and the electron-rich benzene rings, and in consequence, the original water structuring effect near the hydrophobic PS surface should be protected from the disruption caused by the anions in the aqueous media.

Table 5.2. Principal Parameters of the Applied Anions.

Anion	r (nm)	Δr (nm)	$\Delta_{hyd}G^*$ (kJ/mol)
F^-	0.133	0.079	-465
Cl^-	0.181	0.043	-340
I^-	0.220	0.026	-275
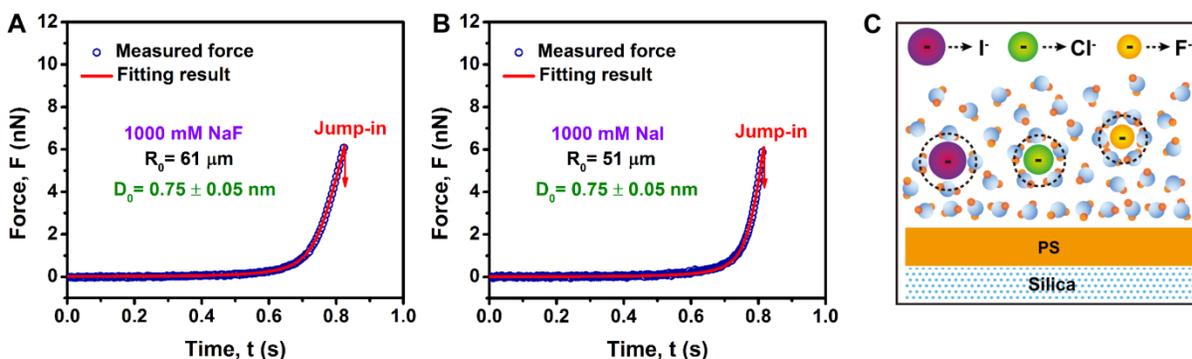
Figure 5.7. (A and B) Interactions between air bubbles (radius ~ 61 μm and 51 μm, respectively) and PS surfaces at velocity of 1 μm/s in 1000 mM NaF and NaI, respectively. (C) Schematic illustration of the non-adsorption of anions onto the PS surfaces.

However, it is impressive to find that the anion specificity appeared to be critical in modulating the HB interactions when it came to the cases involving the PMMA and PDMS surfaces, as shown in Figure 5.8. As compared with the cases of NaF and NaCl, the theoretically fitted decay length D_0 1000 mM NaI decreased from ~ 0.63 ± 0.03 nm to ~ 0.50 ± 0.02 nm for the bubble-PMMA HB interaction, and from 0.73 ± 0.03 nm to 0.59 ± 0.02 nm for the bubble-PDMS HB interaction, respectively. This noticeable variation in the range of the bubble-polymer HB interactions could be attributed to that the preferential adsorption of the heavier halide anions I⁻ onto the hydrophobic polymer surfaces would disorder the structure of the interfacial water molecules and then shorten the range of the HB interactions, while the lighter anions F⁻ and Cl⁻ should be kept away from the hydrophobic polymer surfaces because their presence in the aqueous environment had no detectable effect on the bubble-polymer HB interactions. Identical conclusions have been proposed in several previous MD simulation and experimental studies applying other model hydrophobic materials.[19-21]
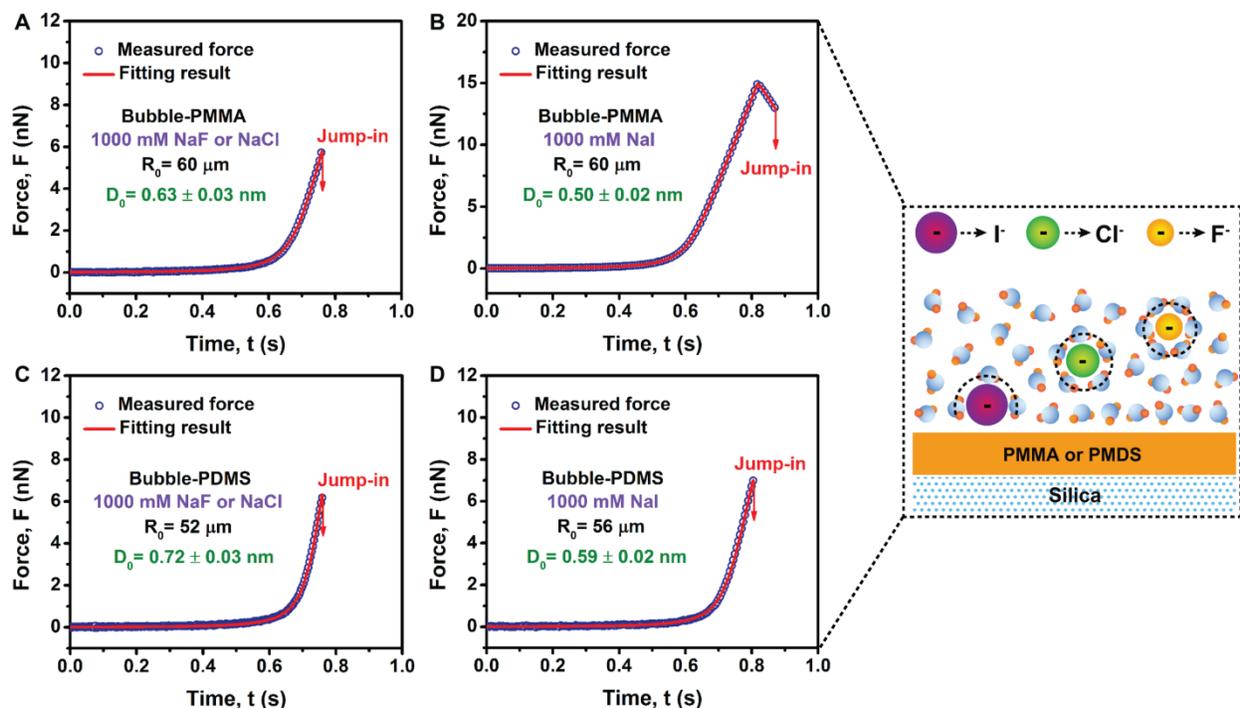
Figure 5.8. Interactions between air bubbles and polymer surfaces at velocity of 1 μm/s in aqueous solutions. (A and B) Bubble-PMMA interactions in 1000 mM NaF (or NaCl) and NaI, respectively. (C and D) Bubble-PDMS interactions in 1000 mM NaF (or NaCl) and NaI, respectively. (E) Schematic illustration of the selective adsorption of anions onto PMMA or PDMS surface.

5.4. Conclusion.

In this work, the hydrophobic (HB) interactions between air bubbles and three representative hydrophobic polymer surfaces, i.e., polystyrene (PS), poly (methyl methacrylate) (PMMA), and polydimethylsiloxane (PDMS), in aqueous environment containing various ions were quantified by coupling bubble probe AFM technique with theoretical analysis through a Stokes-Reynolds-Young-Laplace model. It was found that the interactions between some specific ions and the polymer surfaces could play a key role in modulating the HB interactions.

The decay length of the bubble-PS HB interaction D_0 remained $\sim 0.75 \pm 0.05$ nm in solutions containing 1000 mM larger cations such as Li^+, Na^+ Mg^{2+} and Ca^{2+}, which decreased to $\sim 0.60 \pm 0.05$ nm when the cation was changed to those smaller cations such as Na^+, K^+, NH_4^+ and $N(CH_3)_4^+$. This phenomenon was attributed to that the specific cation-π interactions led to the selective adsorption of the cations with relatively lower charge density and less desolvation penalty onto the aromatic PS surface, which disrupted the water structuring effect at the hydrophobic interface and shortened the range the bubble-PS HB interactions. Nonetheless, varying the anion type had no measurable effect on the bubble-PS HB interaction, with D_0 remaining 0.75 ± 0.05 nm across the cases of F^-, Cl^- and I^-, which implied that the anions cannot bind to the PS surface. On the contrary, the anion specificity, rather than the cation specificity, can affect the bubble-PMMA and bubble-PDMS HB interactions. D_0 was determined to be $\sim 0.63 \pm 0.03$ nm and $\sim 0.72 \pm 0.03$ nm for the bubble-PMMA and bubble-PDMS HB interactions, respectively, in 1000 mM F^- or Cl^-, regardless of the applied cations, indicating no specific interactions between cations and these two polymers; however, D_0 decreased to 0.50 ± 0.02 nm and $\sim 0.59 \pm 0.02$ nm, respectively, when the anion was switched to I^-, which may suggest that the heavier halide I^- would preferentially bind to the PMMA and PDMS surfaces, disordering the structure of the interfacial water molecules and reducing the range of the HB interactions. Our results provided novel insights into the effect of ion specificity on the hydrophobic interactions involving polymer surfaces and contributed to an improved understanding of the physical mechanism of the HB interaction.

5.5. References.

1.   Cao, M.; Guo, D.; Yu, C.; Li, K.; Liu, M.; Jiang, L., Water-Repellent Properties of Superhydrophobic and Lubricant-Infused "Slippery" Surfaces: A Brief Study on the Functions and Applications. *ACS Appl. Mater. Interfaces* **2015**, *8*, 3615-3623.

2.   Gu, J.; Xiao, P.; Chen, J.; Zhang, J.; Huang, Y.; Chen, T., Janus Polymer/Carbon Nanotube Hybrid Membranes for Oil/Water Separation. *ACS Appl. Mater. Interfaces* **2014**, *6*, 16204-16209.

3.   Yu, C.; Zhu, X.; Li, K.; Cao, M.; Jiang, L., Manipulating Bubbles in Aqueous Environment Via a Lubricant-Infused Slippery Surface. *Adv. Funct. Mater.* **2017**.

4.   Park, J. I.; Nie, Z.; Kumachev, A.; Abdelrahman, A. I.; Binks, B. P.; Stone, H. A.; Kumacheva, E., A Microfluidic Approach to Chemically Driven Assembly of Colloidal Particles at Gas–Liquid Interfaces. *Angew. Chem.* **2009**, *121*, 5404-5408.

5.   Zeng, H.; Shi, C.; Huang, J.; Li, L.; Liu, G.; Zhong, H., Recent Experimental Advances on Hydrophobic Interactions at Solid/Water and Fluid/Water Interfaces. *Biointerphases* **2016**, *11*, 018903.

6.   Chandler, D., Interfaces and the Driving Force of Hydrophobic Assembly. *Nature* **2005**, *437*, 640-647.

7.   Israelachvili, J.; Pashley, R., The Hydrophobic Interaction Is Long Range, Decaying Exponentially with Distance. *Nature* **1982**, *300*, 341-342.

8.   Shi, C.; Cui, X.; Xie, L.; Liu, Q.; Chan, D. Y.; Israelachvili, J. N.; Zeng, H., Measuring Forces and Spatiotemporal Evolution of Thin Water Films between an Air Bubble and Solid Surfaces of Different Hydrophobicity. *ACS Nano* **2014**, *9*, 95-104.

9.   Cui, X.; Shi, C.; Zhang, S.; Xie, L.; Liu, J.; Jiang, D.; Zeng, H., Probing the Effect of Salinity and Ph on Surface Interactions between Air Bubbles and Hydrophobic Solids: Implications for Colloidal Assembly at Air/Water Interfaces. *Chem. - Asian J.* **2017**, *12*, 1568-1577.

10.   Stock, P.; Utzig, T.; Valtiner, M., Direct and Quantitative Afm Measurements of the Concentration and Temperature Dependence of the Hydrophobic Force Law at Nanoscopic Contacts. *J. Colloid Interface Sci.* **2015**, *446*, 244-251.

11.   Tabor, R. F.; Wu, C.; Grieser, F.; Dagastine, R. R.; Chan, D. Y., Measurement of the Hydrophobic Force in a Soft Matter System. *J. Phys. Chem. Lett.* **2013**, *4*, 3872-3877.

12.   Donaldson Jr, S. H.; Røyne, A.; Kristiansen, K.; Rapp, M. V.; Das, S.; Gebbie, M. A.; Lee, D. W.; Stock, P.; Valtiner, M.; Israelachvili, J., Developing a General Interaction Potential for Hydrophobic and Hydrophilic Interactions. *Langmuir* **2014**, *31*, 2051-2064.

13.   Faghihnejad, A.; Zeng, H., Hydrophobic Interactions between Polymer Surfaces: Using Polystyrene as a Model System. *Soft Matter* **2012**, *8*, 2746-2759.

14.   Cui, X.; Shi, C.; Xie, L.; Liu, J.; Zeng, H., Probing Interactions between Air Bubble and Hydrophobic Polymer Surface: Impact of Solution Salinity and Interfacial Nanobubbles. *Langmuir* **2016**, *32*, 11236-11244.

15.   Zhang, Y.; Cremer, P. S., Interactions between Macromolecules and Ions: The Hofmeister Series. *Curr. Opin. Chem. Biol.* **2006**, *10*, 658-663.

16.   Kunz, W.; Nostro, P. L.; Ninham, B. W., The Present State of Affairs with Hofmeister Effects. *Curr. Opin. Colloid Interface Sci.* **2004**, *9*, 1-18.

17.   Baldwin, R. L., How Hofmeister Ion Interactions Affect Protein Stability. *Biophys. J.* **1996**, *71*, 2056-2063.

18.   Zangi, R.; Hagen, M.; Berne, B., Effect of Ions on the Hydrophobic Interaction between Two Plates. *J. Am. Chem. Soc.* **2007**, *129*, 4678-4686.

19.   Horinek, D.; Netz, R. R., Specific Ion Adsorption at Hydrophobic Solid Surfaces. *Phys. Rev. Lett.* **2007**, *99*, 226104.

20.   Schwierz, N.; Horinek, D.; Netz, R. R., Anionic and Cationic Hofmeister Effects on Hydrophobic and Hydrophilic Surfaces. *Langmuir* **2013**, *29*, 2602-2614.

21.   Stock, P.; Müller, M.; Utzig, T.; Valtiner, M., How Specific Halide Adsorption Varies Hydrophobic Interactions. *Biointerphases* **2016**, *11*, 019007.

22.   Du, Q.; Freysz, E.; Shen, Y. R., Surface Vibrational Spectroscopic Studies of Hydrogen Bonding and Hydrophobicity. *Science* **1994**, *264*, 826-827.

23.   Du, Q.; Superfine, R.; Freysz, E.; Shen, Y., Vibrational Spectroscopy of Water at the Vapor/Water Interface. *Phys. Rev. Lett.* **1993**, *70*, 2313.

24.   Denkov, N. D.; Subramanian, V.; Gurovich, D.; Lips, A., Wall Slip and Viscous Dissipation in Sheared Foams: Effect of Surface Mobility. *Colloids Surf., A* **2005**, *263*, 129-145.

25.   Mura, S.; Nicolas, J.; Couvreur, P., Stimuli-Responsive Nanocarriers for Drug Delivery. *Nat. Mater.* **2013**, *12*, 991.

26.   Schutt, E. G.; Klein, D. H.; Mattrey, R. M.; Riess, J. G., Injectable Microbubbles as Contrast Agents for Diagnostic Ultrasound Imaging: The Key Role of Perfluorochemicals. *Angew. Chem. Int. Ed.* **2003**, *42*, 3218-3235.

27.   Yu, C.; Cao, M.; Dong, Z.; Li, K.; Yu, C.; Wang, J.; Jiang, L., Aerophilic Electrode with Cone Shape for Continuous Generation and Efficient Collection of H2 Bubbles. *Adv. Funct. Mater.* **2016**, *26*, 6830-6835.

28.   Bhushan, B.; Jung, Y. C., Natural and Biomimetic Artificial Surfaces for Superhydrophobicity, Self-Cleaning, Low Adhesion, and Drag Reduction. *Prog. Mater Sci.* **2011**, *56*, 1-108.

29.   Donaldson Jr, S. H.; Das, S.; Gebbie, M. A.; Rapp, M.; Jones, L. C.; Roiter, Y.; Koenig, P. H.; Gizaw, Y.; Israelachvili, J. N., Asymmetric Electrostatic and Hydrophobic–Hydrophilic Interaction Forces between Mica Surfaces and Silicone Polymer Thin Films. *ACS Nano* **2013**, *7*, 10094-10104.

30.   Tabor, R. F.; Manica, R.; Chan, D. Y.; Grieser, F.; Dagastine, R. R., Repulsive Van Der Waals Forces in Soft Matter: Why Bubbles Do Not Stick to Walls. *Phys. Rev. Lett.* **2011**, *106*, 064501.

31.   Tabor, R. F.; Chan, D. Y.; Grieser, F.; Dagastine, R. R., Anomalous Stability of Carbon Dioxide in Ph-Controlled Bubble Coalescence. *Angew. Chem. Int. Ed.* **2011**, *50*, 3454-3456.

32.   Xie, L.; Shi, C.; Cui, X.; Zeng, H., Surface Forces and Interaction Mechanisms of Emulsion Drops and Gas Bubbles in Complex Fluids. *Langmuir* **2017**, *33*, 3911-3925.

33.   Hutter, J. L.; Bechhoefer, J., Calibration of Atomic-Force Microscope Tips. *Rev. Sci. Instrum.* **1993**, *64*, 1868-1873.

34.   Tabor, R. F.; Grieser, F.; Dagastine, R. R.; Chan, D. Y., Measurement and Analysis of Forces in Bubble and Droplet Systems Using Afm. *J. Colloid Interface Sci.* **2012**, *371*, 1-14.

35.   Vakarelski, I. U.; Manica, R.; Tang, X.; O'Shea, S. J.; Stevens, G. W.; Grieser, F.; Dagastine, R. R.; Chan, D. Y., Dynamic Interactions between Microbubbles in Water. *Proc. Natl. Acad. Sci.* **2010**, *107*, 11177-11182.

36.   Chan, D. Y.; Klaseboer, E.; Manica, R., Theory of Non-Equilibrium Force Measurements Involving Deformable Drops and Bubbles. *Adv. Colloid Interface Sci.* **2011**, *165*, 70-90.

37.   Dagastine, R. R.; Manica, R.; Carnie, S. L.; Chan, D.; Stevens, G. W.; Grieser, F., Dynamic Forces between Two Deformable Oil Droplets in Water. *Science* **2006**, *313*, 210-213.

38.   Chan, D. Y.; Klaseboer, E.; Manica, R., Film Drainage and Coalescence between Deformable Drops and Bubbles. *Soft Matter* **2011**, *7*, 2235-2264.

39.   Israelachvili, J. N., *Intermolecular and Surface Forces*; Academic press, 2015.

40.   Marcus, Y., Thermodynamics of Solvation of Ions. Part 5.—Gibbs Free Energy of Hydration at 298.15 K. *J. Chem. Soc., Faraday Trans.* **1991**, *87*, 2995-2999.

41.   Strazdaite, S.; Versluis, J.; Backus, E. H.; Bakker, H. J., Enhanced Ordering of Water at Hydrophobic Surfaces. *J. Chem. Phys.* **2014**, *140*, 054711.

42.   Richmond, G., Molecular Bonding and Interactions at Aqueous Surfaces as Probed by Vibrational Sum Frequency Spectroscopy. *Chem. Rev.* **2002**, *102*, 2693-2724.

43.   Ma, J. C.; Dougherty, D. A., The Cation−Π Interaction. *Chem. Rev.* **1997**, *97*, 1303-1324.

44.   Mahadevi, A. S.; Sastry, G. N., Cation−Π Interaction: Its Role and Relevance in Chemistry, Biology, and Material Science. *Chem. Rev.* **2012**, *113*, 2100-2138.

45.   Cabarcos, O. M.; Weinheimer, C. J.; Lisy, J. M., Size Selectivity by Cation–Π Interactions: Solvation of K+ and Na+ by Benzene and Water. *J. Chem. Phys.* **1999**, *110*, 8429-8435.

46.   Cabarcos, O. M.; Weinheimer, C. J.; Lisy, J. M., Competitive Solvation of K+ by Benzene and Water: Cation-Π Interactions and Π-Hydrogen Bonds. *J. Chem. Phys.* **1998**, *108*, 5151-5154.

47.   Lu, Q.; Oh, D. X.; Lee, Y.; Jho, Y.; Hwang, D. S.; Zeng, H., Nanomechanics of Cation−Π Interactions in Aqueous Solution. *Angew. Chem.* **2013**, *125*, 4036-4040.

48.   Kumpf, R. A.; Dougherty, D. A., A Mechanism for Ion Selectivity in Potassium Channels: Computational Studies of Cation-Pi Interactions. *Science* **1993**, *261*, 1708-1710.

49.   Shi, C.; Chan, D. Y.; Liu, Q.; Zeng, H., Probing the Hydrophobic Interaction between Air Bubbles and Partially Hydrophobic Surfaces Using Atomic Force Microscopy. *J. Phys. Chem. C* **2014**, *118*, 25000-25008.

50.   Shen, Y. R.; Ostroverkhov, V., Sum-Frequency Vibrational Spectroscopy on Water Interfaces: Polar Orientation of Water Molecules at Interfaces. *Chem. Rev.* **2006**, *106*, 1140-1154.

51.   Russell, T. P.; Chai, Y., 50th Anniversary Perspective: Putting the Squeeze on Polymers: A Perspective on Polymer Thin Films and Interfaces. *Macromolecules* **2017**, *50*, 4597-4609..

52.   Chai, Y.; Salez, T.; McGraw, J. D.; Benzaquen, M.; Dalnoki-Veress, K.; Raphaël, E.; Forrest, J. A., A Direct Quantitative Measure of Surface Mobility in a Glassy Polymer. *Science* **2014**, *343*, 994-999.

53.   Yang, Z.; Fujii, Y.; Lee, F. K.; Lam, C.-H.; Tsui, O. K., Glass Transition Dynamics and Surface Layer Mobility in Unentangled Polystyrene Films. *Science* **2010**, *328*, 1676-1679.

54.   Hanakata, P. Z.; Douglas, J. F.; Starr, F. W., Interfacial Mobility Scale Determines the Scale of Collective Motion and Relaxation Rate in Polymer Films. *Nat. Commun.* **2014**, *5*, 4163.

Chapter 6   Modulation of Hydrophobic Interaction by Mediating Surface Mobility and Chemistry

6.1. Introduction.

As a major nonspecific surface interaction, hydrophobic (HB) interaction plays a key role in a variety of technological and engineering applications, such as froth flotation,[1] oil-water separation,[2] gas transport,[3] protein purification,[4] and controlled drug delivery.[5] Ruling out some indirectly hydrophobic artifacts such as bridging of interfacial nanobubbles and electrostatic attraction due to overturning of surfactant monolayers,[6-7] the driving force underlying the intrinsic HB interaction is highly related to the fact that specific orientation and arrangement of water molecules near hydrophobic surfaces decreases their configurational entropy significantly, and thus the hydrophobic substances tend to aggregate in aqueous media to minimize their surface area exposed to water and reduce the free energy of the system, manifested as a strong attraction that cannot be explained by the classical Derjaguin-Landau-Verwey-Overbeek (DLVO) theory.[8]

Since the pioneering attempt by Israelachivili and Pasheley who proposed that HB interaction exponentially decays with separation,[9] a huge wave of experimental efforts have been devoted to quantitatively probing the HB interactions between two extended hydrophobic surfaces in aqueous media during the last three decades, mainly using nano-mechanical tools such as surface forces apparatus (SFA) and atomic force microscopy (AFM).[10-13] A recently developed bubble/droplet AFM technique coupled with theoretical modeling allows the quantification of HB interactions involving deformable gas bubbles and oil droplets.[14-17] Notably, the agreement in the force law of HB interaction has not been achieved, considering that the

reported decay length ranges from ~ 0.3 nm between two perfluorocarbon oil droplets to ~ 0.6-1.6 nm for systems involving various hydrophobic solid surfaces. On the basis of these previous results, this striking discrepancy can be attributed to that the applied hydrophobic materials vary significantly in surface mobility and chemical composition, which can potentially lead to different degree of the interfacial water structuring effect. The influences of surface mobility and chemistry have been studied in terms of the adhesion between two hydrophobic surfaces;[18-19] however, the evidence is still missing in supporting that the range of HB interaction can be modulated by mediating surface mobility and chemistry, which is of great importance in explicating the physical mechanism of HB interaction.

Here, in order to systematically illuminate the effects of surface mobility and chemistry on HB interaction, a bubble probe AFM coupled with theoretical analysis based on Stokes-Reynolds-Young-Laplace model was applied for the first time to quantify the HB interactions between air bubbles and two representative hydrophobic substrates in aqueous media, i.e., alkanethiol self-assembled monolayers (SAMs) adsorbed on gold wafers whose surface mobility and chemistry can be effectively mediated by altering the chain length and tail groups of the thiol molecules,[20-26] and slippery liquid-infused porous surfaces (SLIPSs) featuring a stable fully liquid over-layer of lubricant.[27-28] The bubble surface is intrinsically hydrophobic and molecularly smooth, which can facilitate the precise quantification of the HB interactions. The experimental setup using bubble probe AFM is illustrated in Figure 6.1. The aqueous condition was fixed as 1000 mM NaCl of pH ~ 5.6 to screen electrical double-layer (EDL) interaction, and the cantilever velocity was set as 1 μm/s to reduce hydrodynamic effect.[29]
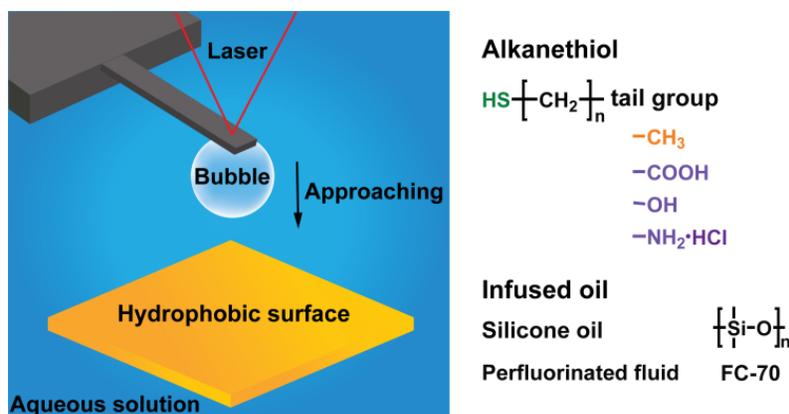
Figure 6.1. Left: Experimental setup of the force measurement using bubble probe AFM. Right: Chemical structures of the applied alkanethiols and infused lubricants, 1-undercanethiol (C11), 1-octanethiol (C8), 1-propanethiol (C3), 11-mercaptoundecanoic acid (C10COOH), 3-mercaptopropionic acid (C2COOH), 11-mercapto-undecanol (C11OH), 11-amino-1-undecanethiol hydrochloride (C11NH$_2$•HCl), silicone oil and perfluorinated FC-70.

6.2. Experimental section.

6.2.1. Materials.

1-propanethiol (C3, 99%), 1-octanethiol (C8, ≥ 98.5%), 1-undecanethiol (C11, 98%), 3-mercaptopropionic acid (C2COOH, ≥ 99%), 11-mercaptoundecanoic acid (C10COOH, 98%), 11-mercapto-1-undecanol (C11OH, 97%), 11-amino-1-undecanethiol hydrochloride (C11NH$_2$, 99%), silicone oil, Fluorinert^{TM} FC-70 lubricating oil and polytetrafluoroethylene (PTFE) filter membrane (pore size ~ 0.2 μm) were purchased from Sigma-Aldrich. Sodium chloride (NaCl, ≥ 99.0%) and ethanol (anhydrous, ≤ 0.005% water) were purchased from Fisher Scientific, Canada. The NaCl aqueous solution was prepared using Milli-Q water with a resistivity of ≥ 18.2 MΩ.cm, and then was degassed through sonication under vacuum followed by purging with nitrogen. All the chemicals were used as received without further purification.

6.2.2. Preparation of SAMs and SLIPSs with various surface compositions.

Smooth gold surfaces were prepared through an template-stripping method which has been elaborated in previous studies.[30-31] The SAMs were prepared by immersing the fresh and clean gold surfaces into ethanoic solutions containing 10 mM single-component thiols or binary-component thiols with different chain lengths or tail groups at specific molar ratios. After being incubated for 24 h at room temperature, the surfaces were removed from the ethanoic solutions, extensively rinsed with a large amount of ethanol, and thoroughly dried with nitrogen gas flow. Afterwards, the surfaces were immediately transferred into a vacuum desiccator and ready for the use of AFM force measurements. It should be mentioned that for C11/C10COOH, C8/C10COOH and C3/C2COOH SAMs, the molar ratio of methyl-ended species to carboxyl-ended species in solution was set as 1/1, 1/1 and 7/3, respectively, leading to similar surface coverage of carboxyl groups which will be verified by X-ray photoelectron spectroscopy (XPS) characterization in a later section. The SLIPSs were prepared by infusing lubricants with low surface energy (i.e. silicone oil and FC-70 in this work) into PTFE membranes. Owing to the matching chemistry, porosity and roughness of the membranes, the lubricant could spontaneously spread throughout the whole membrane due to the capillary wicking. After being immersing in the lubricant for 10 minutes, the completely wetted membrane was taken out, tilted and mildly treated using nitrogen gas flow to remove the excess lubricating oil.

6.2.3. Characterization of the prepared SAM and SLIPS surfaces.

The prepared alkanethiol SAMs exhibit similar surface morphology with root-mean-square roughness ~ 0.4 nm (Figure 6.2) which was imaged through AFM tapping mode (MFP-3D, Asylum Research, Santa, Barbara, CA). The thickness of the SAMs was measured using a

spectroscopic ellipsometer (Sopra GESP-5, France) and shown in Figure S1b, which were in good consistent with the values in previous studies. The thickness of the over-coated oil layer could be calculated to be ~ 20 μm for FC-70 infused SLIPS and ~ 30 μm for silicone oil infused SLIPS, based on the weight of the pristine and wetted PTFE membrane, the surface area and thickness of the membrane and the density of the PTFE and the lubricating oil.[27]
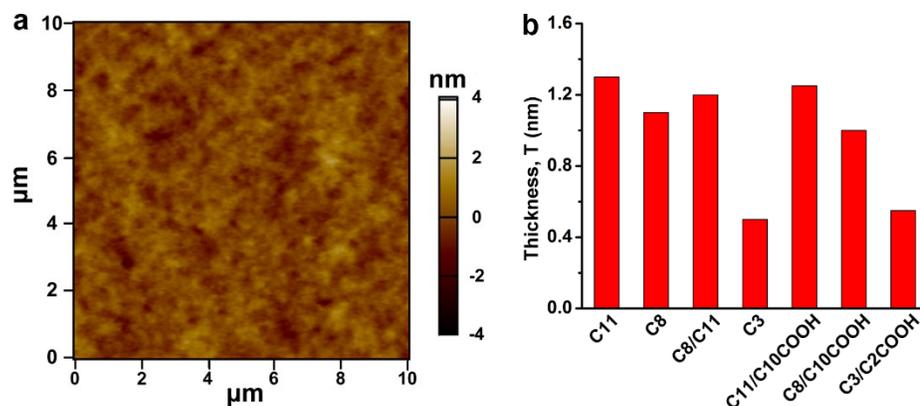
Figure 6.2. (a) Typical morphology of the prepared SAM surface characterized by AFM tapping mode imaging. (b) Thickness of the prepared SAMs with various surface composition measured by ellipsometry.

The static water contact angle θ_c on the prepared SAMs and SLIPSs were measured using a contact angle tensiometer (Ramé-hart Instrument Company, USA) at room temperature, as shown in Figures 6.3. The volume of water droplet applied here was ~ 5 μL through this work.
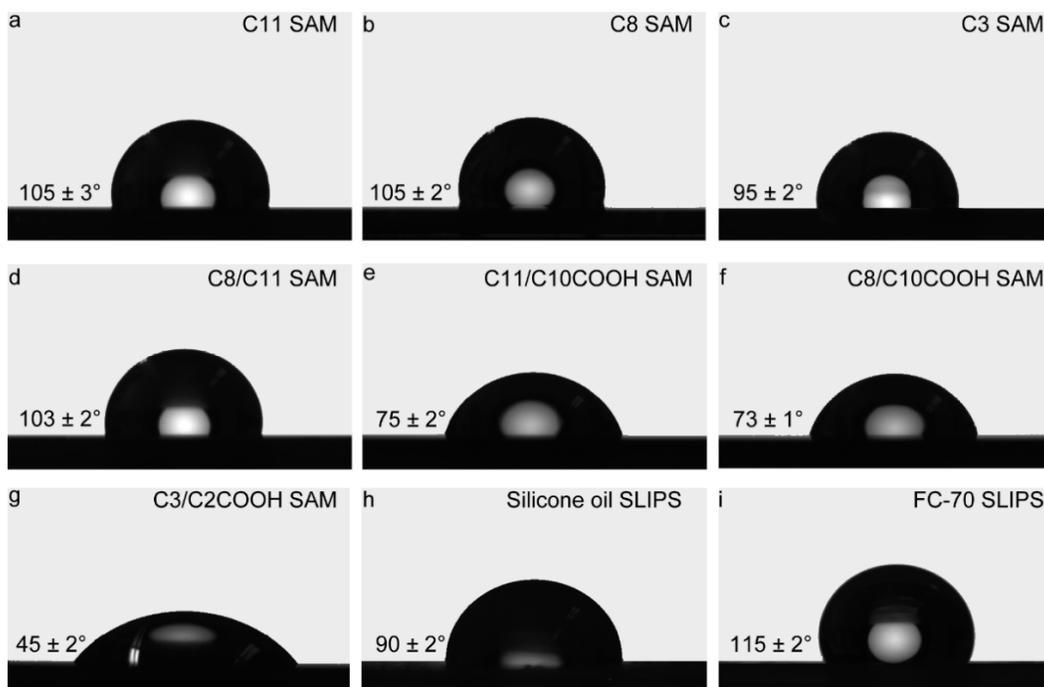
Figure 6.3. Images of static water contact angle in air θ_c on the prepared alkanethiol SAMs and SLIPS with various surface composition.

The surface compositions of the prepared methyl/carboxyl-ended SAMs were characterized by XPS in a vacuum chamber, and the results were illustrated in Figure 6.4 with the binding energies referenced to C1s peak at 284.8 eV. The green curves in Figures 6.4a to 6.4c denote the oxygen signals (O1s) for C11/C10COOH, C8/C10COOH and C3/C2COOH SAM surfaces, respectively. The wide peaks at around 532 eV could be attributed to the overlapping of the signals from two states (C-O and C=O at around 531.5 eV and 533 eV, respectively). Figures 6.4d to 6.4f display the sulfur signals (red curves) for these three types of SAMs, exhibiting characteristic doublet peaks at around 162.1 eV ($2p_{3/2}$) and 163.3 eV ($2p_{1/2}$) which could be assigned to the bounding of thiol to gold wafer. Based on the XPS characterization results, it can be inferred that these three binary-component SAMs exhibit similar surface composition, with

the percentage of surface carboxyl group of ~ 48%, 47% and 45% for C11/C10COOH, C8/C10COOH and C3/C2COOH SAM surfaces, respectively.
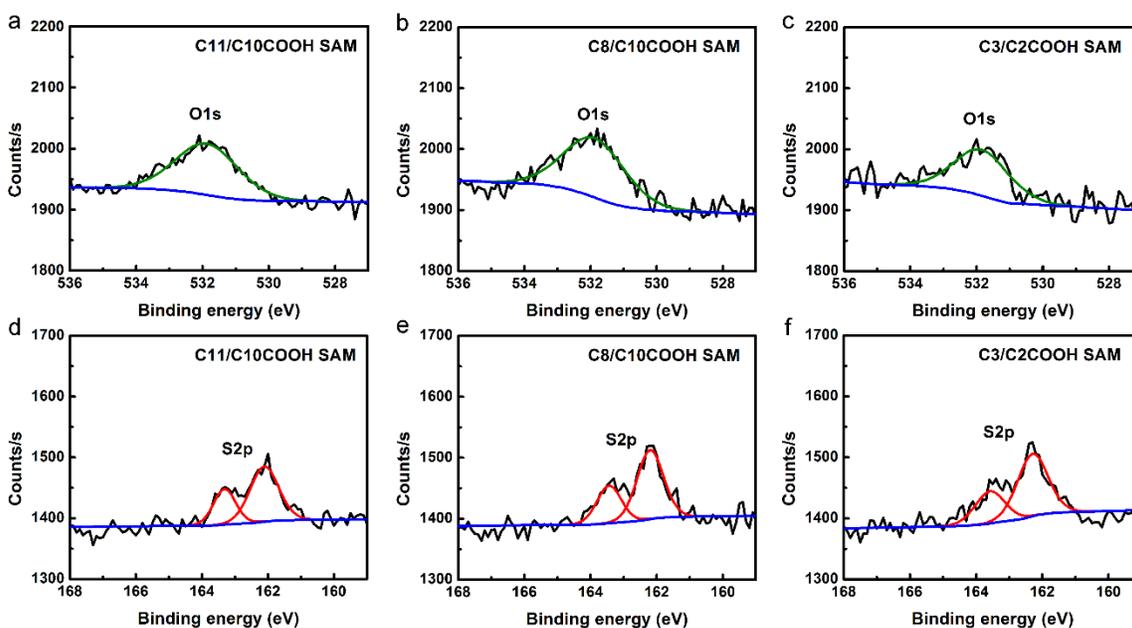
Figure 6.4. Results of XPS characterization of the prepared methyl/carboxyl-ended SAM surfaces. (a-c) Oxygen signals (green) and (d-f) sulfur signals (red) for the C11/C10COOH, C8/C10COOH and C3/C2COOH SAMs, respectively.

6.2.4. Force measurement using bubble probe AFM technique.

The interactions between air bubbles and hydrophobic surfaces in NaCl solutions were measured using a MFP-3D AFM mounted on an inverted Nikon Ti-U microscope. The AFM cantilever applied in our work is a customized rectangular tipless cantilever (400 × 70 × 2 μm) with a circular gold patch (diameter ~ 65 μm, thickness~ 30 nm) at its front end. The spring constant of the cantilever was determined to be 0.3-0.4 N/m using Hutter-Bechhoefer method.[32] The tipless cantilever was immersed in an ethanoic solution containing 10 mM 1-undecanethiol for 24 h prior to the force measurement, in order to hydrophobize the gold patch to make it favorable to anchor an air bubble.[32-33] For each AFM force measurement, the air bubbles were

generated on the glass slide of the fluid cell filled with NaCl solution by carefully injecting air

through an ultra-sharp pipet. And then, the hydrophobized tipless cantilever was slowly lowered

down to pick up an applicable air bubble (radius ~ 50-100 μm). Afterwards, the bubble probe

was manipulated to interact with the hydrophobic surface which had been previously placed in

the fluid cell. The interaction force and cantilever deflection were recorded by the AFM and

ready for the theoretical analysis through MATLAB software.[14, 17, 34-35]

6.2.5. Theoretical model for analysis of the measured interaction force.

The theoretical model applied to analyze the AFM force measurement results is based on

Reynolds lubrication theory and augmented Young-Laplace equation by including the effects of

disjoining pressure which arises from surface interactions (e.g. VDW, EDL and HB interactions).

The drainage behavior of the thin water film with real-time thickness $h(r,t)$ confined by the air

bubble and the hydrophobic surface is described by equation 6.1, where μ is the viscosity of the

aqueous solution, $p(r,t)$ denotes the excessive hydrodynamic pressure within the thin film

relative to that in the bulk solution and r is the radical coordinate.[15, 34, 36]

$$\frac{\partial h(r,t)}{\partial t} = \frac{1}{12\mu}\frac{\partial}{\partial r}(rh^3(r,t)\frac{\partial p(r,t)}{\partial r})$$

(6.1)

Different from rigid particles, air bubbles would easily deform in response to external force. The

deformation of the bubble probe during the AFM force measurement could be expressed by the

equation 6.2,

$$\frac{\gamma}{r}\frac{\partial}{\partial r}\left(r\frac{\partial h(r,t)}{\partial r}\right) = \frac{2\gamma}{R_0} - p(r,t) - \prod[h(r,t)]$$

(6.2)

where γ is the interfacial tension of the aqueous solution with air, R_0 is the radius of air bubble,

and $\prod$ is the overall disjoining pressure that arises from surface interactions.[37-38] The aqueous

salinity is 1000 mM NaCl and consequently the electrical double-layer (EDL) interaction is almost fully screened and could be negligible to influence the overall disjoining pressure. The contributions from van der Waals (VDW) interactions for the cases of SAMs and SLIPSs could be quantitatively determined by equation 6.3 and equation 6.4, respectively, based on the classical Derjaguin-Landau-Verwey-Overbeek (DLVO) theory,[38]

$$\Pi_{VDW}[h(r,t)] = -\frac{A_{AWG}}{6\pi[h(r,t)+T]^3} \tag{6.3}$$

$$\Pi_{VDW}[h(r,t)] = -\frac{A_{AWO}}{6\pi h^3(r,t)} \tag{6.4}$$

where T denotes the thickness of the alkanethiol SAM, A represent the Hamaker constant. Here, the Hamaker constant for the bubble-SAM VDW interaction is considered to be that for the air/water/gold system, A_{AWG}, because the thickness of the SAM is less than 2 nm, making its effect on the VDW interaction negligible. The Hamaker constant for the bubble-SLIPS VDW interaction is applied as that for the air/water/oil system, because the thickness of the lubricant over-layer reached above 20 nm which can get rid of the impact of the membrane substrate. The values of these Hamaker constants were calculated based on the Lifshitz theory.[14, 39]

It has been well accepted that the free energy of HB interaction per unit area decays exponentially with the separation between two hydrophobic surfaces, as described in equation 6.5,[9, 11, 31, 39]

$$W_{HB}[h(r,t)] = -C_0 \exp\left(-\frac{h(r,t)}{D_0}\right) \tag{6.5}$$

where C_0 is the pre-exponential factor regarding the interaction free energy per unit area, and D_0 is the characteristic decay length. For the attachment process of an air bubble onto a hydrophobic surface, C_0 could be derived from the aspect of thermodynamics and expressed as the change in

surface free energy of the system, $C_0 = \gamma + \gamma_{SW} - \gamma_{SA}$, where γ, γ_{SW} and γ_{SA} represent the air/water, surface/water and surface/air interfacial energy, respectively. By incorporating this expression with Young-Duprè equation $\gamma_{SA} = \gamma_{SW} + \gamma\cos\theta_c$, C_0 could be given as $C_0 = \gamma\,(1 - \cos\theta_c)$, and therefore, the HB interaction between air bubble and hydrophobic surface could be quantified by equation 6.6 as[9, 14]

$$\Pi_{HB}[h(r,t)] = -\frac{dW_{HB}}{dh(r,t)} = -\frac{C_0}{D_0}\exp\left(-\frac{h(r,t)}{D_0}\right) = -\frac{\gamma(1-\cos\theta_c)}{D_0}\exp\left(-\frac{h(r,t)}{D_0}\right) \qquad (6.6)$$

The overall interaction force is calculated based on the integration equation incorporating $p(r,t)$ and $\Pi[h(r,t)]$, as shown in equation 6.7.[17, 37]

$$F(t) = 2\pi\int_0^{r_{max}} \left\{p(r,t) + \Pi\big[h(r,t)\big]\right\} r\,dr \qquad (6.7)$$

6.3. Results and discussion.

Figures 6.5a-6.5c show the interactions of air bubbles with single-component C11, C3 and binary-component C8/C11 SAMs, respectively. As the bubble probe approached the substrate, a repulsion due to van der Waals (VDW) interaction was observed in the force curve. Then, a sudden "jump-in" behavior (denoted by the red arrow) occurred, corresponding to the observed bubble attachment onto the SAM substrate. For the case of C11 SAM, θ_c was measured to be ~ 105 ± 3° resulting in C_0 ~ 0.093 J/m^2, and D_0 was theoretically fitted to be ~ 1.60 ± 0.03 nm. However, when the methylene unit was decreased to 3, the SAM exhibited a relatively lower surface hydrophobicity with θ_c ~ 95 ± 2° and C_0 ~ 0.080 J/m^2, and particularly, the fitted D_0 decreased to ~ 1.25 ± 0.05 nm (Figure 6.5b), much smaller than that in the C11 or C8 case. Besides, it is interesting to find that D_0 for the C8/C11 case was also ~ 1.25 ± 0.05 nm (Figure 6.5c), despite θ_c ~ 103 ± 2° and C_0 ~ 0.090 J/m^2. Given the similar SAM chemistry, these

quantitative results could imply that surface mobility may be critical in determining the range of HB interaction. The SAMs composed of long-chain thiols (n ≥ 8) possessed an ordered crystalline-like structure of densely packed and highly oriented hydrocarbon chains (Figure 6.5d), while short-chain thiols (n ≤ 5) adsorbed on gold wafer formed an amorphous liquid-like SAM with low packing density (Figure 6.5e).[21-22, 25] Surface mobility can also be introduced within the SAM by coadsorbing two thiol species with different chain length.[20, 23, 25] As shown in Figure 6.5f, the inner region resembled a crystalline structure which could account for the approximate θ_c of the C11 and C8/C11 SAMs, while the outer region exhibited liquid-like characteristic akin to the mobile C3 SAM, which underlay the consistency in D_0 between the C8/C11 and C3 cases. To gain further insight, the interactions between air bubbles and SLIPSs were also studied (Figure 6.6). The fully liquid over-layer of the SLIPSs bore much more mobile and flexible interfaces with water than the SAM surfaces. Regardless of the applied lubricants (i.e., silicone oil and FC-70), the bubble-SLIPS HB interaction was found to decay exponentially with a much smaller $D_0 \sim 0.35 \pm 0.05$ nm, roughly equal to that between deformable hydrophobic interfaces.[16]
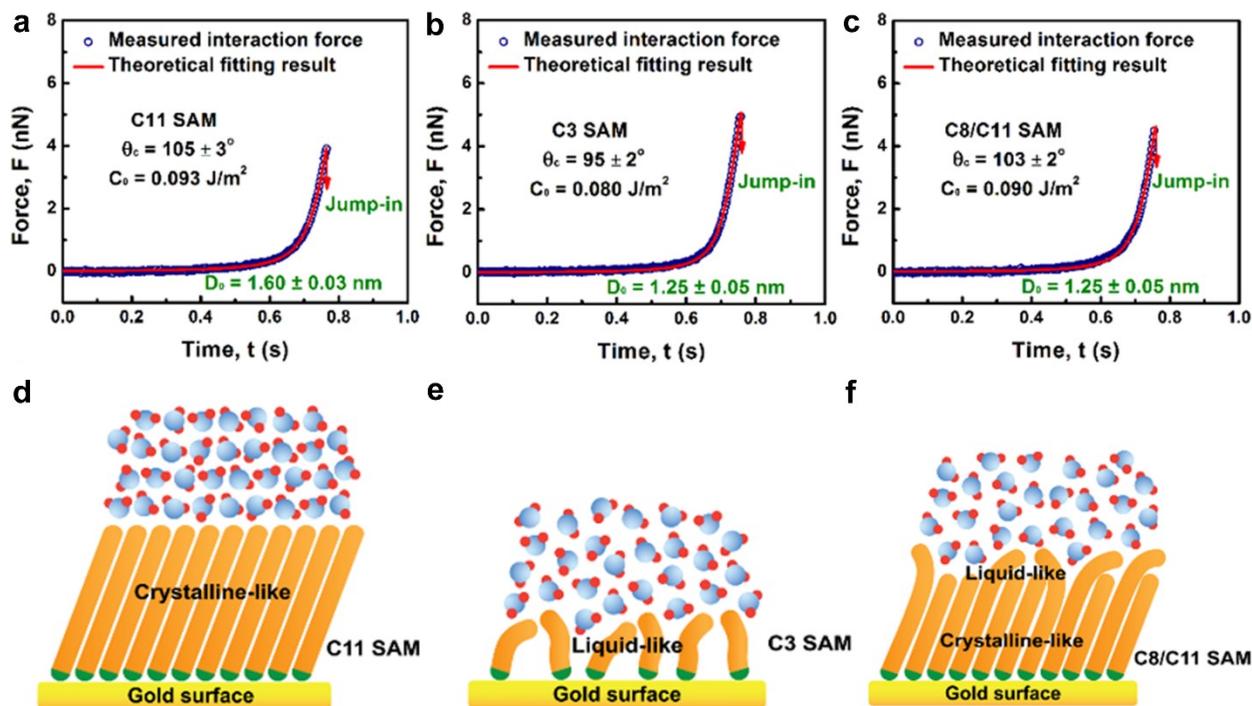
Figure 6.5. Interactions between air bubbles (radius ~ 55, 52 and 56 μm, respectively) and C11, C3 and C8/C11 SAMs, respectively. (a-c) Measured interaction forces (open symbols) and theoretically fitting results (solid curves), respectively. (d-f) Schematics of the corresponding SAMs in contact with water.
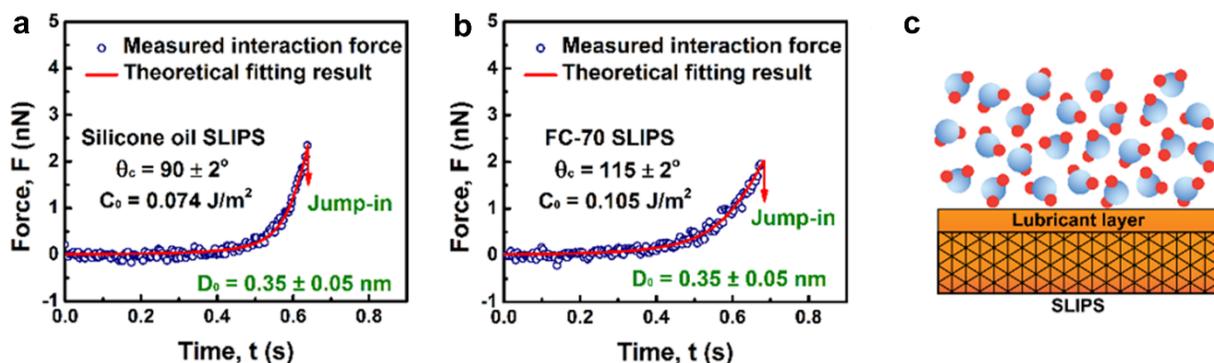
Figure 6.6. (a and b) Interactions between air bubbles (radius ~ 53 and 60 μm, respectively) and SLIPSs infused with silicone oil and FC-70 lubricant, respectively. (c) Schematic of the SLIPS in contact with water.

In addition to surface mobility, surface chemistry can also be essential in modulating HB interaction. Immobilization of hydrophilic moieties proximal to hydrophobic domains could generate nano-scaled chemical heterogeneity within the SAMs.[20, 24, 26] Figures 6.7a-6.7c display the interactions between air bubbles and binary-component SAMs terminated with methyl and carboxyl groups, i.e., C11/C10COOH, C8/C10COOH and C3/C2COOH SAMs, respectively. The coverage of surface carboxyl groups was controlled in the range from 45% to 50% by mediating the molar fractions of the alkanethiol species, as confirmed by XPS characterization. These SAMs showed relatively lower surface hydrophobicity, $\theta_c \sim 75 \pm 2°$, $73 \pm 1°$ and $45 \pm 2°$ and $C_0 \sim 0.055$ J/m^2, 0.052 J/m^2 and 0.024 J/m^2, respectively, and more importantly, D_0 could be further decreased to 1.08 ± 0.02 nm, 1.05 ± 0.03 nm, 1.00 ± 0.02, as compared to the corresponding cases of methyl-ended C11, C8/C11 and C3 SAMs, respectively. The effects of proximally immobilized amino and hydroxyl groups on the bubble-SAM HB interaction were also investigated and the corresponding C_0 and D_0 were listed in Table 6.1, which also indicated that nano-scaled chemical heterogeneity could effectively reduce the range of HB interaction.
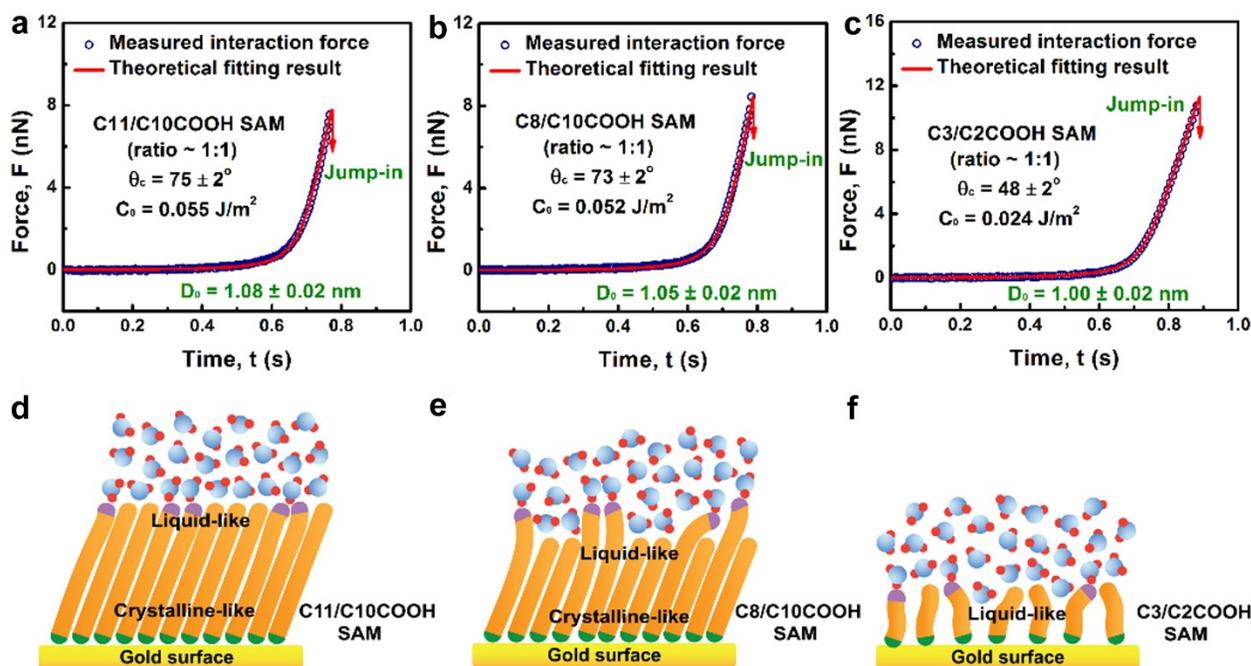
Figure 6.7. Interactions between air bubbles (radius ~59 μm, 61 μm and 63 μm, respectively) and methyl/carboxyl-ended C11/C10COOH, C8/C10COOH and C3/C2COOH SAMs, respectively. (a-c) Measured interaction forces (open symbols) and theoretically results (solid curve), respectively. (d-f) Schematic diagrams of the corresponding SAMs in contact with water, respectively.

Table 6.1. Values of C_0 and D_0 of the Interactions between Air Bubbles and SAMs with Various Surface Chemistry.

SAM	C11/C10COOH			C11/C11OH			C11/C11NH$_2$		
Ratio in solution	3/7	1/1	7/3	3/7	1/1	7/3	3/7	1/1	7/3
C_0 (J/m^2)	0.022	0.054	0.076	0.022	0.055	0.074	0.026	0.057	0.079
D_0 (nm)	1.08	1.08	1.08	1.14	1.14	1.14	1.22	1.22	1.22

The dependence of HB interaction on surface mobility and chemistry could be well interpreted in terms of the unique water structuring effects near various hydrophobic surfaces, which has been extensively explored by the relevant sum frequency generation (SFG) and molecular dynamics (MD) simulations and X-ray reflectivity studies.[40-44] Without hydrogen bond (H-bond) acceptors, the hydrophobic surface forces the interfacial water molecules to sacrifice some H-bonds to accommodate the interface, featuring a population of dangling OHs not engaged in any H-bond. Such H-bond depletion extends the lag time to reorient water dipole moments, and the resultant hindered H-bond exchange between water molecules facilitates the occurrence of long-lived water dipole pairs. The dipole-dipole correlation due to the fluctuating H-bond network gives rise to a structured water shell and a polarization field decaying exponentially with distance from the surface.[45-47] The extent of this correlation effect can vary greatly at different hydrophobic interfaces, depending on the number of the dangling OHs and the degree of the consequent water ordering governed by the specific surface mobility and chemistry.

It has been revealed that the dangling OHs predominantly exist at the interface of water with a rigid hydrophobic SAM of closely packed hydrocarbon chains, intensively restricting several layers of interfacial water molecules into an ordered, ice-like structure through dipolar correlation, which is responsible for the long-range HB interaction. In contrast, as the surface mobility increases, particularly for a highly flexible water/oil interface which undergoes continuous thermal fluctuation, the number of dangling OHs is largely reduced, relaxing the physical restriction and preventing the interfacial water molecules from being bond-ordered.[40, 48-49]. Consequently, only the molecular correlation within a single water layer could be induced,

accounting for the significantly shortened range of the HB interaction between two deformable hydrophobic surfaces. The immobilized hydrophilic moieties can strongly interact with the neighboring water molecules through either hydration or H-bonding, and are flexible to change their configuration which results in a 3D freedom introducing further surface mobility. These two mechanisms synergistically contribute to the reduction in the number of the dangling OHs, the relaxation of the physical restriction for the molecular rearrangement.[50-52] As a result, the ordering of the interfacial water molecules would be disrupted, inhibiting the formation of the long-range H-bond network and dipolar correlation effect, which evidently shortens the range of the HB interaction. The slight discrepancy in D_0 for the cases involving different hydrophilic moieties may reflect the variation in the strength of their interactions with water.

6.4. Conclusions.

In summary, by virtue of bubble probe AFM coupled with theoretical analysis based on Stokes-Reynolds-Young-Laplace model, we quantified the HB interactions between air bubbles and alkanethiol SAMs and SLIPSs with various surface properties. For the first time, we systematically demonstrated that mediating surface mobility and chemistry could effectively modulate HB interaction, by correlating our AFM experimental results with previous SFG and MD simulation studies on the water structuring effects at hydrophobic interfaces. Increasing surface mobility and proximal immobilization of hydrophilic moieties were found to be able to shorten the range of HB interaction by relaxing the physical restriction that orderly organizes the interfacial water molecules and suppressing the extent of the dipolar correlation effect. Our work provides novel insights in the physical mechanism of HB interaction, which is of vital

importance in quantitatively elucidate the colloidal and interfacial phenomena driven by HB interaction and guiding the relevant engineering applications.

6.5. References

1.   Rao, S. R., *Surface Chemistry of Froth Flotation: Volume 1: Fundamentals*; Springer Science & Business Media, 2013.

2.   Yang, H. C.; Hou, J.; Chen, V.; Xu, Z. K., Janus Membranes: Exploring Duality for Advanced Separation. *Angew. Chem. Int. Ed.* **2016**, *55*, 13398-13407.

3.   Yu, C.; Zhu, X.; Li, K.; Cao, M.; Jiang, L., Manipulating Bubbles in Aqueous Environment Via a Lubricant-Infused Slippery Surface. *Adv. Funct. Mater.* **2017**.

4.   Janson, J.-C., *Protein Purification: Principles, High Resolution Methods, and Applications*; John Wiley & Sons, 2012; Vol. 151.

5.   Mura, S.; Nicolas, J.; Couvreur, P., Stimuli-Responsive Nanocarriers for Drug Delivery. *Nat. Mater.* **2013**, *12*, 991-1003.

6.   Meyer, E. E.; Lin, Q.; Hassenkam, T.; Oroudjev, E.; Israelachvili, J. N., Origin of the Long-Range Attraction between Surfactant-Coated Surfaces. *Proc. Natl. Acad. Sci. U.S.A.* **2005**, *102*, 6839-6842.

7.   Attard, P., Nanobubbles and the Hydrophobic Attraction. *Adv. Colloid Interface Sci.* **2003**, *104*, 75-91.

8.   Chandler, D., Interfaces and the Driving Force of Hydrophobic Assembly. *Nature* **2005**, *437*, 640-647.

9.   Israelachvili, J.; Pashley, R., The Hydrophobic Interaction Is Long Range, Decaying Exponentially with Distance. *Nature* **1982**, *300*, 341-342.

10.   Zeng, H.; Shi, C.; Huang, J.; Li, L.; Liu, G.; Zhong, H., Recent Experimental Advances on Hydrophobic Interactions at Solid/Water and Fluid/Water Interfaces. *Biointerphases* **2016**, *11*, 018903.

11.   Donaldson Jr, S. H.; Røyne, A.; Kristiansen, K.; Rapp, M. V.; Das, S.; Gebbie, M. A.; Lee, D. W.; Stock, P.; Valtiner, M.; Israelachvili, J., Developing a General Interaction Potential for Hydrophobic and Hydrophilic Interactions. *Langmuir* **2014**, *31*, 2051-2064.

12.   Stock, P.; Utzig, T.; Valtiner, M., Direct and Quantitative Afm Measurements of the Concentration and Temperature Dependence of the Hydrophobic Force Law at Nanoscopic Contacts. *J. Colloid Interface Sci.* **2015**, *446*, 244-251.

13.   Tabor, R. F.; Grieser, F.; Dagastine, R. R.; Chan, D. Y., The Hydrophobic Force: Measurements and Methods. *Phys. Chem. Chem. Phys.* **2014**, *16*, 18065-18075.

14.   Shi, C.; Cui, X.; Xie, L.; Liu, Q.; Chan, D. Y.; Israelachvili, J. N.; Zeng, H., Measuring Forces and Spatiotemporal Evolution of Thin Water Films between an Air Bubble and Solid Surfaces of Different Hydrophobicity. *ACS Nano* **2014**, *9*, 95-104.

15.   Cui, X.; Shi, C.; Xie, L.; Liu, J.; Zeng, H., Probing Interactions between Air Bubble and Hydrophobic Polymer Surface: Impact of Solution Salinity and Interfacial Nanobubbles. *Langmuir* **2016**, *32*, 11236-11244.

16.   Tabor, R. F.; Wu, C.; Grieser, F.; Dagastine, R. R.; Chan, D. Y., Measurement of the Hydrophobic Force in a Soft Matter System. *J. Phys. Chem. Lett.* **2013**, *4*, 3872-3877.

17.   Xie, L.; Shi, C.; Cui, X.; Zeng, H., Surface Forces and Interaction Mechanisms of Emulsion Drops and Gas Bubbles in Complex Fluids. *Langmuir* **2017**, *33*, 3911-3925.

18.   Yeon, H.; Wang, C.; Van Lehn, R. C.; Abbott, N. L., Influence of Order within Nonpolar Monolayers on Hydrophobic Interactions. *Langmuir* **2017**, *33*, 4628-4637.

19.   Ma, C. D.; Wang, C.; Acevedo-Vélez, C.; Gellman, S. H.; Abbott, N. L., Modulation of Hydrophobic Interactions by Proximally Immobilized Ions. *Nature* **2015**, *517*, 347-350.

20.   Bain, C. D.; Whitesides, G. M., Modeling Organic Surfaces with Self-Assembled Monolayers. *Angew. Chem., Int. Ed. Engl.* **1989**, *28*, 506-512.

21.   Porter, M. D.; Bright, T. B.; Allara, D. L.; Chidsey, C. E., Spontaneously Organized Molecular Assemblies. 4. Structural Characterization of N-Alkyl Thiol Monolayers on Gold by Optical Ellipsometry, Infrared Spectroscopy, and Electrochemistry. *J. Am. Chem. Soc.* **1987**, *109*, 3559-3568.

22.   Bain, C. D.; Troughton, E. B.; Tao, Y. T.; Evall, J.; Whitesides, G. M.; Nuzzo, R. G., Formation of Monolayer Films by the Spontaneous Assembly of Organic Thiols from Solution onto Gold. *J. Am. Chem. Soc.* **1989**, *111*, 321-335.

23.   Bain, C. D.; Whitesides, G. M., Correlations between Wettability and Structure in Monolayers of Alkanethiols Adsorbed on Gold. *J. Am. Chem. Soc.* **1988**, *110*, 3665-3666.

24.   Bain, C. D.; Evall, J.; Whitesides, G. M., Formation of Monolayers by the Coadsorption of Thiols on Gold: Variation in the Head Group, Tail Group, and Solvent. *J. Am. Chem. Soc.* **1989**, *111*, 7155-7164.

25.   Bain, C. D.; Whitesides, G. M., Formation of Monolayers by the Coadsorption of Thiols on Gold: Variation in the Length of the Alkyl Chain. *J. Am. Chem. Soc.* **1989**, *111*, 7164-7175.

26.   Arima, Y.; Iwata, H., Effect of Wettability and Surface Functional Groups on Protein Adsorption and Cell Adhesion Using Well-Defined Mixed Self-Assembled Monolayers. *Biomaterials* **2007**, *28*, 3074-3082.

27.   Wong, T.-S.; Kang, S. H.; Tang, S. K.; Smythe, E. J.; Hatton, B. D.; Grinthal, A.; Aizenberg, J., Bioinspired Self-Repairing Slippery Surfaces with Pressure-Stable Omniphobicity. *Nature* **2011**, *477*, 443.

28.   Cui, J.; Daniel, D.; Grinthal, A.; Lin, K.; Aizenberg, J., Dynamic Polymer Systems with Self-Regulated Secretion for the Control of Surface Properties and Material Healing. *Nat. Mater.* **2015**, *14*, 790.

29.   Israelachvili, J. N., *Intermolecular and Surface Forces*; Academic press, 2011.

30.   Chai, L.; Klein, J., Large Area, Molecularly Smooth (0.2 Nm Rms) Gold Films for Surface Forces and Other Studies. *Langmuir* **2007**, *23*, 7777-7783.

31.   Donaldson Jr, S. H.; Das, S.; Gebbie, M. A.; Rapp, M.; Jones, L. C.; Roiter, Y.; Koenig, P. H.; Gizaw, Y.; Israelachvili, J. N., Asymmetric Electrostatic and Hydrophobic–Hydrophilic Interaction Forces between Mica Surfaces and Silicone Polymer Thin Films. *ACS Nano* **2013**, *7*, 10094-10104.

32.   Hutter, J. L.; Bechhoefer, J., Calibration of Atomic-Force Microscope Tips. *Rev. Sci. Instrum.* **1993**, *64*, 1868-1873.

33.   Epstein, A. K.; Wong, T.-S.; Belisle, R. A.; Boggs, E. M.; Aizenberg, J., Liquid-Infused Structured Surfaces with Exceptional Anti-Biofouling Performance. *Proc. Natl. Acad. Sci.* **2012**, *109*, 13182-13187.

34.   Tabor, R. F.; Manica, R.; Chan, D. Y.; Grieser, F.; Dagastine, R. R., Repulsive Van Der Waals Forces in Soft Matter: Why Bubbles Do Not Stick to Walls. *Phys. Rev. Lett.* **2011**, *106*, 064501.

35.   Tabor, R. F.; Chan, D. Y.; Grieser, F.; Dagastine, R. R., Anomalous Stability of Carbon Dioxide in Ph-Controlled Bubble Coalescence. *Angew. Chem. Int. Ed.* **2011**, *50*, 3454-3456.

36.   Manor, O.; Vakarelski, I. U.; Tang, X.; O'Shea, S. J.; Stevens, G. W.; Grieser, F.; Dagastine, R. R.; Chan, D. Y., Hydrodynamic Boundary Conditions and Dynamic Forces between Bubbles and Surfaces. *Phys. Rev. Lett.* **2008**, *101*, 024501.

37.   Shi, C.; Chan, D. Y.; Liu, Q.; Zeng, H., Probing the Hydrophobic Interaction between Air Bubbles and Partially Hydrophobic Surfaces Using Atomic Force Microscopy. *J. Phys. Chem. C* **2014**, *118*, 25000-25008.

38.   Chan, D. Y.; Klaseboer, E.; Manica, R., Film Drainage and Coalescence between Deformable Drops and Bubbles. *Soft Matter* **2011**, *7*, 2235-2264.

39.   Israelachvili, J. N., *Intermolecular and Surface Forces*; Academic press, 2015.

40.   Du, Q.; Freysz, E.; Shen, Y. R., Surface Vibrational Spectroscopic Studies of Hydrogen Bonding and Hydrophobicity. *Science* **1994**, *264*, 826-827.

41.   Richmond, G., Molecular Bonding and Interactions at Aqueous Surfaces as Probed by Vibrational Sum Frequency Spectroscopy. *Chem. Rev.* **2002**, *102*, 2693-2724.

42.   Stirnemann, G.; Rossky, P. J.; Hynes, J. T.; Laage, D., Water Reorientation, Hydrogen-Bond Dynamics and 2d-Ir Spectroscopy Next to an Extended Hydrophobic Surface. *Faraday Discuss.* **2010**, *146*, 263-281.

43.   Godawat, R.; Jamadagni, S. N.; Garde, S., Characterizing Hydrophobicity of Interfaces by Using Cavity Formation, Solute Binding, and Water Correlations. *Proc. Natl. Acad. Sci.* **2009**, *106*, 15119-15124.

44.   Mezger, M.; Sedlmeier, F.; Horinek, D.; Reichert, H.; Pontoni, D.; Dosch, H., On the Origin of the Hydrophobic Water Gap: An X-Ray Reflectivity and Md Simulation Study. *J. Am. Chem. Soc.* **2010**, *132*, 6735-6741.

45.   Despa, F.; Fernández, A.; Berry, R. S., Dielectric Modulation of Biological Water. *Phys. Rev. Lett.* **2004**, *93*, 228104.

46.   Kanth, J. M. P.; Vemparala, S.; Anishetty, R., Long-Distance Correlations in Molecular Orientations of Liquid Water and Shape-Dependent Hydrophobic Force. *Phys. Rev. E* **2010**, *81*, 021201.

47.   Despa, F.; Berry, R. S., The Origin of Long-Range Attraction between Hydrophobes in Water. *Biophys. J.* **2007**, *92*, 373-378.

48.   Scatena, L.; Brown, M.; Richmond, G., Water at Hydrophobic Surfaces: Weak Hydrogen Bonding and Strong Orientation Effects. *Science* **2001**, *292*, 908-912.

49.   Miranda, P.; Shen, Y., Liquid Interfaces: A Study by Sum-Frequency Vibrational Spectroscopy. *J. Phys. Chem. B* **1999**, *103*, 3292-3307.

50.   Du, Q.; Freysz, E.; Shen, Y. R., Vibrational Spectra of Water Molecules at Quartz/Water Interfaces. *Phys. Rev. Lett.* **1994**, *72*, 238.

51.   Patel, A. J.; Varilly, P.; Chandler, D., Fluctuations of Water near Extended Hydrophobic and Hydrophilic Surfaces. *J. Phys. Chem. B* **2010**, *114*, 1632.

52.   Miranda, P.; Xu, L.; Shen, Y.; Salmeron, M., Icelike Water Monolayer Adsorbed on Mica at Room Temperature. *Phys. Rev. Lett.* **1998**, *81*, 5876.

Chapter 7   Conclusions and Future Work

7.1. Major conclusions

In this project, the interactions between air bubbles and various hydrophobic surfaces under different aqueous conditions have been directly measured using bubble probe AFM technique, and the involved surface interactions have been quantified by theoretically analyzing the measured force data based on the Stoke-Reynolds-Young-Laplace model incorporating the effect of disjoining pressure. This work contributes to an improved understanding of the mechanisms of the surface interactions especially HB interaction between air bubbles and hydrophobic surfaces, and clarifies the effects of a series of principal parameters which can potentially impact the surface interactions.

The interactions between air bubbles and OTS-hydrophobized mica substrates have been investigated in aqueous solutions with different salinity and pH. It was found that the EDL interaction could be significantly suppressed by either lowering the aqueous pH or increasing the solution salinity, either making both the air bubble and the OTS-mica substrate less negatively charged or compressing the Debye length, respectively. However, the variation in salinity and pH was found to have no detectable effect on the HB interaction whose decay length D_0 remained constant (~ 1.0 nm) across all the studied cases. At high pH (e.g., ~ 10.0) or low salinity (~ 1 mM NaCl), the strong EDL interaction made the major contribution to the repulsive disjoining pressure, which was able to resist the HB attraction and sustain the thin water film confined by the air bubble and the OTS-mica substrate. On the contrary, at low pH (e.g., ~ 3.0) or high salinity (e.g., 1000 mM NaCl), the HB attraction dominated the bubble-substrate interaction and overcame the repulsive VDW and EDL repulsions, rupturing the thin water film

and triggering the bubble attachment featured by a characteristic "jump-in" behavior in the interaction force curve.

Different from the cases of hydrocarbon SAMs, the investigation of interactions between air bubbles and hydrophobic polymers surfaces exhibited distinctive results and phenomena. INBs could spontaneously nucleate on the hydrophobic PS surfaces upon immersing in aqueous environment. By virtue of AFM TM and PF-QNM imaging, the morphology and distribution of the INBs were found to be sensitive to the variation in aqueous salinity. By correlating the AFM imaging and force measurement results, the roles of the INBs on the bubble-PS interactions were revealed. At low salinity (e.g., ~ 1 mM NaCl), there existed a dense layer of INBs on the PS surface, and the strong EDL repulsion dominated the interaction between the bubble probe and the PS surface covered with INBs, stabilizing the confined thin water film and preventing the bubble attachment. At high salinity (e.g., ~ 500 and 1000 mM NaCl), the INBs were greatly reduced in both density and size, even disappeared, leading to the exposure of the pristine PS surface to the aqueous media. By applying $D_0 \sim 0.75$ nm for the intrinsic HB interaction between the bubble and the PS surface, the theoretically fitting result could agree well with the measured interaction force at high salinity. However, an unexpected discrepancy was found at intermediate salinity (i.e., 100 mM NaCl) between the experimental results and the theoretical calculations, which could not be interpreted by the classical DLVO theory incorporating the effect of HB interaction. The air bubble should have attached onto the PS surface because the VDW and suppressed EDL repulsions were not able to resist the strong HB attraction. Whereas, the presence of the layer of INBs imposed an additional non-DLVO repulsion resembling a certain hydration force against the bubble and inhibited the bubble attachment.

Besides, it was found that the HB interactions between air bubbles and hydrophobic polymers could be modulated by the presence of some specific ions in the aqueous environment. By conducting the AFM force measurements at high salinity (~ 1000 mM), the negative effect of the INBs can be effectively ruled out. For the bubble-PS HB interaction, the decay length D0 was reduced from ~ 0.75 nm in solutions of LiCl or NaCl to ~ 0.60 nm when the cation was switched to K^+ or NH_4^+. This shortened range of the bubble-PS HB interaction could arise from the cation-π interaction. The cations with relatively low charge density and desolvation penalty (e.g., K^+ and NH_4^+) could selectively bind to the aromatic benzene rings of the PS molecules, disturbing the original ordered structure of the interfacial water molecules and shortening the range of the bubble-PS HB interaction. However, the variation in the anion type had no measurable effect on the bubble-PS HB interaction, which could be attributed to the possible repulsion between the cations and the electro-rich benzene rings. Oppositely, the bubble-PMMA and bubble-PDMS HB interactions were found to be sensitive to the specific anionic effects rather than cationic effects. D_0 was reduced from ~ 0.63 nm and ~ 0.72 nm to ~ 0.50 nm and ~ 0.59 nm, respectively, when F^- or Cl^- was changed to I^-. This phenomenon could be due to the preferential adsorption of the heavier I^- over the lighter F^- and Cl^- onto the PMMA and PDMS surfaces which could also disorder the network of the interfacial water molecules and reduce the range of the HB interaction.

In addition to water chemistry, the inherent physical and chemical properties of the hydrophobic surfaces, such as the surface mobility and chemistry, can also be crucial factors in determining the range and magnitude of the HB interactions in different hydrophobic systems. Such effects have been deeply and comprehensively investigated by quantifying the HB interactions between air bubbles and various alkanethiol SAMs and SLIPSs. The SAMs

composed of a layer of uniform long-chain alkanethiols ($n \geq 8$) possessed an ordered crystalline-like structure. Adsorbing short-chain thiols ($n \leq 5$) or coadsorbing two species of thiol molecules with different chain length could effectively introduce the surface mobility into the SAM surface, resembling an amorphous liquid-like surface. The SLIPSs featured an over-coating of lubricating oil, exhibiting a thermodynamically flexible pure liquid surface. For these three distinctive hydrophobic surfaces, D_0 of their HB interactions with air bubbles was ~ 1.60 nm, ~ 1.25 nm, and ~ 0.35 nm, respectively. This result can reflect that increasing the mobility of the hydrophobic surface would relax the physical restriction that orderly reorganized the interfacial water molecules, and thus shorten the range of the HB interaction. Besides, D_0 could also be effectively modulated by proximally immobilizing hydrophilic moieties (e.g., hydroxyl, amine and carboxyl groups) to hydrophobic domains within the SAM. The presence of the hydrophilic moieties with high affinity for water can interfere with the ordering of the interfacial water molecules. And the resultant nano-scaled chemical heterogeneity could introduce extra three-dimensional freedom, which could further disrupt the packing of the thiol molecules, relaxing the physical restriction and shortening the range of the HB interaction.

7.2 Original contributions.

This work offers a reliable and effective methodology to directly measure the interactions between air bubbles and various hydrophobic surfaces under different aqueous conditions, and quantitatively study the involved surface interactions by coupling bubble probe AFM technique with the theoretical analysis based on the Stokes-Reynolds-Young-Laplace model. Applying this method, it is feasible to precisely interpret the measured interaction forces, establish the accurate force-separation profiles of the surface interactions and identify the effects of the potential

influencing factors, which is of great significance in not only fundamentally understanding the surface interaction mechanisms involving deformable bubbles, but also practically offering quantitative guidance for a variety of industrial and engineering applications, such as froth flotation in mineral processing, oil production and wastewater treatment, emulsion stabilization and encapsulation technique in food, drug and cosmetic industries, multimodal imaging and stimulus-responsive drug/gene delivery in biomedical diagnostics and therapeutics, and fabrication of novel materials in catalysis, lithium battery, microreactors and gas evolution reaction.

In addition to the target of investigating the surface interactions between air bubbles and hydrophobic surfaces, the application of air bubbles as the AFM probes possesses unparalleled advantages in precisely measuring and quantifying the HB interactions because the bubble surface generally exhibits molecular smoothness and intrinsic hydrophobicity. By quantitatively study the HB interactions between air bubbles and various hydrophobic surfaces under different aqueous conditions, this work unravels the effects of a series of principal parameters which can significantly modulate the HB interaction, including water chemistry such as salinity, aqueous pH and ion specificity, and the inherent properties of the hydrophobic surfaces such as the surface mobility and chemistry. Therefore, this work makes a great contribution to advancing the basic knowledge of the HB interactions involved in a variety of hydrophobic systems, and sheds novel lights on the understanding of the related colloidal and interfacial phenomena driven by HB interaction. Besides, an improved understanding of the hydrophobic interaction mechanism would provide theoretical instructions on how to optimize the associated industrial and bioengineering operations and to innovate the fabrication procedures of novel advanced functional materials.

Moreover, this methodology can be extensively utilized to study the interactions involving other gas bubbles and oil droplets in complex aqueous media and the interactions involving water droplets in oil phases, which can be of great importance in studying the mechanisms of emulsion stabilization and destabilization in various complicated fluidic systems and the self-assembly behaviors of particles and macromolecules at the different interfaces.

7.3. Suggestions for future work.

(1). This method can be extensively applied to measure and analyze the interactions between various oil droplets (e.g., aromatic, aliphatic and fluoro hydrocarbons) and surfaces with different hydrophobicity, aiming to probe the surface interactions, especially the HB interactions involving the oil/water interfaces, which are expected to provide novel insight on the process of water/oil separation.

(2). Some surface active agents such as cationic, anionic and zwitterionic surfactants, amphiphilic macromolecules and proteins, and colloidal particles are commonly present in a variety of complex aqueous systems in both natural environment and engineering processes. The spontaneous adsorption and assembly at the oil/water, gas/water and solid/water interfaces would complicate the interactions between deformable droplets and hydrophobic surfaces and lead to some distinctive phenomena, which deserves to be intensively studied.

(3). SFG characterization and MD simulation can be utilized to explore the orientation and organization of the water molecules at the interfaces of water with gas, oil and amorphous and crystalline solid surfaces, in order to elucidate the specific ordering effect of the interfacial water molecules at different hydrophobic surfaces. In this way, the range and magnitude of the HB interactions in different hydrophobic systems can be correlated with the corresponding water

structuring effects, which offers a deeper understanding of the HB interaction mechanism at nanoscale.

(4). This project provided novel insight into the surface interaction mechanisms between deformable droplets and hydrophobic surfaces. Based on the results of this fundamental research, novel advanced materials applied for gas transport and separation of oil/water mixtures and emulsions can be designed and developed, and the relevant preparation procedures can be optimized.

Bibliography

1.   Dickinson, E., Food Emulsions and Foams: Stabilization by Particles. *Curr. Opin. Colloid Interface Sci.* **2010**, *15*, 40-49.

2.   Park, J. I.; Jagadeesan, D.; Williams, R.; Oakden, W.; Chung, S.; Stanisz, G. J.; Kumacheva, E., Microbubbles Loaded with Nanoparticles: A Route to Multiple Imaging Modalities. *ACS Nano* **2010**, *4*, 6579-6586.

3.   Klibanov, A. L., Microbubble Contrast Agents: Targeted Ultrasound Imaging and Ultrasound-Assisted Drug-Delivery Applications. *Invest. Radiol.* **2006**, *41*, 354-362.

4.   Gao, W.; Pei, A.; Wang, J., Water-Driven Micromotors. *ACS Nano* **2012**, *6*, 8432-8438.

5.   Lou, X. W. D.; Archer, L. A.; Yang, Z., Hollow Micro-/Nanostructures: Synthesis and Applications. *Adv. Mater.* **2008**, *20*, 3987-4019.

6.   Zeng, H.; Shi, C.; Huang, J.; Li, L.; Liu, G.; Zhong, H., Recent Experimental Advances on Hydrophobic Interactions at Solid/Water and Fluid/Water Interfaces. *Biointerphases* **2016**, *11*, 018903.

7.   Xie, L.; Shi, C.; Cui, X.; Zeng, H., Surface Forces and Interaction Mechanisms of Emulsion Drops and Gas Bubbles in Complex Fluids. *Langmuir* **2017**, *33*, 3911-3925.

8.   Israelachvili, J. N., *Intermolecular and Surface Forces*; Academic press, 2011.

9.   Hogg, R.; Healy, T. W.; Fuerstenau, D., Mutual Coagulation of Colloidal Dispersions. *Trans. Faraday Soc.* **1966**, *62*, 1638-1651.

10.   Carnie, S. L.; Chan, D. Y.; Gunning, J. S., Electrical Double Layer Interaction between Dissimilar Spherical Colloidal Particles and between a Sphere and a Plate: The Linearized Poisson-Boltzmann Theory. *Langmuir* **1994**, *10*, 2993-3009.

11.   Ralston, J.; Fornasiero, D.; Hayes, R., Bubble–Particle Attachment and Detachment in Flotation. *Int. J. Miner. Process.* **1999**, *56*, 133-164.

12.   Gu, J.; Xiao, P.; Chen, J.; Zhang, J.; Huang, Y.; Chen, T., Janus Polymer/Carbon Nanotube Hybrid Membranes for Oil/Water Separation. *ACS Appl. Mater. Interfaces* **2014**, *6*, 16204-16209.

13.   Gonzenbach, U. T.; Studart, A. R.; Tervoort, E.; Gauckler, L. J., Ultrastable Particle-Stabilized Foams. *Angew. Chem. Int. Ed.* **2006**, *45*, 3526-3530.

14.   Yu, C.; Zhu, X.; Li, K.; Cao, M.; Jiang, L., Manipulating Bubbles in Aqueous Environment Via a Lubricant-Infused Slippery Surface. *Adv. Funct. Mater.* **2017**.

15.   Janson, J.-C., *Protein Purification: Principles, High Resolution Methods, and Applications*; John Wiley & Sons, 2012; Vol. 151.

16.   Chandler, D., Interfaces and the Driving Force of Hydrophobic Assembly. *Nature* **2005**, *437*, 640.

17.   Tabor, R. F.; Grieser, F.; Dagastine, R. R.; Chan, D. Y., The Hydrophobic Force: Measurements and Methods. *Phys. Chem. Chem. Phys.* **2014**, *16*, 18065-18075.

18.   Israelachvili, J.; Pashley, R., The Hydrophobic Interaction Is Long Range, Decaying Exponentially with Distance. *Nature* **1982**, *300*, 341-342.

19.   Faghihnejad, A.; Zeng, H., Hydrophobic Interactions between Polymer Surfaces: Using Polystyrene as a Model System. *Soft Matter* **2012**, *8*, 2746-2759.

20.   Donaldson Jr, S. H.; Røyne, A.; Kristiansen, K.; Rapp, M. V.; Das, S.; Gebbie, M. A.; Lee, D. W.; Stock, P.; Valtiner, M.; Israelachvili, J., Developing a General Interaction Potential for Hydrophobic and Hydrophilic Interactions. *Langmuir* **2014**, *31*, 2051-2064.

21.   Xie, L.; Wang, J.; Shi, C.; Cui, X.; Huang, J.; Zhang, H.; Liu, Q.; Liu, Q.; Zeng, H., Mapping the Nanoscale Heterogeneity of Surface Hydrophobicity on the Sphalerite Mineral. *J. Phys. Chem. C* **2017**, *121*, 5620-5628.

22.   Stock, P.; Utzig, T.; Valtiner, M., Direct and Quantitative Afm Measurements of the Concentration and Temperature Dependence of the Hydrophobic Force Law at Nanoscopic Contacts. *J. Colloid Interface Sci.* **2015**, *446*, 244-251.

23.   Meyer, E. E.; Lin, Q.; Hassenkam, T.; Oroudjev, E.; Israelachvili, J. N., Origin of the Long-Range Attraction between Surfactant-Coated Surfaces. *Proc. Natl. Acad. Sci. U.S.A.* **2005**, *102*, 6839-6842.

24.   Nguyen, A. V.; Nalaskowski, J.; Miller, J. D.; Butt, H.-J., Attraction between Hydrophobic Surfaces Studied by Atomic Force Microscopy. *Int. J. Miner. Process.* **2003**, *72*, 215-225.

25.   Ishida, N.; Sakamoto, M.; Miyahara, M.; Higashitani, K., Attraction between Hydrophobic Surfaces with and without Gas Phase. *Langmuir* **2000**, *16*, 5681-5687.

26.   Pushkarova, R. A.; Horn, R. G., Surface Forces Measured between an Air Bubble and a Solid Surface in Water. *Colloids Surf., A* **2005**, *261*, 147-152.

27.   Fielden, M. L.; Hayes, R. A.; Ralston, J., Surface and Capillary Forces Affecting Air Bubble− Particle Interactions in Aqueous Electrolyte. *Langmuir* **1996**, *12*, 3721-3727.

28.   Preuss, M.; Butt, H.-J., Direct Measurement of Particle− Bubble Interactions in Aqueous Electrolyte: Dependence on Surfactant. *Langmuir* **1998**, *14*, 3164-3174.

29.   Dagastine, R. R.; Manica, R.; Carnie, S. L.; Chan, D.; Stevens, G. W.; Grieser, F., Dynamic Forces between Two Deformable Oil Droplets in Water. *Science* **2006**, *313*, 210-213.

30.   Shi, C.; Cui, X.; Xie, L.; Liu, Q.; Chan, D. Y.; Israelachvili, J. N.; Zeng, H., Measuring Forces and Spatiotemporal Evolution of Thin Water Films between an Air Bubble and Solid Surfaces of Different Hydrophobicity. *ACS Nano* **2014**, *9*, 95-104.

31.   Tabor, R. F.; Manica, R.; Chan, D. Y.; Grieser, F.; Dagastine, R. R., Repulsive Van Der Waals Forces in Soft Matter: Why Bubbles Do Not Stick to Walls. *Phys. Rev. Lett.* **2011**, *106*, 064501.

32.   Cui, X.; Shi, C.; Xie, L.; Liu, J.; Zeng, H., Probing Interactions between Air Bubble and Hydrophobic Polymer Surface: Impact of Solution Salinity and Interfacial Nanobubbles. *Langmuir* **2016**, *32*, 11236-11244.

33.   Cui, X.; Shi, C.; Zhang, S.; Xie, L.; Liu, J.; Jiang, D.; Zeng, H., Probing the Effect of Salinity and Ph on Surface Interactions between Air Bubbles and Hydrophobic Solids: Implications for Colloidal Assembly at Air/Water Interfaces. *Chem. - Asian J.* **2017**, 12, 1568-1577.

34.   Chan, D. Y.; Klaseboer, E.; Manica, R., Film Drainage and Coalescence between Deformable Drops and Bubbles. *Soft Matter* **2011**, *7*, 2235-2264.

35.   Tabor, R. F.; Lockie, H.; Mair, D.; Manica, R.; Chan, D. Y.; Grieser, F.; Dagastine, R. R., Combined Afm− Confocal Microscopy of Oil Droplets: Absolute Separations and Forces in Nanofilms. *J. Phys. Chem. Lett.* **2011**, *2*, 961-965.

36.   Barrett. J.C. www.Barrett-Group.Mcgill.Ca. **2008**.

37.   Parker, J. L.; Claesson, P. M.; Attard, P., Bubbles, Cavities, and the Long-Ranged Attraction between Hydrophobic Surfaces. *J. Phys. Chem.* **1994**, *98*, 8468-8480.

38.   Yakubov, G. E.; Butt, H.-J.; Vinogradova, O. I., Interaction Forces between Hydrophobic Surfaces. Attractive Jump as an Indication of Formation of "Stable" Submicrocavities. *J. Phys. Chem. B* **2000**, *104*, 3407-3410.

39.   Lohse, D.; Zhang, X., Surface Nanobubbles and Nanodroplets. *Rev. Mod. Phys.* **2015**, *87*, 981.

40.   Meyer, E. E.; Rosenberg, K. J.; Israelachvili, J., Recent Progress in Understanding Hydrophobic Interactions. *Proc. Natl. Acad. Sci.* **2006**, *103*, 15739-15746.

41.   Tabor, R. F.; Wu, C.; Grieser, F.; Dagastine, R. R.; Chan, D. Y., Measurement of the Hydrophobic Force in a Soft Matter System. *J. Phys. Chem. Lett.* **2013**, *4*, 3872-3877.

42.   Shi, C.; Chan, D. Y.; Liu, Q.; Zeng, H., Probing the Hydrophobic Interaction between Air Bubbles and Partially Hydrophobic Surfaces Using Atomic Force Microscopy. *J. Phys. Chem. C* **2014**, *118*, 25000-25008.

43.   Hutter, J. L.; Bechhoefer, J., Calibration of Atomic-Force Microscope Tips. *Rev. Sci. Instrum.* **1993**, *64*, 1868-1873.

44.   Xue, Y.; Li, X.; Li, H.; Zhang, W., Quantifying Thiol-Gold Interactions Towards the Efficient Strength Control. *Nat. Commun.* **2014**, *5*, 4348.

45.   Vakarelski, I. U.; Manica, R.; Tang, X.; O'Shea, S. J.; Stevens, G. W.; Grieser, F.; Dagastine, R. R.; Chan, D. Y., Dynamic Interactions between Microbubbles in Water. *Proc. Natl. Acad. Sci.* **2010**, *107*, 11177-11182.

46.   Xie, L.; Shi, C.; Wang, J.; Huang, J.; Lu, Q.; Liu, Q.; Zeng, H., Probing the Interaction between Air Bubble and Sphalerite Mineral Surface Using Atomic Force Microscope. *Langmuir* **2015**, *31*, 2438-2446.

47.   Tabor, R. F.; Chan, D. Y.; Grieser, F.; Dagastine, R. R., Anomalous Stability of Carbon Dioxide in Ph-Controlled Bubble Coalescence. *Angew. Chem. Int. Ed.* **2011**, *50*, 3454-3456.

48.   Hendrix, M. H.; Manica, R.; Klaseboer, E.; Chan, D. Y.; Ohl, C.-D., Spatiotemporal Evolution of Thin Liquid Films During Impact of Water Bubbles on Glass on a Micrometer to Nanometer Scale. *Phys. Rev. Lett.* **2012**, *108*, 247803.

49.   Manor, O.; Vakarelski, I. U.; Stevens, G. W.; Grieser, F.; Dagastine, R. R.; Chan, D. Y., Dynamic Forces between Bubbles and Surfaces and Hydrodynamic Boundary Conditions. *Langmuir* **2008**, *24*, 11533-11543.

50.   Manica, R.; Chan, D. Y., Drainage of the Air–Water–Quartz Film: Experiments and Theory. *Phys. Chem. Chem. Phys.* **2011**, *13*, 1434-1439.

51.   Park, J. I.; Nie, Z.; Kumachev, A.; Abdelrahman, A. I.; Binks, B. P.; Stone, H. A.; Kumacheva, E., A Microfluidic Approach to Chemically Driven Assembly of Colloidal Particles at Gas–Liquid Interfaces. *Angew. Chem.* **2009**, *121*, 5404-5408.

52.   Zhang, X.; Lohse, D., Perspectives on Surface Nanobubbles. *Biomicrofluidics* **2014**, *8*, 041301.

53.   Fameau, A. L.; Carl, A.; Saint-Jalmes, A.; Von Klitzing, R., Responsive Aqueous Foams. *ChemPhysChem* **2015**, *16*, 66-75.

54.   Binks, B. P.; Murakami, R., Phase Inversion of Particle-Stabilized Materials from Foams to Dry Water. *Nat. Mater.* **2006**, *5*, 865-869.

55.   Zhou, C.; Zhao, Y.; Bian, T.; Shang, L.; Yu, H.; Wu, L.-Z.; Tung, C.-H.; Zhang, T., Bubble Template Synthesis of Sn 2 Nb 2 O 7 Hollow Spheres for Enhanced Visible-Light-Driven Photocatalytic Hydrogen Production. *Chem. Commun.* **2013**, *49*, 9872-9874.

56. Mao, Z.; Xu, H.; Wang, D., Molecular Mimetic Self-Assembly of Colloidal Particles. *Adv. Funct. Mater.* **2010**, *20*, 1053-1074.

57. Xu, J.; Li, X.; Wu, X.; Wang, W.; Fan, R.; Liu, X.; Xu, H., Hierarchical Cuo Colloidosomes and Their Structure Enhanced Photothermal Catalytic Activity. *J. Phys. Chem. C* **2016**, *120*, 12666-12672.

58. Zhang, L.; Zheng, M.; Liu, X.; Sun, J., Layer-by-Layer Assembly of Salt-Containing Polyelectrolyte Complexes for the Fabrication of Dewetting-Induced Porous Coatings. *Langmuir* **2010**, *27*, 1346-1352.

59. Wu, C.; Xie, Y.; Lei, L.; Hu, S.; OuYang, C., Synthesis of New-Phased Vooh Hollow "Dandelions" and Their Application in Lithium-Ion Batteries. *Adv. Mater.* **2006**, *18*, 1727-1732.

60. Fan, X.; Zhang, Z.; Li, G.; Rowson, N., Attachment of Solid Particles to Air Bubbles in Surfactant-Free Aqueous Solutions. *Chem. Eng. Sci.* **2004**, *59*, 2639-2645.

61. Wang, X.; Feng, J.; Bai, Y.; Zhang, Q.; Yin, Y., Synthesis, Properties, and Applications of Hollow Micro-/Nanostructures. *Chem. Rev.* **2016**, *116*, 10983-11060.

62. Butt, H.-J.; Graf, K.; Kappl, M., *Physics and Chemistry of Interfaces*; John Wiley & Sons, 2006.

63. Hammer, M. U.; Anderson, T. H.; Chaimovich, A.; Shell, M. S.; Israelachvili, J., The Search for the Hydrophobic Force Law. *Faraday Discuss.* **2010**, *146*, 299-308.

64. Davis, J. G.; Gierszal, K. P.; Wang, P.; Ben-Amotz, D., Water Structural Transformation at Molecular Hydrophobic Interfaces. *Nature* **2012**, *491*, 582-585.

65. Lam, S.; Velikov, K. P.; Velev, O. D., Pickering Stabilization of Foams and Emulsions with Particles of Biological Origin. *Curr. Opin. Colloid Interface Sci.* **2014**, *19*, 490-500.

66.   Bournival, G.; Ata, S.; Wanless, E. J., The Roles of Particles in Multiphase Processes: Particles on Bubble Surfaces. *Adv. Colloid Interface Sci.* **2015**, *225*, 114-133.

67.   Butt, H.-J., A Technique for Measuring the Force between a Colloidal Particle in Water and a Bubble. *J. Colloid Interface Sci.* **1994**, *166*, 109-117.

68.   Ducker, W. A.; Xu, Z.; Israelachvili, J. N., Measurements of Hydrophobic and DLVO Forces in Bubble-Surface Interactions in Aqueous Solutions. *Langmuir* **1994**, *10*, 3279-3289.

69.   Ishida, N., Direct Measurement of Hydrophobic Particle–Bubble Interactions in Aqueous Solutions by Atomic Force Microscopy: Effect of Particle Hydrophobicity. *Colloids Surf., A* **2007**, *300*, 293-299.

70.   Vakarelski, I. U.; Lee, J.; Dagastine, R. R.; Chan, D. Y.; Stevens, G. W.; Grieser, F., Bubble Colloidal Afm Probes Formed from Ultrasonically Generated Bubbles. *Langmuir* **2008**, *24*, 603-605.

71.   Xie, L.; Wang, J.; Yuan, D.; Shi, C.; Cui, X.; Zhang, H.; Liu, Q.; Liu, Q.; Zeng, H., Interaction Mechanisms between Air Bubble and Molybdenite Surface: Impact of Solution Salinity and Polymer Adsorption. *Langmuir* **2017**, *33*, 2353-2361.

72.   Webber, G. B.; Manica, R.; Edwards, S. A.; Carnie, S. L.; Stevens, G. W.; Grieser, F.; Dagastine, R. R.; Chan, D. Y., Dynamic Forces between a Moving Particle and a Deformable Drop. *J. Phys. Chem. C* **2008**, *112*, 567-574.

73.   Tabor, R. F.; Grieser, F.; Dagastine, R. R.; Chan, D. Y., Measurement and Analysis of Forces in Bubble and Droplet Systems Using Afm. *J. Colloid Interface Sci.* **2012**, *371*, 1-14.

74.   Tabor, R. F.; Morfa, A. J.; Grieser, F.; Chan, D. Y.; Dagastine, R. R., Effect of Gold Oxide in Measurements of Colloidal Force. *Langmuir* **2011**, *27*, 6026-6030.

75.   Horozov, T. S.; Aveyard, R.; Clint, J. H.; Binks, B. P., Order− Disorder Transition in Monolayers of Modified Monodisperse Silica Particles at the Octane− Water Interface. *Langmuir* **2003**, *19*, 2822-2829.

76.   Wang, J.; Li, J.; Xie, L.; Shi, C.; Liu, Q.; Zeng, H., Interactions between Elemental Selenium and Hydrophilic/Hydrophobic Surfaces: Direct Force Measurements Using Afm. *Chem. Eng. J.* **2016**, *303*, 646–654.

77.   Paunov, V. N., Novel Method for Determining the Three-Phase Contact Angle of Colloid Particles Adsorbed at Air− Water and Oil− Water Interfaces. *Langmuir* **2003**, *19*, 7970-7976.

78.   Klaseboer, E.; Chevaillier, J. P.; Gourdon, C.; Masbernat, O., Film Drainage between Colliding Drops at Constant Approach Velocity: Experiments and Modeling. *J. Colloid Interface Sci.* **2000**, *229*, 274-285.

79.   Yiantsios, S. G.; Davis, R. H., Close Approach and Deformation of Two Viscous Drops Due to Gravity and Van Der Waals Forces. *J. Colloid Interface Sci.* **1991**, *144*, 412-433.

80.   Stankovich, J.; Carnie, S. L., Electrical Double Layer Interaction between Dissimilar Spherical Colloidal Particles and between a Sphere and a Plate: Nonlinear Poisson− Boltzmann Theory. *Langmuir* **1996**, *12*, 1453-1461.

81.   Donaldson Jr, S. H.; Das, S.; Gebbie, M. A.; Rapp, M.; Jones, L. C.; Roiter, Y.; Koenig, P. H.; Gizaw, Y.; Israelachvili, J. N., Asymmetric Electrostatic and Hydrophobic–Hydrophilic Interaction Forces between Mica Surfaces and Silicone Polymer Thin Films. *ACS Nano* **2013**, *7*, 10094-10104.

82.   Manica, R.; Connor, J. N.; Dagastine, R. R.; Carnie, S. L.; Horn, R. G.; Chan, D. Y., Hydrodynamic Forces Involving Deformable Interfaces at Nanometer Separations. *Phys. Fluids* **2008**, *20*, 032101.

83.   Creux, P.; Lachaise, J.; Graciaa, A.; Beattie, J. K.; Djerdjev, A. M., Strong Specific Hydroxide Ion Binding at the Pristine Oil/Water and Air/Water Interfaces. *J. Phys. Chem. B* **2009**, *113*, 14146-14150.

84.   Takahashi, M., Z Potential of Microbubbles in Aqueous Solutions: Electrical Properties of the Gas-Water Interface. *J. Phys. Chem. B* **2005**, *109*, 21858-21864.

85.   Yang, C.; Dabros, T.; Li, D.; Czarnecki, J.; Masliyah, J. H., Measurement of the Zeta Potential of Gas Bubbles in Aqueous Solutions by Microelectrophoresis Method. *J. Colloid Interface Sci.* **2001**, *243*, 128-135.

86.   Lützenkirchen, J.; Richter, C., Zeta-Potential Measurements of Ots-Covered Silica Samples. *Adsorption* **2013**, *19*, 217-224.

87.   Hozumi, A.; Sugimura, H.; Yokogawa, Y.; Kameyama, T.; Takai, O., Z-Potentials of Planar Silicon Plates Covered with Alkyl-and Fluoroalkylsilane Self-Assembled Monolayers. *Colloids Surf., A* **2001**, *182*, 257-261.

88.   Schweiss, R.; Welzel, P. B.; Werner, C.; Knoll, W., Dissociation of Surface Functional Groups and Preferential Adsorption of Ions on Self-Assembled Monolayers Assessed by Streaming Potential and Streaming Current Measurements. *Langmuir* **2001**, *17*, 4304-4311.

89.   Chen, K.; Shan, L.; He, S.; Hu, G.; Meng, Y.; Tian, Y., Biphasic Resistive Pulses and Ion Concentration Modulation During Particle Translocation through Cylindrical Nanopores. *J. Phys. Chem. C* **2015**, *119*, 8329-8335.

90.   Gonzenbach, U. T.; Studart, A. R.; Tervoort, E.; Gauckler, L. J., Stabilization of Foams with Inorganic Colloidal Particles. *Langmuir* **2006**, *22*, 10983-10988.

91.   Stocco, A.; Rio, E.; Binks, B. P.; Langevin, D., Aqueous Foams Stabilized Solely by Particles. *Soft Matter* **2011**, *7*, 1260-1267.

59.   Khademhosseini, A.; Langer, R.; Borenstein, J.; Vacanti, J. P. Microscale technologies for tissue engineering and biology. *Proc. Natl. Acad. Sci. U. S. A.* **2006,** *103*, 2480-2487.

60.   Sanguansri, P.; Augustin, M. A. Nanoscale materials development–a food industry perspective. *Trends Food Sci. Technol.* **2006,** *17*, 547-556.

61.   Nguyen, A.; Nalaskowski, J.; Miller, J. A study of bubble–particle interaction using atomic force microscopy. *Miner. Eng.* **2003,** *16*, 1173-1181.

62.   Wangsa-Wirawan, N.; Ikai, A.; O'Neill, B.; Middelberg, A. Measuring the interaction forces between protein inclusion bodies and an air bubble using an atomic force microscope. *Biotechnol. Prog.* **2001,** *17*, 963-969.

63.   Preuss, M.; Butt, H.-J. Measuring the contact angle of individual colloidal particles. *J. Colloid Interface Sci.* **1998,** *208*, 468-477.

64.   Walczyk, W.; Schön, P. M.; Schönherr, H. The effect of PeakForce tapping mode AFM imaging on the apparent shape of surface nanobubbles. *J. Phys.: Condens. Matter* **2013,** *25*, 184005.

65.   Zhao, B.; Song, Y.; Wang, S.; Dai, B.; Zhang, L.; Dong, Y.; Lü, J.; Hu, J. Mechanical mapping of nanobubbles by PeakForce atomic force microscopy. *Soft Matter* **2013,** *9*, 8837-8843.

66.   Wang, X.; Zhao, B.; Ma, W.; Wang, Y.; Gao, X.; Tai, R.; Zhou, X.; Zhang, L. Interfacial Nanobubbles on Atomically Flat Substrates with Different Hydrophobicities. *ChemPhysChem* **2015,** *16*, 1003-1007.

67.   Simonsen, A. C.; Hansen, P. L.; Klösgen, B. Nanobubbles give evidence of incomplete wetting at a hydrophobic interface. *J. Colloid Interface Sci.* **2004,** *273*, 291-299.

68.   Hampton, M.; Nguyen, A. Nanobubbles and the nanobubble bridging capillary force. *Adv. Colloid Interface Sci.* **2010,** *154*, 30-55.

69.   Zhang, X. H.; Quinn, A.; Ducker, W. A. Nanobubbles at the interface between water and a hydrophobic solid. *Langmuir* **2008,** *24*, 4756-4764.

70.   Bhushan, B.; Jung, Y. C. Natural and biomimetic artificial surfaces for superhydrophobicity, self-cleaning, low adhesion, and drag reduction. *Prog. Mater Sci.* **2011,** *56*, 1-108.

71.   Weijs, J. H.; Lohse, D. Why surface nanobubbles live for hours. *Phys. Rev. Lett.* **2013,** *110*, 054501.

72.   Yang, J.; Duan, J.; Fornasiero, D.; Ralston, J. Very small bubble formation at the solid-water interface. *J. Phys. Chem. B* **2003,** *107*, 6139-6147.

73.   Ducker, W. A. Contact angle and stability of interfacial nanobubbles. *Langmuir* **2009,** *25*, 8907-8910.

74.   Brenner, M. P.; Lohse, D. Dynamic equilibrium mechanism for surface nanobubble stabilization. *Phys. Rev. Lett.* **2008,** *101*, 214505.

75.   Seddon, J. R.; Zandvliet, H. J.; Lohse, D. Knudsen gas provides nanobubble stability. *Phys. Rev. Lett.* **2011,** *107*, 116101.

76.   Attard, P. Bridging bubbles between hydrophobic surfaces. *Langmuir* **1996,** *12*, 1693-1695.

77.   Carambassis, A.; Jonker, L. C.; Attard, P.; Rutland, M. W. Forces measured between hydrophobic surfaces due to a submicroscopic bridging bubble. *Phys. Rev. Lett.* **1998,** *80*, 5357.

78.   Tyrrell, J. W.; Attard, P. Images of nanobubbles on hydrophobic surfaces and their interactions. *Phys. Rev. Lett.* **2001,** *87*, 176104.

79.   Azadi, M.; Nguyen, A. V.; Yakubov, G. E. Attractive forces between hydrophobic solid surfaces measured by AFM on the first approach in salt solutions and in the presence of dissolved gases. *Langmuir* **2015,** *31*, 1941-1949.

80.   Carnie, S. L.; Chan, D. Y.; Lewis, C.; Manica, R.; Dagastine, R. R. Measurement of dynamical forces between deformable drops using the atomic force microscope. I. Theory. *Langmuir* **2005,** *21*, 2912-2922.

81.   Manor, O.; Vakarelski, I. U.; Tang, X.; O'Shea, S. J.; Stevens, G. W.; Grieser, F.; Dagastine, R. R.; Chan, D. Y. Hydrodynamic boundary conditions and dynamic forces between bubbles and surfaces. *Phys. Rev. Lett.* **2008,** *101*, 024501.

82.   Xu, R. Progress in nanoparticles characterization: Sizing and zeta potential measurement. *Particuology* **2008,** *6*, 112-115.

83.   Carrique, F.; Zurita, L.; Delgado, A. Dielectric relaxation in polystyrene suspensions. Effect of ionic strength. *Colloids Surf., A* **1994,** *92*, 9-21.

84.   Carrique, F.; Zurita, L.; Delgado, A. Correlation of the dielectric and conductivity properties of polystyrene suspensions with zeta potential and electrolyte concentration. *J. Colloid Interface Sci.* **1994,** *166*, 128-132.

85.   Wang, Y.; Bhushan, B.; Zhao, X. Nanoindents produced by nanobubbles on ultrathin polystyrene films in water. *Nanotechnology* **2008,** *20*, 045301.

86.   Craig, V.; Ninham, B.; Pashley, R. Effect of electrolytes on bubble coalescence. *Nature* **1993,** *364*, 317-319.

87.   Craig, V. S.; Ninham, B. W.; Pashley, R. M. The effect of electrolytes on bubble coalescence in water. *J. Phys. Chem.* **1993,** *97*, 10192-10197.

88.   Clasohm, L. Y.; Vakarelski, I. U.; Dagastine, R. R.; Chan, D. Y.; Stevens, G. W.; Grieser, F. Anomalous pH dependent stability behavior of surfactant-free nonpolar oil drops in aqueous electrolyte solutions. *Langmuir* **2007,** *23*, 9335-9340.

89.   Walczyk, W.; Schönherr, H. Characterization of the interaction between AFM tips and surface nanobubbles. *Langmuir* **2014,** *30*, 7112-7126.

90.   Song, Y.; Zhao, B.; Zhang, L.; Lü, J.; Wang, S.; Dong, Y.; Hu, J. The Origin of the "Snap-In" in the Force Curve between AFM Probe and the Water/Gas Interface of Nanobubbles. *ChemPhysChem* **2014,** *15*, 492-499.

91.   Li, D.; Jing, D.; Pan, Y.; Wang, W.; Zhao, X. Coalescence and stability analysis of surface nanobubbles on the polystyrene/water interface. *Langmuir* **2014,** *30*, 6079-6088.

92.   Zhao, B.; Wang, X.; Song, Y.; Hu, J.; Lü, J.; Zhou, X.; Tai, R.; Zhang, X.; Zhang, L. Stiffness and evolution of interfacial micropancakes revealed by AFM quantitative nanomechanical imaging. *Phys. Chem. Chem. Phys.* **2015,** *17*, 13598-13605.

93.   Walczyk, W.; Schönherr, H. Dimensions and the Profile of Surface Nanobubbles: Tip–Nanobubble Interactions and Nanobubble Deformation in Atomic Force Microscopy. *Langmuir* **2014,** *30*, 11955-11965.

127.   Cao, M.; Guo, D.; Yu, C.; Li, K.; Liu, M.; Jiang, L., Water-Repellent Properties of Superhydrophobic and Lubricant-Infused "Slippery" Surfaces: A Brief Study on the Functions and Applications. *ACS Appl. Mater. Interfaces* **2015**, *8*, 3615-3623.

128.   Zhang, Y.; Cremer, P. S., Interactions between Macromolecules and Ions: The Hofmeister Series. *Curr. Opin. Chem. Biol.* **2006**, *10*, 658-663.

129.   Kunz, W.; Nostro, P. L.; Ninham, B. W., The Present State of Affairs with Hofmeister Effects. *Curr. Opin. Colloid Interface Sci.* **2004**, *9*, 1-18.

130. Baldwin, R. L., How Hofmeister Ion Interactions Affect Protein Stability. *Biophys. J.* **1996**, *71*, 2056-2063.

131. Zangi, R.; Hagen, M.; Berne, B., Effect of Ions on the Hydrophobic Interaction between Two Plates. *J. Am. Chem. Soc.* **2007**, *129*, 4678-4686.

132. Horinek, D.; Netz, R. R., Specific Ion Adsorption at Hydrophobic Solid Surfaces. *Phys. Rev. Lett.* **2007**, *99*, 226104.

133. Schwierz, N.; Horinek, D.; Netz, R. R., Anionic and Cationic Hofmeister Effects on Hydrophobic and Hydrophilic Surfaces. *Langmuir* **2013**, *29*, 2602-2614.

134. Stock, P.; Müller, M.; Utzig, T.; Valtiner, M., How Specific Halide Adsorption Varies Hydrophobic Interactions. *Biointerphases* **2016**, *11*, 019007.

135. Du, Q.; Freysz, E.; Shen, Y. R., Surface Vibrational Spectroscopic Studies of Hydrogen Bonding and Hydrophobicity. *Science* **1994**, *264*, 826-827.

136. Du, Q.; Superfine, R.; Freysz, E.; Shen, Y., Vibrational Spectroscopy of Water at the Vapor/Water Interface. *Phys. Rev. Lett.* **1993**, *70*, 2313.

137. Denkov, N. D.; Subramanian, V.; Gurovich, D.; Lips, A., Wall Slip and Viscous Dissipation in Sheared Foams: Effect of Surface Mobility. *Colloids Surf., A* **2005**, *263*, 129-145.

138. Mura, S.; Nicolas, J.; Couvreur, P., Stimuli-Responsive Nanocarriers for Drug Delivery. *Nat. Mater.* **2013**, *12*, 991.

139. Schutt, E. G.; Klein, D. H.; Mattrey, R. M.; Riess, J. G., Injectable Microbubbles as Contrast Agents for Diagnostic Ultrasound Imaging: The Key Role of Perfluorochemicals. *Angew. Chem. Int. Ed.* **2003**, *42*, 3218-3235.

140.   Yu, C.; Cao, M.; Dong, Z.; Li, K.; Yu, C.; Wang, J.; Jiang, L., Aerophilic Electrode with Cone Shape for Continuous Generation and Efficient Collection of H2 Bubbles. *Adv. Funct. Mater.* **2016**, *26*, 6830-6835.

141.   Chan, D. Y.; Klaseboer, E.; Manica, R., Theory of Non-Equilibrium Force Measurements Involving Deformable Drops and Bubbles. *Adv. Colloid Interface Sci.* **2011**, *165*, 70-90.

142.   Marcus, Y., Thermodynamics of Solvation of Ions. Part 5.—Gibbs Free Energy of Hydration at 298.15 K. *J. Chem. Soc., Faraday Trans.* **1991**, *87*, 2995-2999.

143.   Strazdaite, S.; Versluis, J.; Backus, E. H.; Bakker, H. J., Enhanced Ordering of Water at Hydrophobic Surfaces. *J. Chem. Phys.* **2014**, *140*, 054711.

144.   Richmond, G., Molecular Bonding and Interactions at Aqueous Surfaces as Probed by Vibrational Sum Frequency Spectroscopy. *Chem. Rev.* **2002**, *102*, 2693-2724.

145.   Ma, J. C.; Dougherty, D. A., The Cation−Π Interaction. *Chem. Rev.* **1997**, *97*, 1303-1324.

146.   Mahadevi, A. S.; Sastry, G. N., Cation−Π Interaction: Its Role and Relevance in Chemistry, Biology, and Material Science. *Chem. Rev.* **2012**, *113*, 2100-2138.

147.   Cabarcos, O. M.; Weinheimer, C. J.; Lisy, J. M., Size Selectivity by Cation–Π Interactions: Solvation of K+ and Na+ by Benzene and Water. *J. Chem. Phys.* **1999**, *110*, 8429-8435.

148.   Cabarcos, O. M.; Weinheimer, C. J.; Lisy, J. M., Competitive Solvation of K+ by Benzene and Water: Cation-Π Interactions and Π-Hydrogen Bonds. *J. Chem. Phys.* **1998**, *108*, 5151-5154.

149.   Lu, Q.; Oh, D. X.; Lee, Y.; Jho, Y.; Hwang, D. S.; Zeng, H., Nanomechanics of Cation−Π Interactions in Aqueous Solution. *Angew. Chem.* **2013**, *125*, 4036-4040.

150.   Kumpf, R. A.; Dougherty, D. A., A Mechanism for Ion Selectivity in Potassium Channels: Computational Studies of Cation-Pi Interactions. *Science* **1993**, *261*, 1708-1710.

151.   Shen, Y. R.; Ostroverkhov, V., Sum-Frequency Vibrational Spectroscopy on Water Interfaces: Polar Orientation of Water Molecules at Interfaces. *Chem. Rev.* **2006**, *106*, 1140-1154.

152.   Russell, T. P.; Chai, Y., 50th Anniversary Perspective: Putting the Squeeze on Polymers: A Perspective on Polymer Thin Films and Interfaces. *Macromolecules* **2017**, *50*, 4597-4609.

153.   Chai, Y.; Salez, T.; McGraw, J. D.; Benzaquen, M.; Dalnoki-Veress, K.; Raphaël, E.; Forrest, J. A., A Direct Quantitative Measure of Surface Mobility in a Glassy Polymer. *Science* **2014**, *343*, 994-999.

154.   Yang, Z.; Fujii, Y.; Lee, F. K.; Lam, C.-H.; Tsui, O. K., Glass Transition Dynamics and Surface Layer Mobility in Unentangled Polystyrene Films. *Science* **2010**, *328*, 1676-1679.

155.   Hanakata, P. Z.; Douglas, J. F.; Starr, F. W., Interfacial Mobility Scale Determines the Scale of Collective Motion and Relaxation Rate in Polymer Films. *Nat. Commun.* **2014**, *5*, 4163.

156.   Rao, S. R., *Surface Chemistry of Froth Flotation: Volume 1: Fundamentals*; Springer Science & Business Media, 2013.

157.   Yang, H. C.; Hou, J.; Chen, V.; Xu, Z. K., Janus Membranes: Exploring Duality for Advanced Separation. *Angew. Chem. Int. Ed.* **2016**, *55*, 13398-13407.

158.   Attard, P., Nanobubbles and the Hydrophobic Attraction. *Adv. Colloid Interface Sci.* **2003**, *104*, 75-91.

159.   Yeon, H.; Wang, C.; Van Lehn, R. C.; Abbott, N. L., Influence of Order within Nonpolar Monolayers on Hydrophobic Interactions. *Langmuir* **2017**, *33*, 4628-4637.

160.   Ma, C. D.; Wang, C.; Acevedo-Vélez, C.; Gellman, S. H.; Abbott, N. L., Modulation of Hydrophobic Interactions by Proximally Immobilized Ions. *Nature* **2015**, *517*, 347-350.

161. Bain, C. D.; Whitesides, G. M., Modeling Organic Surfaces with Self-Assembled Monolayers. *Angew. Chem., Int. Ed. Engl.* **1989**, *28*, 506-512.

162. Porter, M. D.; Bright, T. B.; Allara, D. L.; Chidsey, C. E., Spontaneously Organized Molecular Assemblies. 4. Structural Characterization of N-Alkyl Thiol Monolayers on Gold by Optical Ellipsometry, Infrared Spectroscopy, and Electrochemistry. *J. Am. Chem. Soc.* **1987**, *109*, 3559-3568.

163. Bain, C. D.; Troughton, E. B.; Tao, Y. T.; Evall, J.; Whitesides, G. M.; Nuzzo, R. G., Formation of Monolayer Films by the Spontaneous Assembly of Organic Thiols from Solution onto Gold. *J. Am. Chem. Soc.* **1989**, *111*, 321-335.

164. Bain, C. D.; Whitesides, G. M., Correlations between Wettability and Structure in Monolayers of Alkanethiols Adsorbed on Gold. *J. Am. Chem. Soc.* **1988**, *110*, 3665-3666.

165. Bain, C. D.; Evall, J.; Whitesides, G. M., Formation of Monolayers by the Coadsorption of Thiols on Gold: Variation in the Head Group, Tail Group, and Solvent. *J. Am. Chem. Soc.* **1989**, *111*, 7155-7164.

166. Bain, C. D.; Whitesides, G. M., Formation of Monolayers by the Coadsorption of Thiols on Gold: Variation in the Length of the Alkyl Chain. *J. Am. Chem. Soc.* **1989**, *111*, 7164-7175.

167. Arima, Y.; Iwata, H., Effect of Wettability and Surface Functional Groups on Protein Adsorption and Cell Adhesion Using Well-Defined Mixed Self-Assembled Monolayers. *Biomaterials* **2007**, *28*, 3074-3082.

168. Wong, T.-S.; Kang, S. H.; Tang, S. K.; Smythe, E. J.; Hatton, B. D.; Grinthal, A.; Aizenberg, J., Bioinspired Self-Repairing Slippery Surfaces with Pressure-Stable Omniphobicity. *Nature* **2011**, *477*, 443.

169.   Cui, J.; Daniel, D.; Grinthal, A.; Lin, K.; Aizenberg, J., Dynamic Polymer Systems with Self-Regulated Secretion for the Control of Surface Properties and Material Healing. *Nat. Mater.* **2015**, *14*, 790.

170.   Chai, L.; Klein, J., Large Area, Molecularly Smooth (0.2 Nm Rms) Gold Films for Surface Forces and Other Studies. *Langmuir* **2007**, *23*, 7777-7783.

171.   Epstein, A. K.; Wong, T.-S.; Belisle, R. A.; Boggs, E. M.; Aizenberg, J., Liquid-Infused Structured Surfaces with Exceptional Anti-Biofouling Performance. *Proc. Natl. Acad. Sci.* **2012**, *109*, 13182-13187.

172.   Stirnemann, G.; Rossky, P. J.; Hynes, J. T.; Laage, D., Water Reorientation, Hydrogen-Bond Dynamics and 2d-Ir Spectroscopy Next to an Extended Hydrophobic Surface. *Faraday Discuss.* **2010**, *146*, 263-281.

173.   Godawat, R.; Jamadagni, S. N.; Garde, S., Characterizing Hydrophobicity of Interfaces by Using Cavity Formation, Solute Binding, and Water Correlations. *Proc. Natl. Acad. Sci.* **2009**, *106*, 15119-15124.

174.   Mezger, M.; Sedlmeier, F.; Horinek, D.; Reichert, H.; Pontoni, D.; Dosch, H., On the Origin of the Hydrophobic Water Gap: An X-Ray Reflectivity and Md Simulation Study. *J. Am. Chem. Soc.* **2010**, *132*, 6735-6741.

175.   Despa, F.; Fernández, A.; Berry, R. S., Dielectric Modulation of Biological Water. *Phys. Rev. Lett.* **2004**, *93*, 228104.

176.   Kanth, J. M. P.; Vemparala, S.; Anishetty, R., Long-Distance Correlations in Molecular Orientations of Liquid Water and Shape-Dependent Hydrophobic Force. *Phys. Rev. E* **2010**, *81*, 021201.

177.   Despa, F.; Berry, R. S., The Origin of Long-Range Attraction between Hydrophobes in Water. *Biophys. J.* **2007**, *92*, 373-378.

178.   Scatena, L.; Brown, M.; Richmond, G., Water at Hydrophobic Surfaces: Weak Hydrogen Bonding and Strong Orientation Effects. *Science* **2001**, *292*, 908-912.

179.   Miranda, P.; Shen, Y., Liquid Interfaces: A Study by Sum-Frequency Vibrational Spectroscopy. *J. Phys. Chem. B* **1999**, *103*, 3292-3307.

180.   Du, Q.; Freysz, E.; Shen, Y. R., Vibrational Spectra of Water Molecules at Quartz/Water Interfaces. *Phys. Rev. Lett.* **1994**, *72*, 238-241.

181.   Patel, A. J.; Varilly, P.; Chandler, D., Fluctuations of Water near Extended Hydrophobic and Hydrophilic Surfaces. *J. Phys. Chem. B* **2010**, *114*, 1632-1637.

182.   Miranda, P.; Xu, L.; Shen, Y.; Salmeron, M., Icelike Water Monolayer Adsorbed on Mica at Room Temperature. *Phys. Rev. Lett.* **1998**, *81*, 5876-5879.